STOCHASTIC ANALYSIS AND OPTIMIZATION OF POWER SYSTEM STEADY-STATE WITH WIND FARMS AND ELECTRIC VEHICLES

by

GAN LI

A thesis submitted to
The University of Birmingham
for the degree of
DOCTOR OF PHILOSOPHY

School of Electronic,
Electrical and Computer Engineering
The University of Birmingham
June 2012

To my parents

ACKNOWLEDGEMENTS

First and foremost, I would like to express my sincere appreciation to my supervisor, Prof. Xiao-Ping Zhang, for his support, guidance, inspiration and patience during my PhD study. I have greatly benefited from his knowledge and experience.

I am also grateful to Associate Prof. Zhigang Wu and Associate Prof. Xuefeng Bai for their support and advices on my research. Many thanks to Mr. Dechao Kong, Mr. Zhou Li and Mr. Bo Fan for sharing their valuable ideas with me. I would also like to thank my dear colleagues Miss Rui Shi, Mr. Jingchao Deng, Mr. Xuan Yang, and Mr. Suyang Zhou for their discussions and kind assistance during my study.

Finally, I would like to thank my families and all my friends. Without their encouragement, support and understanding, completion of my thesis would not be possible.

ABSTRACT

Since the end of last century, power systems are more often operating under highly stressed and unpredictable conditions because of not only the market-oriented reform but also the rising of renewable generation and electric vehicles. The uncertain factors resulting from these changes lead to higher requirements for the reliability of power grids. In this situation, conventional deterministic analysis and optimization methods cannot fulfil these requirements very well, so stochastic analysis and optimization methods become more and more important.

This thesis tries to cover different aspects of stochastic analysis and optimization of the power systems from a perspective of its steady state operation. Its main research topics consist of four parts: deterministic power flow calculations, modelling of wind farm power output and electric vehicle charging demand, probabilistic power flow calculations, as well as stochastic optimal power flow. These different topics involve modelling, analysis and optimization, which could establish a whole stochastic methodology of the power system with wind farms and electric vehicles.

TABLE OF CONTENTS

LIST OF FIGURES

LIST OF TABLES

LIST OF ABBREVIATIONS

ANR	Accelerated Newton-Raphson power flow
FNR	Fixed Newton-Raphson power flow
NR	Newton-Raphson power flow
FD	Fast Decoupled power flow
MRV	Modifying right-hand-side vector
LDS	Large diagonal strategy
FOR	Forced outage rate
i.i.d.	Independent, identically distributed
PPF	Probabilistic power flow
CM	Cumulant method
PEM	Point estimate method
MCS	Monte Carlo simulation
OPF	Optimal power flow
D-OPF	Deterministic optimal power flow
S-OPF	Stochastic optimal power flow

CHAPTER 1 INTRODUCTION

1.1 Research Background

1.1.1 Energy and Environment

In the 21st century, our modern industry still relies on the fossil fuels, e.g. oil, gas, coal etc., as the dominant energy source. However, the exploitation and utilization of fossil fuels brings negative impact on the environment, such as air pollution, greenhouse effect, extreme climate and so on. The developed countries have to spend a lot of resources and time treating the environmental problems left over during their industrialization process, while developing countries are also troubled by the contradiction between environment protection and economic development. On the other hand, the limited mineable reserves of fossil fuels and their difference in regional distribution lead to worldwide concerns about energy security, especially after three oil crises successively occurred in the mid and late 20th century [1].

Since the last decade of the 20th century, as the depletion trend of fossil fuels becomes widely recognized along with the environmental challenge mainly due to global warming resulting from excessive greenhouse gas emissions, the international community has reached an agreement that it is necessary to reform the existing mode of production and consumption, which excessively relies on fossil fuels, to a sustainable mode with cleaner alternative energy and less greenhouse gas emissions [2]. From the energy supply side, the large scale exploitation of renewable energy generation, such as solar energy, tidal energy, and especially wind energy, is developing very fast and renewable energy sources have taken an important role in the supply of energy [3]; on the energy demand side, electric vehicles are becoming popular because of their high energy efficiency and low off-gas emissions, and an emerging

marketplace of electric vehicles is forming in both developing countries and developed countries in recent years [4].

In pursuit of environmental sustainability and energy security, most developed countries and developing countries have made their mid and long term strategic plans to promote renewable energy and electric vehicle industry in the 21st century [5], so it can be expected that with the rising of renewable energy and the popularization of electric vehicles, great changes are happening in the supply and demand chain of energy in next several decades. As an irreplaceable part of this chain, the power system performs the important task of transferring electric power from its generation side to its demand side, and is inevitably involved in these series of changes. Therefore, it's necessary to study the influence of large-scale integration of renewable energy and electric vehicles into power systems, and develop corresponding qualitative and quantitative analysis and optimization methods.

1.1.2 Wind Generation Development

Wind power is the conversion of wind energy existing in air flowing into a useful form of energy. It is clean, safe and sustainable. There has been a long history of its utilization. In early days, kinetic energy was extracted from wind power, e.g. sails to propel ships, or further converted to mechanical power, e.g. windmills to pump water. In the late 19th century, a wind generator was first invented by the Danish, and then the first wind farm was built in Denmark, which disclosed a new page of the history of wind energy.

During 1970s-1980s, in order to overcome energy crisis and environment stress, more and more attention was paid on sustainable energy including wind power generation. In 1980, the first 55kW wind generator was successfully developed, which marked a breakthrough in the

modern wind power industry, and since then wind power generation entered a new period of fast growth [8]. As the progress in technology, the capacity of single wind generator grows to the MW order, and its reliability and efficiency is significantly improved. Moreover, the cost of wind power generation steadily falls and is now competitive in price with conventional coal on most sites [9]. Therefore, wind power generation has been one of the most promising renewable energy sources.

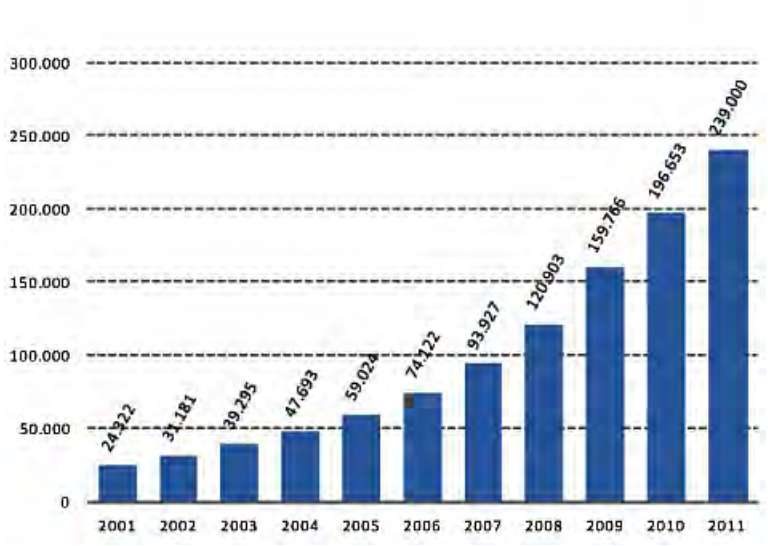

Figure 1-1 World total installed wind power capacity (GW)

By the end of 2000, the worldwide installed wind power capacity reached 17.7GW, among which developed countries, such as Germany, Spain, Denmark and USA, together took a share of 80% [3]. In the 21st century, main developing countries such as China, India and Brazil, joined the development of wind power generation. The huge market of these developing countries greatly stimulated the wind power industry, and the development of wind power generation was once again accelerated over the last decade. As shown in Figure 1-1, the worldwide installed wind power capacity surged to 239GW by the end of 2011, among which the five leading countries are China, USA, Germany, Spain and India, together

representing a total share of 74% of the global wind capacity, and a number of new markets are also arising in East Europe and Central and South America [10].

UK is the windiest country in Europe, but when compared to Germany, Denmark and USA etc., its wind power generation dated from 1990s, but was accelerated since the beginning of the 21th century as shown in Figure 1-2 [11]:

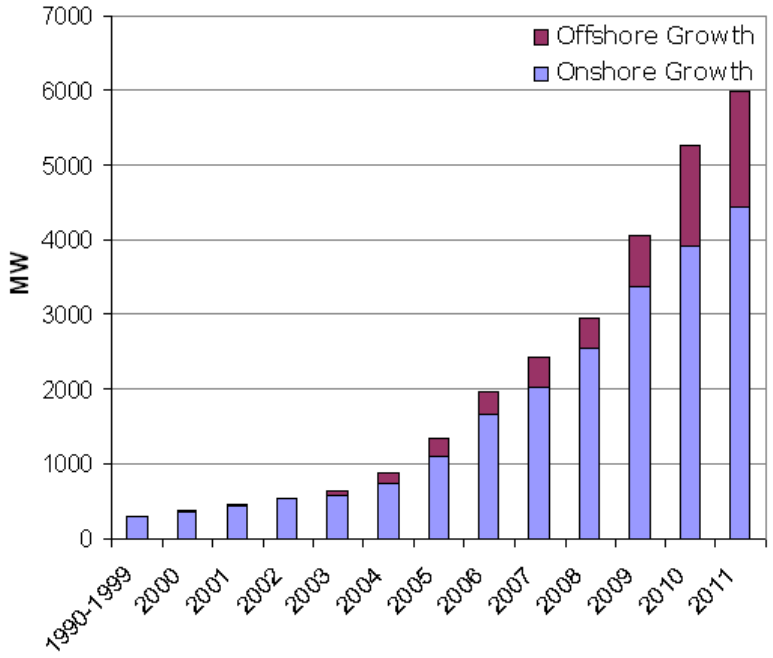

Figure 1-2 UK installed wind power capacity (MW)

At the beginning of March 2012, the installed capacity of wind power in UK reached 6.58GW with 333 operational wind farms accounting about 10% of its electricity supply, and UK is ranked as the world's eighth largest producer of wind power [11]. Wind power is expected to continue growing in UK for the foreseeable future, especially offshore wind power, because UK has been estimated to have over a third of Europe's total offshore wind resource, which is equivalent to three times its current electricity need, although this is only at times when the wind blows [12]. In fact, UK government planned 13GW of offshore wind power capacity by 2020, and had completed 3 rounds of offshore wind farm project bidding since 1998. In

October 2008, UK overtook Denmark and became the world leader of offshore wind power generation [13]. Currently, UK has 1.86GW of operational nameplate capacity, with a further 2.05GW in construction [11].

Figure 1-3 UK offshore wind farms (Source: Crown Estate)

1.1.3 Electric Vehicle Popularization

The rapid development of wind power generation along with other renewable energy causes an optimization in power supply side for environment protection and sustainability, while

power demand side is also undergoing a reformation, which is represented by the rising of electric vehicles.

Automobile transportation consumes the most fossil fuel, mainly oil (e.g. in USA, about 15.4 million barrels of oil are used each day, while 2/3 of these are refined into automobile fuel [14]); On the other hand, automobile exhaust is one of the main sources of greenhouse gases and harmful gases especially in urban areas (e.g. in Europe, automobile exhaust accounts about 25% of greenhouse gas emissions [15]). In order to relieve energy supply stress and reduce exhaust emissions, both developed countries and main developing countries are trying to popularize electric vehicles.

An electric vehicle is an automobile which can be propelled partially or fully by electric motor(s), using electricity stored in its onboard rechargeable or replaceable batteries or another energy storage device [16]. Electric vehicles were once popular in the late 19th and early 20th century, until mass manufacturing of cheaper internal combustion engine based automobiles led to their decline. The energy crises along with environment problem since the late 20th century raised renewed interest in electric vehicles due mainly to concerns about rapidly increasing oil prices and the need to curb greenhouse gas emissions [17].

Electric vehicles have several advantages as compared to conventional internal combustion based automobiles in energy efficiency and exhaust emissions [17]-[18]: Internal combustion engines are relatively inefficient at converting on-board fuel energy to propulsion (only about 15%-20%); in contrast, electric motors are more efficient in converting stored electric energy into propulsion (around 80%), and electric vehicles do not consume energy while coasting, and some of the energy lost when braking can be captured and reused through regenerative braking, which captures as much as one fifth of the energy normally lost during braking. On

the other hand, electric vehicles contribute to cleaner local air because they reduce or even produce no harmful exhaust, especially when power supply side is integrated with more clean renewable generation sources such as wind farms and solar power station.

Despite their potential benefits, the widespread adoption of electric vehicles still faces several hurdles and limitations [17]-[18]: Currently, high cost of power batteries leads to the disadvantage of electric vehicles in market competition with conventional internal combustion engine based vehicles; the lack of public and private recharging infrastructure and limited driving distance also reduce customer desire for purchasing electric vehicles. However, several governments, including USA, UK and China, have established policies and economic incentives to promote the sales of electric vehicles, and to fund further development of new electric vehicles [19]-[20].

As the prices of electric vehicles, especially plug-in hybrid electric vehicles which have realized industrialization, are coming down with mass production in recent years, there is a steady growth in the market share of electric vehicles in USA, Japan and European. For example, over 2 million hybrid electric cars and SUVs have been sold in USA by mid-2011 [21]; hybrid electric cars have already accounted 16% of market in Japan [22]. Since the beginning of 2011, UK government also launched a £5000 electric car grant scheme to both business and private buyers as an incentive [23]. Moreover, the world's first national electric vehicle charging network along main motorways was also launched in UK later in the same year [24]. By the end of 2011, UK has become one of the leading European markets and its total number of hybrid electric cars reached over a hundred thousand [25].

Above all, electric vehicles are now perceived as a core segment of the future automobile market. While the worldwide market for all vehicles will grow by about four percent per year

over the next six years, analysts estimate that electric vehicle market will grow at a rate of almost 20 percent over the same time frame [26].

1.1.4 Challenges and Opportunities

Due to the inherent fluctuation and intermittency of wind energy, the large integration of wind power generation could lead to negative effects on the power grids in terms of reliability, stability and power quality [27]. From the perspective of power system steady-state operation, because wind power generation is still not as reliable or controllable as conventional thermal power or hydropower plants are, extra reserve capacity should be supplemented into power systems as the penetration of wind power generation grows, otherwise system dispatching could be made more difficult.

Early wind generators draw reactive power during their operation, thus wind farms should be equipped with reactive power compensation devices. Though current wind generators don't have this problem, but dynamic reactive power compensation devices are still necessary in wind farms for voltage regulation. All these factors could reduce the economic value of wind power generation. Moreover, a lot of factors such as a too fast or too slow wind speed and voltage fluctuation could make a large number of wind generators in the same region offline, and this would result in great impact on the power flows.

On the other hand, with the popularization of electric vehicles into transportation, the electric energy sector will encounter a dramatic change due to this important and expected issue. The impact of electric vehicles on power systems mainly occurs in the demand side [28]-[29]: The number of electric vehicles directly determines the degree of their impact on power grids. As the rapid growth of electric vehicles in recent years, their charging demand will become an

important part of system loads. For example, Table 1-1 shows the projected concentrations of electric vehicles in major USA metro areas when 1 million vehicles are deployed nationally, where the charging loads of electric vehicles are considerable [4]:

Table 1-1 MW Load and Charging Projections for US Metro Areas in 2009

Metro Area	Total Electric Vehicles	MW Load if Everyone Charges at the Same Time	MW Load if Charging at the Stages over 8 Hours	MW Load if Charging at the Stages over 12 Hours
New York	54,069	299	33	22
Los Angeles	119,069	658	147	98
Chicago	27,892	154	34	23
Washington D.C.	37,520	207	46	31
San Francisco	91,005	503	112	75
Philadelphia	18,319	101	23	15
Boston	31,976	177	40	26
Detroit/Ann Arbor	10,718	59	13	9
Dallas/Fort Worth	10,961	61	14	9
Houston	12,032	67	15	10

Due to the differences in individual electric vehicles, their charging behaviour tends to be uncertain. A lot of factors could influence the charging behaviour of electric vehicles, such as the type and status of the power battery, the charging duration, and the operation mode. For example, the power batteries of an electric car and an electric bus are different in terms of capacity and operating characteristics, which leads to different charging voltage and current levels; while an electric bus prefers to replace a fully charged battery and leave the empty one to be gradually charged at the station; in contrast, a private electric car can choose to be charged at a rapid charging station and/or at home.

Besides the uncertainty in electric vehicle charging, the mobility of electric vehicles also adds new difficulty to the power system planning and scheduling, because it is difficult to exactly

calculate the number of electric vehicles running at a certain site during a particular time period, and how many of them will be connected to the power grid for charging.

Above all, due to the continuing rapid growth in wind power generation and electric vehicles, from its supply side to its demand side, the power system is encountered with more uncertainties in generation and load, which put more strict requirements on power system reliability, planning and operation. Therefore, it is necessary to establish corresponding mechanism for its analysis, evaluation and optimization.

1.2 Research Focuses of This Study

Just as its title shows, this study focuses on how to analyse and optimize the power system with large scale integration of wind farms and electric vehicles from a perspective of power system steady-state operation. Since both the power output of a wind farm and the charging demand of electric vehicles tend to be uncertain over a certain period, a natural idea is to describe such uncertainties using probability distributions, i.e. to view them as random variables.

A probability distribution of a random variable includes not only its numerical information, but also corresponding possibility, thus stochastic analysis of power systems can reveal more information than conventional deterministic analysis. However, due to the non-linearity and complexity of the power system, it is not easy to determine the unknown system outputs, state variables or reliability indices of interest directly from random system inputs which are described as probability distributions.

Fortunately, a lot of research work has been done in stochastic analysis and optimization of the power system, and a series of literature has been published over last several decades.

Based on the achievement of research before, this study is aimed at overcoming some drawbacks and improving the performance of existing methods in this field. Main efforts of this study include the following aspects:

1. **Deterministic AC power flow calculations.**

Deterministic AC power flow is fundamental to the analysis of power systems and is always a hot research topic. Although a lot of algorithms have been proposed on its calculations, the Newton-Raphson power flow and the Fast Decoupled power flow are currently dominant. The Fast Decoupled power flow is simpler and faster, but it cannot totally substitute for the Newton-Raphson power flow due to its assumptions on branch impedance. In this study, an improvement will be proposed to accelerate the conventional Newton-Raphson power flow.

2. Modelling the charging demand of electric vehicles.

Electric vehicles are more and more popular in recent years. Due to various factors influencing their charging behaviour, the overall charging demand of electric vehicles tends to be uncertain. As the number of electric vehicles increases, their charging demand will become an important part of the system load. Therefore, it is necessary establish a methodology to model such a new type of loads.

3. Probabilistic power flow calculations.

Probabilistic power flow is fundamental to the stochastic analysis of power systems. It is able to reveal the uncertainty of system status and outputs through the uncertain system inputs described as probability distributions. Currently, main methods of probabilistic power flow calculations have different disadvantages: Some of them suffer from large computational burden, while others are based on some unrealistic assumptions. In this study, a comparison of three mainstream methods, i.e. Monte Carlo simulation, the Cumulant Method, and the Point Estimate Method, will be given and an improvement will be done to the fastest

Cumulant method, in order to remove its assumption on the independence between system inputs.

4. Chance-constrained stochastic optimal power flow problem.

Deterministic optimal power flow neither reveals the influences of uncertainties, nor provides information on the degree of importance or likelihood of constraint violations. In contrast, the chance-constrained stochastic optimal power flow is more suitable when such uncertainties should be considered. However, currently the solution approach to stochastic optimal power flow is still an open research area. Some approaches have been proposed but they rely on the assumption that system inputs are independent, and can only deal with Gaussian distributed system inputs. In this study, a heuristic approach will be proposed to overcome these two limitations.

The next section will give a detailed literature review on the above four research topics of this thesis.

1.3 Literature Review

1.3.1 Deterministic AC Power Flow

The AC power flow problem is aimed at determining the bus complex voltages from the given bus power injections and electric network configuration in steady state. It is usually formulated as a set of non-linear algebraic equations and solved by iterative methods such as Gauss-Seidel, Newton-Raphson, Fast Decoupled power flow, and so on. As one of the fundamentals of power system analysis, many efforts have been paid to improve the robustness and/or efficiency of its solution in different ways:

The Newton-Raphson power flow was first proposed in [30], which utilizes the Newton method to achieve local quadratic convergence [31]. However, it is time consuming to factorize the Jacobian matrix in the correction equations at each iteration in the Newton-Raphson power flow calculations [32]. Therefore, the Fast Decoupled power flow was developed in [33], which separates the correction equation set into the two decoupled sets with constant coefficient matrices to achieve much better time efficiency. However, in some areas the Newton-Raphson power flow is still superior. For example, when the system is operating near its stability limits, some assumptions on the Fast Decoupled power flow don't hold any more so that the Newton-Raphson power flow becomes the only available method [34]. Moreover, due to the fast development of renewable energy and the deregulation of power systems, highly stressed system conditions are nowadays not rare. On the other hand, the assumption on the low R/X ratio of branches also limits the applicability of the Fast Decoupled power flow [35].

As the Newton-Raphson power flow is still irreplaceable, different efforts have been done to improve its robustness and speed: A new power flow formulation based on bus current injections was presented in [36]. Its case studies showed this formulation can achieve a consistent speed-up of about 20% in comparison with the conventional formulation based on bus power injections. The conventional power flow formulation based on bus power injections was expanded in [37] to include injected current based equations. Such a mixed formulation leads to a better time efficiency, which is particularly advantageous in the presence of a large number of zero-injection buses, though the number of equations is duplicated. The injected current based power flow formulation proposed in [38] retains the second order terms and uses an optimal step size factor to acquire not only better computational efficiency but also better robustness even when the conventional power flow

formulation is not solvable. An alternative injected current based power flow formulation was proposed in [39] for better efficiency, where the formation of the Jacobian matrix is simplified. A comprehensive comparison between the injected current based formulation and the injected power based formulation in different coordinates was done in [40]. Numerical results in [40] have indicated some advantages of the injected current based formulation under heavy loading conditions. Recently, the power flow problem was formulated in [41] as a set of autonomous ordinary differential equations, which was solved by the continuous Newton's method especially for ill-conditioned or badly initialized cases.

On the other hand, besides new power flow formulations, new mathematical methods for solving the non-linear equations were introduced into power flow calculations. In [42], the concept of optimal multiplier was proposed based on the second-order Taylor expansion of the power flow equations, and it was multiplied to the voltage correction in the Newton-Raphson power flow in order to enhance its robustness in ill or highly stressed loading conditions. The optimal multiplier was extended from the rectangular coordinates, as originally presented in [42], to the polar coordinates in [43]. Detailed comparison between these two approaches was presented in [44] and numerical results indicated some advantages of the Newton-Raphson power flow with the optimal multiplier formulated in the polar coordinates. In [45], two schemes based on the tensor methods were proposed to solve the power flow problem, and it was reported that cubic convergence characteristics can be obtained and apparent speedup can be achieved if the computational effort for calculating the quadratic terms is reduced. In addition, a non-iterative power flow algorithm has been established in [46] for voltage stability analysis, where the voltage corrections are represented as the Taylor series expansion of bus injected power mismatches. However, this method may require a large number of expansion terms necessary for convergence, which would be a

serious drawback for its practical application. In [47] and [48], the power flow problem was considered as an optimization problem and solved by the neural network algorithm and the chaotic particle swarm algorithm, respectively. Such algorithms can achieve better robustness than the traditional power flow algorithms under heavy loading conditions but their speed needs to be investigated yet especially for large scale power systems.

Moreover, specific research has been done on the conventional Newton-Raphson power flow to obtain time saving. In [49], the Quasi-Newton method, incorporating best step selection and partial Jacobian matrix updates, was introduced to solve the power flow problem. Case studies have shown that an order of 50% time saving on large power systems compared to the conventional Newton-Raphson power flow algorithm can be achieved. An effective procedure avoiding unnecessary repetitions between the calculations of bus power injections and the calculations of Jacobian matrix elements was presented in [50], which resulted in obvious reduction in power flow solution time. Different techniques for improving the convergence by adjusting the Jacobian matrix iteratively in the Newton-Raphson power flow solution were compared in [51]. In [52], a Newton-like method with the modification of the right-hand-side vector (MRV), which originated from [53], was introduced to solve the power flow problem in branch outage simulations. Such a MRV Newton-like method in [53] is based on a constant Jacobian matrix and a factor to the right-hand-side vector, and numerical results validated its robustness. However, it was only employed in [52] for post-contingency power flow analysis starting with a converged solution.

In this study, we will discuss the possibility of applying a new MRV Newton-like method to the power flow solution with a flat start. As presented [53]-[59], though their names could be various, these MRV Newton-like methods belong to the same category that modifies the

right-hand-side vector in the correction equations and eliminates the necessity of factorizing the Jacobian matrix at each iteration. However, they differ from each other in the way how the right-hand-side vector is modified. Due to its concise formulation and good robustness, the MRV Newton-like method proposed in [58] will be employed, and hence the Accelerated Newton-Raphson power flow will be proposed. Details about this are presented in Chapter 2.

1.3.2 Charging Demand of Electric Vehicles

An electric vehicle is typically equipped with a drive train that at least contains an electrical motor, a battery storage system and a means of recharging the battery system from an external source of electricity [60]. Its battery capacity is usually several kWh or more to power the vehicle in all electric drive mode for several tens of miles [61]. Moreover, an electric vehicle could have an internal combustion engine as well, which is engaged to extend its drive range when its battery's charge is not sufficient [62].

Related research on the impact of electric vehicle charging on the power grid dated from 1980s. It was discovered that their charging demand is likely to coincide with the overall peak load [63], and it is necessary to manage their charging demand when the penetration of electric vehicles increases, otherwise the overall peak load could increase significantly [64]-[65]. Therefore, the concept of smart charging was proposed, which is aimed at optimizing the charging process of electric vehicles [66]-[71]:

A control strategy was proposed in [66] to optimize the energy consumption stemming from electric vehicle charging in a residential use case; another two strategies were presented in [67] to optimize charging time and energy flows of an electric car, considering forecasted electricity price and system auxiliary service. In [68]-[69], the possible benefits of electric

vehicles as a certain type of auxiliary service were discussed and some conceptual framework for its implementation was presented in [70]-[71].

Although smart charging may demonstrate a good application potential in the future smart grid, the consumers in reality may prefer to charge their electric vehicles as fast as possible, so that smart charging control doesn't interfere with their daily drive profile [72]-[73]. On the other hand, rapid charging techniques are also developing fast [74], which could attract more electric vehicle consumers. Moreover, the physical implementation and integration of smart charging is still to be done on a system wide scale in future. Therefore, currently it is still necessary to evaluate the impact of uncontrolled charging of electric vehicles.

As stated before, the overall charging demand of electric vehicles within a certain area tends to be uncertain over a certain period, and stochastic analysis can be applied to its impact on the power systems. Therefore, the first step is how to model the charging demand of electric vehicles and there has been some literature on this topic: A specified operation mode of charging an electric car at home during day and night periods was assumed in [75] with specified charging periods, charging level, battery start/end status and capacity, then a coordinated strategy of charging power was proposed to improve the voltage profile in the residential distribution grid. But this strategy was based on deterministic power flow analysis, so it cannot take uncertainty into consideration. Queuing theory [76] was first introduced in [77] to model the instantaneous charging demand of multiple electric vehicles at a charging station. This model was extended in [78] to describe the total charging and discharging power of electric vehicle in a certain region. However, only one type of electric vehicle was considered in [77]-[78], while other influential factors, e.g. differences in battery capacity and charging level, were neglected. An analytic approach of modelling the daily recharge energy

of electric vehicles in a certain region was presented in [79]. Such an approach considers the vehicle types, the status of batteries and the charging periods as probability distributions, and then obtains the inverted load duration curve of charging power as its probability distribution. The drawback of the approach in [79] is the charging power of multiple vehicles was simply added together, regardless of the potential interactions between electric vehicles themselves.

Besides their drawbacks in the consideration of influential factors, the above models generally expressed the overall charging demand of electric vehicles as a nonlinear function of several random variables. This leads to great difficulty in calculating the numeric characteristics of its probability distribution, which are essential in stochastic analysis of the power system. Therefore, in order to overcome such a difficulty and at the same time to take more influential factors into consideration, a methodology of modelling the overall charging demand of electric vehicles will be proposed in Chapter 3.

1.3.3 Probabilistic Power Flow

For the power system, deterministic power flow is fundamental to its deterministic analysis. Similarly, probabilistic power flow, sometimes also called as stochastic power flow, is fundamental to its stochastic analysis. Probabilistic power flow is aimed at obtaining the probability distributions of system outputs or state variables from that of uncertain system inputs, which are modelled as appropriate probability distributions.

The concept of probabilistic power flow was first proposed in 1974 [80], and over last several decades many papers have been published on how to solve the probabilistic power flow problem [81]-[102]. Basically, these methods can be divided into three categories [103]-[104], namely simulation methods, analytical methods and approximate methods.

Simulation methods [81]-[83] originated from statistical theory and have been applied to reliability assessment for many years due to their simplicity and applicability, among which Monte Carlo simulation [82] is currently most widely used. However, these methods usually suffer from large amount of computation in order to obtain meaningful statistical results. In contrast, analytical methods [84]-[99] are more computationally effective. In the early stages of analytical methods, convolution techniques [84]-[85] were commonly employed to obtain the probability distributions of desired variables. However, the computation efficiency is still low, though some efforts have been made to improve this by fast Fourier transform [87]-[91], so that other analytical methods based on the numerical characteristics of the probability distribution, e.g. moments and cumulants, were developed [92]-[99]. A basic assumption of these methods is the independence between system inputs, and the power flow equations are usually linearized in order to utilize certain properties of these numerical characteristics. The cumulant method [94]-[99] is currently the representative of analytical methods. Because the linearization of power flow equations requires a constant network configuration, some auxiliary techniques should be applied to deal with network changes, e.g. branch outages [95]-[96]. The point estimate method [100]-[102] is well recognized as the representation of approximate methods. Similar to analytical methods, it also utilizes the numerical characteristics of random system inputs, but a different way is adopted: a certain number of locations are extracted from the probability distribution of each random system input with corresponding weights, then the moments of system outputs are calculated straightforwardly from them, so that the linearization of power flow equations are not needed.

Chapter 4 will give a detailed comparative study on the above three methods, and a technique will be presented to improve the cumulant method so that it is able to deal with the correlation among them.

1.3.4 Stochastic Optimal Power Flow

As an extension of the concept of power flow, optimal power flow was first proposed for the economic generation dispatch in 1979 [105], and over last several decades a wide range of optimal power flow models and approaches have been developed to formulate and solve various optimization problems in the operation and planning of the power system. Typically, an optimal power flow problem is aimed at seeking a feasible power flow operating point by adjusting a set of control variables subjected to certain physical, operational and policy constraints, so that the objective function can be maximized or minimized.

Optimal power flow is conventionally formulated as a deterministic optimization problem with fixed model parameters and input variables. Such a formulation neither considers the influence of uncertain factors, such as load forecasting errors, accidental component failures or renewable generation fluctuations, etc., nor provides information on the degree of importance or likelihood of constraint violations [106]. In the deterministic optimal power flow, an overestimation of uncertainties has to be adopted as a widespread practice for the sake of system security, due to the lack of quantitative analysis methods to study the impact of uncertainties. However, such a way of treating uncertainties could lead to conservative optimization results. Therefore, it is necessary to develop a suitable formulation that is capable of revealing the influence of uncertainties on the power system from the perspective of optimal power flow.

The proposal of probabilistic power flow [80] provided a new idea for the development of optimal power flow to take uncertainties into consideration. A literature review has indicated that current research on this topic can be divided into two categories [107], i.e. probabilistic optimal power flow and stochastic optimal power flow:

Probabilistic optimal power flow [108]-[114] retains the deterministic formulation but models uncertain system inputs as random distributions. The analysis methods of probabilistic power flow, e.g. the cumulant method [109]-[111] or the point estimate method [112]-[114], are generally applied. However, due to its deterministic formulation, the randomness of system inputs only determines the probability distributions of control variables instead of their values.

In contrast, stochastic optimal power flow [115]-[119] not only treats uncertain system inputs as random distributions, but also establishes stochastic formulation for the optimal power flow problem. That is, either the objective function or constraints in the optimization model are represented as probability formulation, equations or inequalities, so the randomness of system inputs directly determines the optimal results during its solution process [120].

Early research on stochastic optimal power flow usually employed the expected value model [115], which optimizes the expected value of a certain objective function subject to certain constraints expressed in the form of expected values as well. Although it is simple and straightforward to be solved, this formulation of stochastic optimal power flow only reveals the expected value information but neglects variations and other information. In recent years, the chance-constrained model is introduced into stochastic optimal power flow [116]-[119], where part of or all the constraints become probability inequalities. Different approaches have been developed to solve these chance-constrained stochastic optimal power flow problems: A heuristic approach was proposed in [116], which is able to consider uncorrelated Gaussian loads. It searches the optimal solution of the stochastic optimal power flow problem in the neighbourhood of the optimal solution of a corresponding deterministic optimal power flow problem with a dynamically adjusted feasible set. Another approach was proposed in [117] for optimal reactive power dispatch considering uncorrelated Gaussian loads, where a

stochastic search based on the genetic algorithm was employed. A Monte-Carlo simulation based approach was proposed in [118] for optimal economic generation dispatch considering correlated Gaussian loads. A hybrid intelligent algorithm presented in [120] combining Monte Carlo simulation and neutral network was introduced in [119] to determine the optimal operation strategy of energy storage units at a wind farm with Gaussian wind generation forecast error.

It should be noted that the approaches to chance constrained stochastic optimal power flow proposed in [116]-[117] rely on the assumption of the independence between random system inputs. However, it has been indicated in [97] and [121] that some correlations between uncertain system inputs should be taken into consideration, e.g. the correlation between generation outputs of wind farms in the same region. Although the Monte Carlo simulation based approaches in [118]-[119] are able to deal with correlation, they generally suffer from low computation efficiency and have to be limited to optimization problems of small scale. On the other hand, currently only Gaussian loads are considered in all these approaches [116]-[119], but uncertain system inputs could be non-Gaussian distributions, e.g. the generation outputs of wind farms [97].

In order to overcome the above drawbacks, a new heuristic approach to the chance-constrained stochastic optimal power flow problem will be presented in Chapter 5, taking account of non-Gaussian system inputs as well as the possible correlation among them.

1.4 Thesis Outlines

This thesis is organized as follows:

Chapter 2: A brief introduction on the key mathematical concepts and methods related to stochastic analysis.

Chapter 3: The applicability of a Newton-like method to AC power flow solution is investigated and based on this the Accelerated Newton-Raphson power flow is proposed.

Chapter 4: The probability models of typical power system inputs including the power output of a wind farm will be introduced. Especially, a methodology is proposed in this chapter to model the charging demand of electric vehicles.

Chapter 5: The features of three mainstream methods of probabilistic power flow calculations are introduced and compared through case studies. On the other hand, an improvement is proposed for the cumulant method to deal with the correlation between random system inputs. Moreover, the modelling methodology of electric vehicle charging demand is also verified through case studies in this chapter.

Chapter 6: A heuristic approach to chance-constrained stochastic AC optimal power flow is proposed in this chapter, which is able to deal with non-Gaussian distribution and the possible correlation between system inputs.

Chapter 7: A summary of main contributions is given and possible future research topics are discussed.

CHAPTER 2 ACCELERATED NEWTON-RAPHSON POWER FLOW

2.1 Introduction

In power engineering, the power flow study, also known as load-flow study, is an essential tool involving numerical analysis applied to a power system. AC power flow study usually uses simplified notation of the power system, such as a one-line diagram and the per-unit system, and analyses the power system in normal steady-state operation, which is fundamental to power system planning and operation. Its goal is to determine complete voltage angle and magnitude information for each bus in a power system with specified load, generator real power, voltage, and network conditions. Once this information is known, real and reactive power flow on each branch as well as generator reactive power can be analytically determined. A reasonable solution of the power flow problem is fundamental to the operation of the power system, where the bus voltage magnitudes are kept within a safe range and the power apparatus are working without limit violation. In the planning and expansion of the power system, it is necessary to calculate the power flow solutions under different loading conditions and network configurations.

Due to the nonlinear nature of the AC power flow problem, numerical methods should be employed to obtain a solution that is within an acceptable tolerance. In this chapter, we will discuss the application of a Newton-like method with the modification of the right-hand-side vector (MRV) to solve the AC power flow problem. As presented in [53]-[59], the MRV Newton-like methods belong to the same category of methods that modify the right-hand-side vector in the correction equations and eliminate the necessity of factorizing the Jacobian

matrix at each iteration. However, these methods differ from each other in how the right-hand-side vector is modified. The MRV Newton-like method proposed in [58] is employed in this chapter. In comparison with the other alternatives in [53]-[57] and [59], it employs a simpler modification on the right-hand-side vector of the correction equations and achieves good convergence. Stemming from this MVR Newton-like method, the Accelerated Newton-Raphson (ANR) power flow algorithm is proposed, where a constant Jacobian matrix is employed and the power mismatch vector in the correction equations is multiplied by a special factor.

2.2 Mathematical Formulation

2.2.1 AC Power Flow Formulation

In the AC power flow problem, the buses in the power grid are generally divided into three categories, i.e. PQ, PV and slack buses. A PQ bus is a bus with given both real and reactive power injection. In reality, it can typically be a substation or a power plant with fixed real and reactive power. A PV bus is a bus with given real power injection and bus voltage magnitude. In reality, it is usually a substation with adjustable reactive compensation devices or a power plant with reactive reserves. A slack bus is a bus with given both bus voltage magnitude and phase angle. In reality, a power plant that has adequate capacity and is responsible for frequency control is often selected as a slack bus.

In the power system, there may be a lot of PQ buses, but PV buses may not be necessary. Moreover, in some circumstances, there could be some bus type conversion between a PQ bus and a PV bus. On the other hand, there should be at least one slack bus in the power system. For simplicity, it is assumed in this study that there is only one slack bus in the power system.

Mathematically, the AC power flow problem is usually formulated as a set of nonlinear algebraic equations. The complex voltage at each bus is formulated in two forms according to the preferred coordinates. If the polar coordinates are employed, the voltage at bus *i* is given as $\dot{V}_i = V_i \angle \theta_i$, then the complex power injection at bus *i* can be calculated by

$$\dot{S}_i = \dot{V}_i \sum_j Y_{ij} \dot{V}_j \tag{2.1}$$

where $\dot{S}_i$ is the complex power injection at bus *i*;

$\dot{V}_i$ is the complex voltage of bus *i*;

$\dot{V}_j$ is the complex voltage of bus *j*;

Y_{ij} is the admittance between bus bus *i* and *j*.

For each bus, the calculated power injection should be equal to its specified value, so both the power mismatches ΔP_i and ΔQ_i at bus *i* should be 0, i.e.

$$\Delta P_i = P_{g,i} - P_{d,i} - V_i \sum_j V_j [G_{ij} \cos(\theta_i - \theta_j) + B_{ij} \sin(\theta_i - \theta_j)] = 0 \tag{2.2}$$

$$\Delta Q_i = Q_{g,i} - Q_{d,i} - V_i \sum_j V_j [G_{ij} \sin(\theta_i - \theta_j) - B_{ij} \cos(\theta_i - \theta_j)] = 0 \tag{2.3}$$

where $P_{g,i}$ is the specified real generation injected into bus *i*

$P_{d,i}$ is the specified real load drawn from bus *i*

$Q_{g,i}$ is the specified reactive generation injected at bus *i*

$Q_{d,i}$ is the specified reactive load drawn from bus *i*

G_{ij} is the conductance between bus *i* and *j*, i.e. the real part of Y_{ij}

B_{ij} is the susceptance between bus *i* and *j*, i.e. the imaginary part of Y_{ij}

Equations (2.2) and (2.3) are the well-known power balance equations. Note that, the power mismatches of the slack bus are not included in either Equation (2.2) or (2.3), and the reactive power mismatches of PV buses are not included in Equation (2.3).

2.2.2 Accelerated Newton-Raphson Power Flow

The non-linear power balance equations in Equations (2.2) and (2.3) can be generally represented as the following nonlinear equations

$$\boldsymbol{F}(\boldsymbol{x}) = \boldsymbol{0} \tag{2.4}$$

where $\boldsymbol{F}(\boldsymbol{x})$ is the power mismatch vector $[\Delta\boldsymbol{P},\Delta\boldsymbol{Q}]^{\mathrm{T}}$ and $\boldsymbol{x}$ is the voltage vector $[\boldsymbol{\theta},\boldsymbol{V}]^{\mathrm{T}}$.

According to the conventional Newton's method, the correction equations for Equation (2.4) in the *k*-th iteration can be represented as follows

$$\boldsymbol{F}'(\boldsymbol{x}^{(k)})\Delta\boldsymbol{x}^{(k)} = \left.\frac{\partial \boldsymbol{F}(\boldsymbol{x})}{\partial \boldsymbol{x}}\right|_{\boldsymbol{x}=\boldsymbol{x}^{(k)}} \Delta\boldsymbol{x}^{(k)} = -\boldsymbol{F}(\boldsymbol{x}^{(k)}) \tag{2.5}$$

$$\boldsymbol{x}^{(k+1)} = \boldsymbol{x}^{(k)} + \Delta\boldsymbol{x}^{(k)} \tag{2.6}$$

where $\boldsymbol{F}'(\boldsymbol{x}^{(k)})$ is so called the Jacobian matrix at the *k*-th iteration

$\Delta\boldsymbol{x}^{(k)}$ is the voltage correction vector after the *k*-th iteration

$\boldsymbol{F}(\boldsymbol{x}^{(k)})$ is the power mismatch vector at the *k*-th iteration

In the AC power flow problem, the solution approach as Equations (2.5) and (2.6) is the well-known Newton-Raphson (NR) power flow. Although such an approach demonstrates local quadratic convergence characteristics, it's time consuming to update and factorize the Jacobian matrix $\boldsymbol{F}'(\boldsymbol{x}^{(k)})$ at each iteration, i.e. to solve the linear equations in Equation (2.5).

Therefore, an alternative scheme is to fix the Jacobian matrix in the Newton's method by replacing $\boldsymbol{F}'(\boldsymbol{x}^{(k)})$ in Equation (2.5). If the constant $\boldsymbol{F}'(\boldsymbol{x}^{(0)})$ corresponding to the initial voltage values is employed, then we have

$$\boldsymbol{F}'(\boldsymbol{x}^{(0)})\Delta\boldsymbol{x}^{(k)} = -\boldsymbol{F}(\boldsymbol{x}^{(k)}) \tag{2.7}$$

$$\boldsymbol{x}^{(k+1)} = \boldsymbol{x}^{(k)} + \Delta\boldsymbol{x}^{(k)} \tag{2.8}$$

In the AC power flow problem, the modification in Equations (2.7) and (2.8) is known as the fixed Newton-Raphson (FNR) power flow, which greatly reduces the computation burden because $\boldsymbol{F}'(\boldsymbol{x}^{(0)})$ is only factorized once at the beginning of the iterations. However, an obvious drawback of this replacement would be its unsatisfactory convergence characteristics, especially when only poor initial voltage values $\boldsymbol{x}^{(0)}$ are available.

In order to utilize the fixed Jacobian matrix in power flow calculations while retaining better convergence characteristics at the same time, the Newton-like method proposed in [58] that modifies the right vector $-\boldsymbol{F}(\boldsymbol{x}^{(k)})$ can be employed:

$$\boldsymbol{F}'(\boldsymbol{x}^{(0)})\Delta\boldsymbol{x}^{(k)} = -\alpha_k \boldsymbol{F}(\boldsymbol{x}^{(k)}) \tag{2.9}$$

$$\boldsymbol{x}^{(k+1)} = \boldsymbol{x}^{(k)} + \Delta\boldsymbol{x}^{(k)} \tag{2.10}$$

where the parameter $\alpha_k > 0$.

Equations (2.9) and (2.10) give the basic formulation of the ANR power flow. Note that, when $\alpha_k \equiv 1$, it becomes the iterative format of the FNR power flow as Equations (2.7) and (2.8).

The key to the ANR power flow is how to select a proper value for the parameter α_k, which will be addressed in Section 3.3.2.

2.3 Algorithm Analysis

2.3.1 Proof of Convergence Characteristics

The local convergence characteristics of the ANR power flow in Equations (2.9) and (2.10) can be proved as follows:

Lemma 1 [123]: Let $\boldsymbol{F}$: $R^n \rightarrow R^n$ is continuously differentiable in the neighbourhood of $\boldsymbol{x}^* \in R^n$. Then for any $r > 0$, there exists $\delta > 0$ such that

$$\left\|\boldsymbol{F}(\boldsymbol{x}) - \boldsymbol{F}(\boldsymbol{x}^*) - \boldsymbol{F}'(\boldsymbol{x}^*)(\boldsymbol{x} - \boldsymbol{x}^*)\right\| \le r\left\|\boldsymbol{x} - \boldsymbol{x}^*\right\| \tag{2.11}$$

when $\|\boldsymbol{x} - \boldsymbol{x}^*\| < \delta$.

Note that, $\|\cdot\|$ denotes the 2-norm, i.e. for a vector $\boldsymbol{z} = (z_1, z_2, \ldots, z_n)$,

$$\|\boldsymbol{z}\| = \sqrt{z_1^2 + z_2^2 + \cdots + z_n^2} \tag{2.12}$$

and for a matrix $\boldsymbol{A}$,

$$\|\boldsymbol{A}\| = \max_{\|\boldsymbol{x}\|=1} \|\boldsymbol{A}\boldsymbol{x}\| = \sqrt{\lambda_{\max}} \tag{2.13}$$

where $\lambda_{\max}$ is the largest values of λ such that $\boldsymbol{A}^*\boldsymbol{A} - \lambda\boldsymbol{I} = 0$ ($\boldsymbol{A}^*$ is the conjugate transpose of $\boldsymbol{A}$ and $\boldsymbol{I}$ is the identity matrix).

Lemma 2 [124]: Let $\boldsymbol{M}, \boldsymbol{N} \in R^{n\times n}$. If $\boldsymbol{M}$ is non-singular and

$$\left\| \boldsymbol{M}^{-1}(\boldsymbol{M}-\boldsymbol{N}) \right\| < 1 \tag{2.14}$$

then $\boldsymbol{N}$ is non-singular as well and

$$\left\| \boldsymbol{N}^{-1} \right\| < \frac{\left\| \boldsymbol{M}^{-1} \right\|}{1-\left\| \boldsymbol{M}^{-1}(\boldsymbol{N}-\boldsymbol{M}) \right\|} \tag{2.15}$$

Theorem 3 [58]: Let $\boldsymbol{x}^* \in R^n$ be a zero point of $\boldsymbol{F}$: $R^n \rightarrow R^n$, i.e. $\boldsymbol{F}(\boldsymbol{x}^*) = 0$. Assume that $\boldsymbol{F}'(\boldsymbol{x})$ is continuous in the neighbourhood of $\boldsymbol{x}^*$, $\boldsymbol{F}'(\boldsymbol{x}^*)$ is non-singular, and $\boldsymbol{x}^0$ is sufficiently close to $\boldsymbol{x}^*$. Then there exists $\{\alpha_k > 0\}$ such that the sequence $\{\boldsymbol{x}^{(k)}\}$ generated by Equations (2.9) and (2.10) with α_k at least linearly converges to $\boldsymbol{x}^*$. That is, there exists $0 < r < 1$ such that

$$\left\| \boldsymbol{x}^{(k+1)} - \boldsymbol{x}^* \right\| \le r \left\| \boldsymbol{x}^{(k)} - \boldsymbol{x}^* \right\| \tag{2.16}$$

for all $k = 0, 1, \ldots$.

Proof: According to Equation (2.9),

$$\begin{aligned}
&\boldsymbol{x}^{(k+1)} - \boldsymbol{x}^* \\
&= \boldsymbol{x}^{(k)} - \alpha_k \boldsymbol{J}_0^{-1} \boldsymbol{F}(\boldsymbol{x}^{(k)}) - \boldsymbol{x}^* \\
&= \alpha_k \boldsymbol{J}_0^{-1} \cdot \left[\alpha_k^{-1} \boldsymbol{J}_0 (\boldsymbol{x}^{(k)} - \boldsymbol{x}^*) - \boldsymbol{F}(\boldsymbol{x}^{(k)}) + \boldsymbol{F}(\boldsymbol{x}^*) \right] \\
&= \alpha_k \boldsymbol{J}_0^{-1} \cdot \{ [\alpha_k^{-1} \boldsymbol{J}_0 - \boldsymbol{F}'(\boldsymbol{x}^*)](\boldsymbol{x}^{(k)} - \boldsymbol{x}^*) \\
&\quad - [\boldsymbol{F}(\boldsymbol{x}^{(k)}) - \boldsymbol{F}(\boldsymbol{x}^*) - \boldsymbol{F}'(\boldsymbol{x}^*)(\boldsymbol{x}^{(k)} - \boldsymbol{x}^*)] \}
\end{aligned} \tag{2.17}$$

where $\boldsymbol{J}_0 = \boldsymbol{F}'(\boldsymbol{x}^{(0)})$. Then

$$
\begin{aligned}
&\left\|\boldsymbol{x}^{(k+1)}-\boldsymbol{x}^{*}\right\| \\
&\le\left\|\alpha_k \boldsymbol{J}_0^{-1}\right\| \cdot\left\|[\alpha_k^{-1} \boldsymbol{J}_0-\boldsymbol{F}'(\boldsymbol{x}^{*})](\boldsymbol{x}^{(k)}-\boldsymbol{x}^{*})\right. \\
&\quad\left.-[\boldsymbol{F}(\boldsymbol{x}^{(k)})-\boldsymbol{F}(\boldsymbol{x}^{*})-\boldsymbol{F}'(\boldsymbol{x}^{*})(\boldsymbol{x}^{(k)}-\boldsymbol{x}^{*})]\right\| \\
&\le\left\|\alpha_k \boldsymbol{J}_0^{-1}\right\| \cdot\left\|\alpha_k^{-1} \boldsymbol{J}_0-\boldsymbol{F}'(\boldsymbol{x}^{*})\right\| \cdot\left\|\boldsymbol{x}^{(k)}-\boldsymbol{x}^{*}\right\| \\
&\quad+\left\|\alpha_k \boldsymbol{J}_0^{-1}\right\| \cdot\left\|\boldsymbol{F}(\boldsymbol{x}^{(k)})-\boldsymbol{F}(\boldsymbol{x}^{*})-\boldsymbol{F}'(\boldsymbol{x}^{*})(\boldsymbol{x}^{(k)}-\boldsymbol{x}^{*})\right\|
\end{aligned}
\tag{2.18}
$$

Based on the assumptions of *Theorem* 2 and applying *Lemma* 1, the following holds:

$$
\left\|\boldsymbol{F}(\boldsymbol{x}^{(k)})-\boldsymbol{F}(\boldsymbol{x}^{*})-\boldsymbol{F}'(\boldsymbol{x}^{*})(\boldsymbol{x}^{(k)}-\boldsymbol{x}^{*})\right\| \le r_1\left\|\boldsymbol{x}^{(k)}-\boldsymbol{x}^{*}\right\| \tag{2.19}
$$

where $0 < r_1 < 1$.

Adjusting $\{\alpha_k\}$ so that the assumptions of *Theorem* 2 hold yields

$$
\left\|\alpha_k^{-1} \boldsymbol{J}_0-\boldsymbol{F}'(\boldsymbol{x}^{*})\right\| \cdot\left\|\boldsymbol{x}^{(k)}-\boldsymbol{x}^{*}\right\| \le r_2\left\|\boldsymbol{x}^{(k)}-\boldsymbol{x}^{*}\right\| \tag{2.20}
$$

where $0 < r_2 < 1$.

Applying Equations (2.19) and (2.20) to Equation (2.18) yields

$$
\left\|\boldsymbol{x}^{(k+1)}-\boldsymbol{x}^{*}\right\| \le\left\|\alpha_k \boldsymbol{J}_0^{-1}\right\| \cdot\left(r_1+r_2\right) \cdot\left\|\boldsymbol{x}^{(k)}-\boldsymbol{x}^{*}\right\| \tag{2.21}
$$

Let us define

$$
r=\left\|\alpha_k \boldsymbol{J}_0^{-1}\right\| \cdot\left(r_1+r_2\right) \tag{2.22}
$$

Further adjusting α_k such that $r < 1$, we obtain

$$\left\|\boldsymbol{x}^{(k+1)}-\boldsymbol{x}^{*}\right\| \le r\left\|\boldsymbol{x}^{(k)}-\boldsymbol{x}^{*}\right\| \tag{2.23}$$

The theorem proof has been completed.

It will be discussed in the following how to determine the value of α_k.

2.3.2 Determining Optimal Parameter α_k

The value of $\boldsymbol{F}(\boldsymbol{x})$ at $\boldsymbol{x}=\boldsymbol{x}^{(k+1)}$ is approximated by

$$\boldsymbol{F}(\boldsymbol{x}^{(k+1)}) \approx \boldsymbol{F}(x^{(k)}) + \boldsymbol{J}_k \Delta \boldsymbol{x}^{(k)} \tag{2.24}$$

where $\boldsymbol{J}_k = \boldsymbol{F}'(\boldsymbol{x}^{(k)})$.

In the Newton's method, let $\boldsymbol{F}(\boldsymbol{x}^{(k+1)}) = 0$ so $\boldsymbol{F}(x^{(k)}) + \boldsymbol{J}_k \Delta \boldsymbol{x}^{(k)} = 0$ and its correction vector $\Delta \boldsymbol{x}^{(k)} = -\boldsymbol{J}_k^{-1}\boldsymbol{F}(\boldsymbol{x}^{(k)})$ is obtained. According to Equation (2.9), we have

$$\Delta \boldsymbol{x}^{(k)} = -\alpha_k \boldsymbol{J}_0^{-1}\boldsymbol{F}(\boldsymbol{x}^{(k)}) \tag{2.25}$$

Therefore, α_k can be found by solving the following minimization optimization problem:

$$\begin{aligned} \min G(\alpha_k) &= \min \frac{1}{2}\Delta \boldsymbol{F}_{k+1}^{T}\Delta \boldsymbol{F}_{k+1} \\ &= \min \frac{1}{2}\left\|\boldsymbol{F}(\boldsymbol{x}^{(k)}) + \boldsymbol{J}_k \Delta \boldsymbol{x}^{(k)}\right\|^2 \\ &= \min \frac{1}{2}\left\|\boldsymbol{F}(\boldsymbol{x}^{(k)}) + \boldsymbol{J}_k[-\alpha_k \boldsymbol{J}_0^{-1}\boldsymbol{F}(\boldsymbol{x}^{(k)})]\right\|^2 \\ s.t.\ \alpha_k &\ge 0 \end{aligned} \tag{2.26}$$

Let $\boldsymbol{u} = \boldsymbol{F}(\boldsymbol{x}^{(k)})$, $\boldsymbol{v} = \boldsymbol{J}_0^{-1}\boldsymbol{u}$, $\boldsymbol{w} = \boldsymbol{J}_k\boldsymbol{v}$, then

$$\min G(\alpha_k) = \min \frac{1}{2}\left\|\boldsymbol{u} - \alpha_k \boldsymbol{w}\right\|^2 \quad s.t.\ \alpha_k \geq 0 \tag{2.27}$$

The exact solution of the quadratic optimization problem in Equation (2.27) can be found as follows [125]

$$\alpha_k^{\text{opt}} = \langle \boldsymbol{u}, \boldsymbol{w} \rangle / \langle \boldsymbol{w}, \boldsymbol{w} \rangle \tag{2.28}$$

It should be pointed out that the inversion of $\boldsymbol{J}_0$ is not necessary because $\boldsymbol{v}$ can be solved by $\boldsymbol{J}_0$ $\boldsymbol{v} = \boldsymbol{u}$ according to Equation (2.9) and the constant $\boldsymbol{J}_0$ is only factorized once. On the other hand, $\boldsymbol{J}_k$ is still needed in order to obtain α_k, but its factorization is not necessary.

Once the optimal factor α_k^{opt} is obtained, the correction vector $\Delta\boldsymbol{x}^{(k)}$ can be solved by forward and backward substitution in Equation (2.9):

$$\boldsymbol{J}_0 \Delta\boldsymbol{x}^{(k)} = -\alpha_k^{\text{opt}} \boldsymbol{u} \tag{2.29}$$

Furthermore, because $\boldsymbol{v}$ is a by-product of calculating α_k^{opt} according to Equation (2.28), Equation (2.25) can be simplified as

$$\Delta\boldsymbol{x}^{(k)} = -\alpha_k^{\text{opt}} \boldsymbol{v} \tag{2.30}$$

2.3.3 Computational Complexity

According to Equations (2.25)-(2.30), the computation time required for the ANR power flow calculations mainly consists of 1 sparse LU decomposition of $\boldsymbol{J}_0$, k sparse forward-backward substitutions for calculating $\boldsymbol{v}$, k sparse matrix-vector multiplications for calculating $\boldsymbol{w}$ and $2k$

vector-vector multiplications for calculating α_k^{opt}, where k denotes the total number of iterations for convergence.

The ANR power flow mainly benefits from the fact that the repeated factorization of $\boldsymbol{J}_k$ is avoided, whose computational complexity depends on the non-zero elements in $\boldsymbol{J}_k$. Moreover, the factor α_k is introduced to guarantee at least local linear convergence characteristics so that the total iteration count will not increase significantly.

If the reactive generation limit should be enforced at a PV bus, it is necessary to update the factor table of $\boldsymbol{J}_0$ when PV-PQ bus type conversion occurs. Evidently, this could lead to efficiency deterioration if bus type conversion occurs frequently during the ANR power flow calculations.

In order to deal with this, partial matrix refactorization and the large diagonal strategy (LDS) presented in [126]-[127] can be employed to reduce the computational effort:

1. The row and column in $\boldsymbol{J}_0$ corresponding to the reactive power injection at every PV bus are also formed and their diagonal elements are multiplied by a very large constant value K so that the off-diagonal elements are masked out. However, if K is too large it may cause unacceptable numerical errors, but too small a value cannot mask out the effects of the off-diagonal elements. In this chapter, K is chosen as 10^8 after several heuristic trials and pivot selection is employed to reduce the numerical errors.
2. If a PV bus is changed to a PQ bus, its diagonal element of the corresponding row or column in $\boldsymbol{J}_0$ is reset to its original value. Then partial matrix refactorization is used to update the factor table of $\boldsymbol{J}_0$.

3. If a PQ bus is reversed back to a PV bus, its diagonal element of the corresponding row or column in $\boldsymbol{J}_0$ is multiplied by K again. Then partial matrix refactorization is applied again to update the factor table of $\boldsymbol{J}_0$.

Because partial matrix refactorization requires much less time than rebuilding the whole factor table from scratch, the computational burden resulting from bus type conversion can be significantly reduced.

2.3.4 Flowchart of ANR Power Flow

A basic flowchart of the ANR power flow is given in Figure 2-1, where ε denotes the convergence tolerance, k is the total iteration count and $N_{\max}$ is the allowed maximum iteration count.

It should be noted that, because $\boldsymbol{F}'(\boldsymbol{x}^{(0)})$ is factorized before the first iteration starts and for the sake of simplicity, the factor in first iteration, i.e. α_0 is set to 1, though it is reported in [58] that this might not be the best choice. This actually makes the first iteration of the ANR power flow equivalent to that of the conventional NR power flow.

When the reactive generation limits at PV buses should be enforced, a check of limit violation and bus type adjustment should be added before calculating bus reactive power injections in each iteration step, and partial matrix refactorization should be applied when bus type conversion occurs.

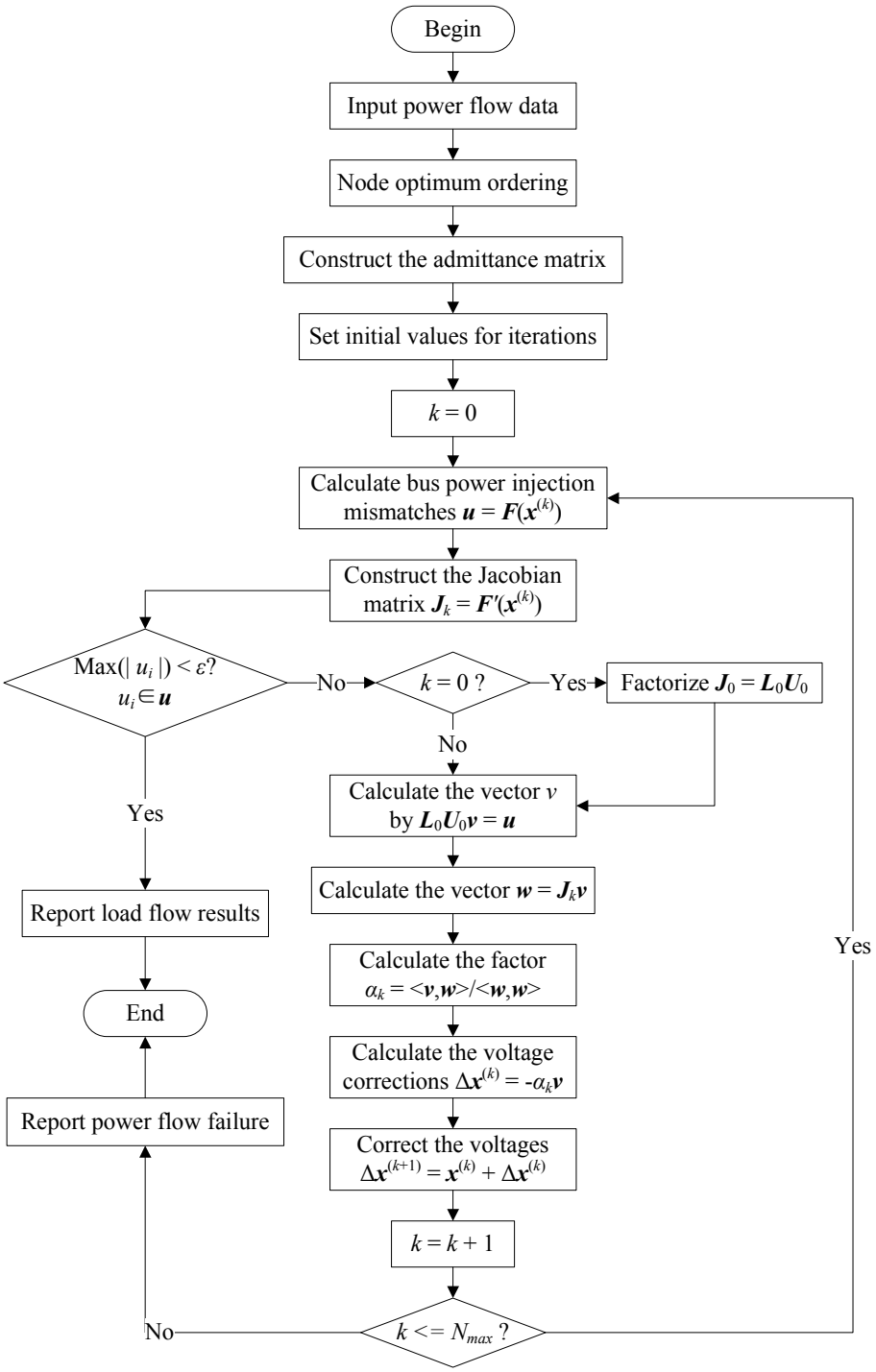

Figure 2-1 Flowchart of the ANR power flow calculations

2.4 Case Studies

In this section, the ANR power flow is compared with the NR power flow and the FNR power

flow on several systems of different sizes. Moreover, because the Jacobian matrix can be fixed from different iteration steps, three schemes for the ANR power flow are tested in this section:

1. ANR^0: The ANR iteration is used throughout the whole power flow calculations.
2. ANR^1: The ANR iteration follows the first conventional NR iteration.
3. ANR^2: The ANR iteration follows the first two conventional NR iterations.

For the sake of comparison, the FNR power flow is also modified to fix the Jacobian matrix after 1 or 2 conventional Newton iterations, the corresponding schemes are denoted as FNR^1 and FNR^2, which are corresponding to $ANR^1$and ANR^2, respectively.

The test systems include the IEEE 118-bus system, the IEEE 300-bus system and two large power systems: the Northwest China transmission grid (1145 buses, 1563 branches, 121 generators and 192 loads) and the East China transmission grid (3141 buses, 4240 branches, 425 generators and 931 loads) respectively. For thorough comparisons, different loading levels are considered here. Flat start is employed in all the tests.

All the test programmes are written in C++ using the Boost.uBLAS library [128] (for sparse matrix storage), the KLU library [129] (for solving the linear equations), and the Boost.Timer [130] library (for measuring the CPU time) and run on a desktop PC with a 2.53GHz Core 2 Duo CPU and 2GB DDR2-800 RAM.

If converged, the solutions of different power flow methods are of the same accuracy for every test system. Table 2-1 shows the total iteration time and the total iteration counts of these different power flow methods under normal loading conditions. It should be noted that the total iteration time of the FNR or ANR power flow is expressed in percentage of that of

the NR power flow in all the following tables.

Table 2-1 Comparison of Power Flow Methods (Tolerance = 1e-6p.u., Load Level = 100%)

(a) Total Iteration Count

Bus Number	Iteration Count					
	NR	FNR^1	FNR^2	ANR^0	ANR^1	ANR^2
118	4	11	5	4	4	4
300	5	18	12	15	9	7
1145	6	×	27	20	11	8
3141	8	×	49	24	17	12

(b) Total Iteration Time

Bus Number	Iteration Time (100%)					
	NR	FNR^1	FNR^2	ANR^0	ANR^1	ANR^2
118	1	0.2209	0.3328	0.9712	0.9107	1.0120
300	1	0.3238	0.4009	0.6240	0.7198	0.7723
1145	1	×	0.3187	0.4123	0.4596	0.5543
3141	1	×	0.7843	0.5105	0.4876	0.5207

It can be clearly seen in the above tables that although the NR power flow achieves the solution with requite accuracy in less number of iterations than the other methods, it takes longer time. It is because the convergence progress achieves by a single iteration of the NR power flow is greater, but it takes more time. The advantage of the ANR power flow in time efficiency becomes more and more apparent as the system scale grows: the ANR power flow is about 1.8–2.4 times as fast as the NR power flow. For the FNR power flow, the FNR^1 scheme failed to converge on large systems while the FNR^2 scheme gradually lost its advantage in efficiency due to the increase of its total iteration number. It should be pointed out that the 3141-bus system includes a large amount of branches with high R/X ratios. This deteriorates the convergence of the FNR power flow, because the constant Jacobian matrix is sensitive to the R/X ratio of network branches. In contrast, the ANR power flow seems to be less influenced by the R/X ratio of the branches because the introduction of the factor α_k

ensures its convergence.

Table 2-2 shows the total iteration time and the total iteration counts under heavier loading levels.

Table 2-2 Comparison of Power Flow Methods (Tolerance = 1e-6p.u., Load level = 140%)

(a) Total Iteration Count

Bus Number	Iteration Count					
	NR	FNR^1	FNR^2	ANR^0	ANR^1	ANR^2
118	5	13	6	6	5	5
300	7	94	46	52	26	18
1145	9	×	34	×	16	12
3141	11	×	×	×	24	18

(b) Total Iteration Time

Bus Number	Iteration Time (100%)					
	NR	FNR^1	FNR^2	ANR^0	ANR^1	ANR^2
118	1	0.2222	0.3457	0.9728	0.9133	0.9908
300	1	0.7196	0.6649	0.9501	0.7133	0.4958
1145	1	×	0.3568	×	0.3673	0.4378
3141	1	×	×	×	0.4040	0.4113

A similar situation can be observed in Table 2-2 except that the ANR^0 scheme failed to converge this time, which means that $\boldsymbol{F}'(\boldsymbol{x}^{(0)})$ might not be a suitable choice under a heavy load level where only flat start is available. For the ANR^1 and ANR^2 schemes, as stressed loading levels involve more iteration counts, the efficiency advantage also becomes more apparent. Moreover, it should be pointed out that for the IEEE 300-bus system, a loading level of 140% is already very close to its maximum loading point. In this situation, the FNR power flow required much more iterations than the others to converge; for 3141-bus system, even the FNR^2 scheme failed to converge, which indicates the influence of high R/X ratios of branches again on the convergence.

Further tests are presented with the situation of PV-PQ bus conversion. The type conversion of each bus is limited within twice during the power flow calculations and the results are shown in Table 2-3.

Table 2-3 Comparison of Power Flow Methods with Bus Type Conversion
(Tolerance = 1e-6p.u., Load level = 100%)

(a) Total Iteration Count

Bus Number	PV to PQ Bus Number	Iteration Count					
		NR	FNR^1	FNR^2	ANR^0	ANR^1	ANR^2
118	6	8	22	10	13	11	9
300	23	14	×	55	58	42	24
1145	8	11	×	53	27	16	13
3141	13	12	×	×	×	21	16

(b) Total Iteration Time

Bus Number	Iteration Time (100%)					
	NR	FNR^1	FNR^2	ANR^0	ANR^1	ANR^2
118	1	0.2548	0.3502	0.7076	0.5926	0.6788
300	1	×	0.6689	0.6628	0.5934	0.4817
1145	1	×	0.3940	0.2935	0.2844	0.3540
3141	1	×	×	×	0.4369	0.4306

As shown in Table 2-3, all the iteration counts increase due to the occurrence of bus type conversion, and even some divergence are caused. Because an ANR iteration is much faster than an NR iteration, and the partial matrix refactorization reduces the computation burden when bus type conversion occurs, the efficiency becomes better again: the ANR power flow is about 1.4–3.5 times as fast as the NR power flow. However, frequent bus type conversion also deteriorates the convergence of both the FNR and ANR power flow, and the former seems to suffer more severely.

The sensitivity of the ANR power flow with respect to different loading levels was tested on the 1145-bus system in comparison to the NR power flow, where the load level is gradually

increased close to its maximum loading level of about 189%. The results are listed in Table 2-4:

Table 2-4 Comparison of Power Flow Methods under Different Loading Levels (Tolerance = 1e-6p.u.)

(a) Total Iteration Count

Load Level	Iteration Count			
	NR	FNR^2	ANR^1	ANR^2
1.50	9	42	16	12
1.55	9	43	16	12
1.60	9	44	19	13
1.65	10	46	20	15
1.70	10	48	22	17
1.75	11	50	25	17
1.80	11	55	28	19
1.85	12	68	35	21

(b) Total Iteration Time

Load Level	Iteration Time (100%)			
	NR	FNR^2	ANR^1	ANR^2
1.50	1	0.3941	0.3680	0.4387
1.55	1	0.4012	0.3677	0.4393
1.60	1	0.4128	0.3721	0.4401
1.65	1	0.4199	0.3739	0.4498
1.70	1	0.4285	0.3880	0.4556
1.75	1	0.4345	0.4101	0.4547
1.80	1	0.4501	0.4259	0.4623
1.85	1	0.5117	0.4407	0.4755

The FNR^1 or the ANR^0 scheme is not listed above because of their unsatisfactory convergence in this test, which means $\boldsymbol{F'}(\boldsymbol{x}^{(0)})$ is not a good choice for a heavily loaded large system. It can be seen that as the loading level gradually approaches near the maximum loading point, all the iteration counts increase correspondingly. But it can be found that the NR power flow is not as sensitive to the loading conditions as that of the ANR or FNR power flow is. This is because the former has a local quadratic convergence characteristic.

Nevertheless, the convergence of the ANR power flow is still satisfactory even under very heavy loading conditions and its total iteration time is not only much less than that of the NR power flow, but also as competitive as that of the FNR^2 scheme.

In order to intuitively illustrate the convergence characteristics of the ANR power flow, the bus power mismatch at each iteration of the IEEE 118-bus system under a loading level of 300% is drawn in Figure 2-2.

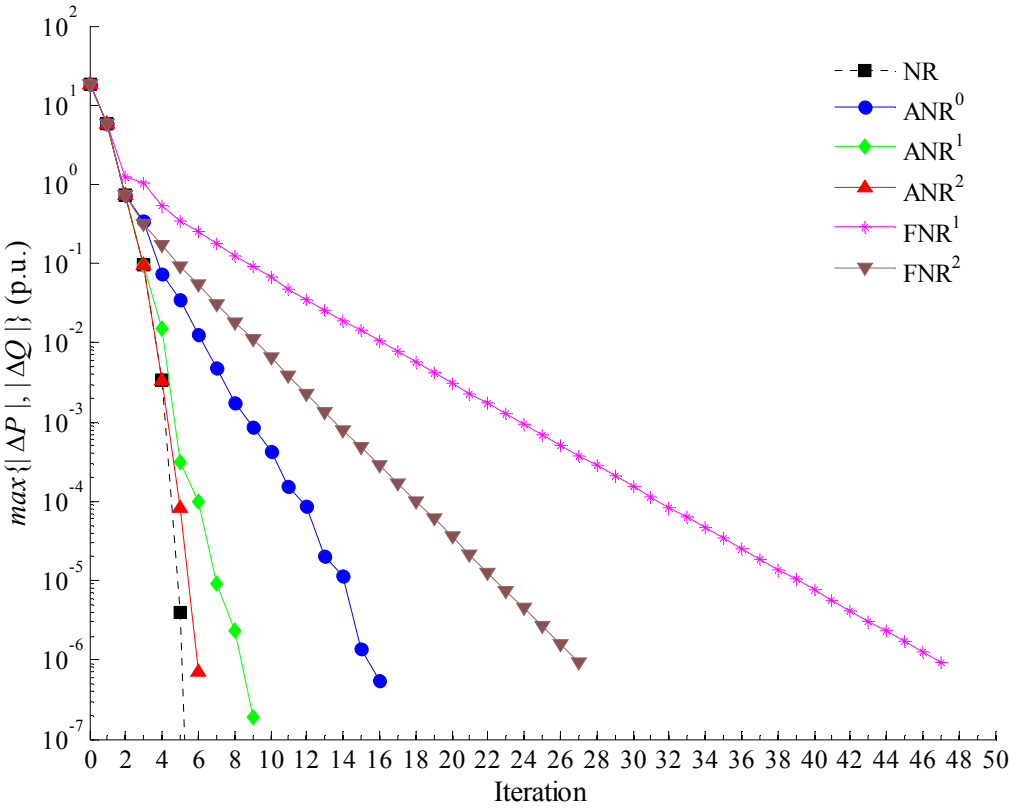

Figure 2-2 Bus power mismatches on the IEEE 118-bus system under loading level 300%

The super-linear convergence characteristics of the ANR power flow are clearly depicted in the above figure, in contrast to the linear convergence characteristics of the FNR power flow.

Moreover, it may be meaningful to show the sensitivity of the ANR power flow with respect to the convergence tolerance. Such a test was carried out on the 3141-bus system by gradually tightening the convergence tolerance and the results are given in Table 2-5:

Table 2-5 Comparison of Power Flow Methods with Different Convergence Tolerance (Load level = 100%)

(a) Total Iteration Count

Tolerance (p.u.)	Iteration Count				
	NR	FNR^2	ANR^0	ANR^1	ANR^2
1e-5	7	34	24	15	11
1e-6	8	49	24	17	12
1e-7	8	65	27	19	12
1e-8	8	79	30	21	14

(b) Total Iteration Time

Tolerance (p.u.)	Iteration Time (100%)				
	NR	FNR^2	ANR^0	ANR^1	ANR^2
1e-5	1	0.5993	0.5719	0.5160	0.5639
1e-6	1	0.7849	0.5101	0.4876	0.5196
1e-7	1	0.8752	0.5557	0.5190	0.5194
1e-8	1	0.9634	0.6037	0.5508	0.5514

Just like the FNR power flow, the ANR power flow is more sensitive to the tolerance than the NR power flow as its iteration counts increase as the tolerance becomes tighter. However, in terms of the total iteration time, the ANR power flow has a relatively stable advantage over the NR power flow, while the FNR^2 scheme lost its advantage due to the rapid increase in its total iteration counts.

Moreover, among the three ANR schemes, it should also be noted that the ANR^0 scheme needs more time than the other two ANR schemes. This is because constant $\boldsymbol{F'}(\boldsymbol{x}^{(0)})$ represents a relatively poor approximation of the actual Jacobian matrix in Equation (2.9), hence such a scheme involves more iterations.

In order to further verify the robustness of the ANR power flow on more operating points, N-1 verification has been done on the IEEE 118-bus system and the 3141-bus system under a heavy loading level (but islanding cases are excluded). The results are given in Table 2-6 and Table 2-7. Note that, the FNR power flow or the ANR^0 scheme is not listed because of their failure in a large number of cases.

Table 2-6 N-1 Verification on the IEEE 118-Bus System
(Total Case = 177, Loading Level = 300%, Tolerance = 1e-6p.u.)

Method	Converged Case	Average Iteration	Minimum Iteration	Maximum Iteration
NR	157	7.00	6	9
ANR^1	157	17.18	9	19
ANR^2	157	10.24	6	13

Table 2-7 N-1 Verification on the 3141-Bus System
(Total Case = 2404, Loading Level = 150%, Tolerance = 1e-6p.u.)

Method	Converged Case	Average Iteration	Minimum Iteration	Maximum Iteration
NR	2380	10.45	7	12
ANR^1	2353	28.48	22	50
ANR^2	2380	18.15	17	22

It should be noted that the average iteration is obtained through dividing the sum of iteration counts in all converged cases by the number of these cases, which reflects an overall convergence performance of the power flow methods.

As shown above, under a heavy load level, the ANR power flow, especially the ANR^2 scheme, performs as well as the NR power flow does with respect to the convergence. Therefore, the ANR^1 and ANR^2 schemes are at least as reliable as the NR power flow.

On the other hand, it has been observed that the variation of α_k in Equation (2.30) during the ANR iterations tends to show different characteristics, depending on whether the ANR power

flow is able to converge or not.

For example, as shown in Figure 2-3, the variation of α_k tends to be a nearly undamped oscillation around 1.0 when the ANR power flow converges, while it tends to be a dying oscillation finally decreases to nearly 0 after a few iterations when the ANR power flow fails to converge. Therefore, by monitoring the value of α_k, we can detect the convergence of the ANR power flow during its iteration process.

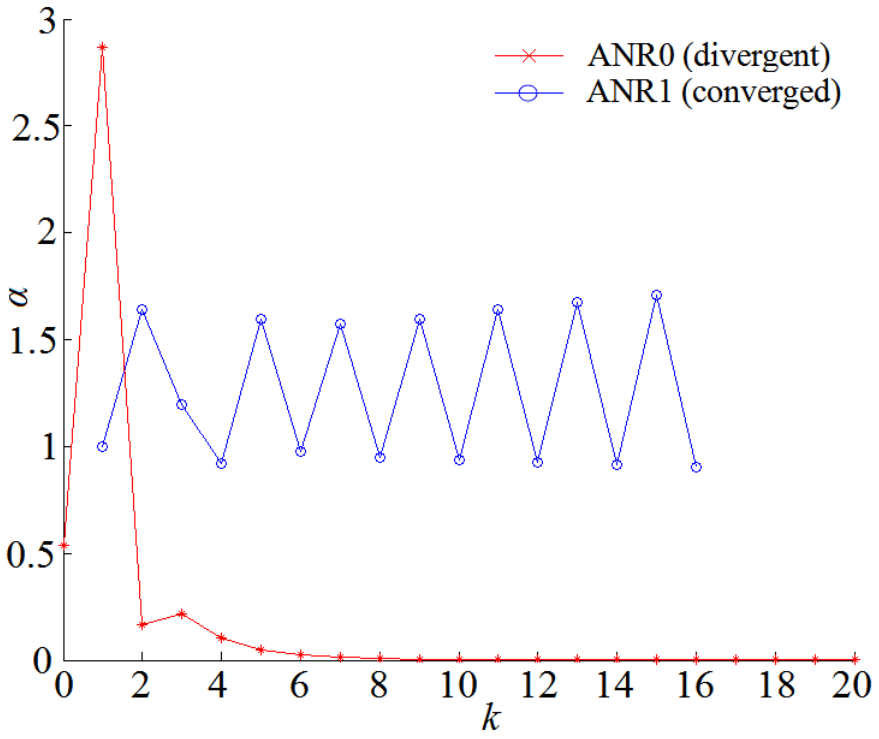

Figure 2-3 The value of α_k during the ANR iterations on the 1145-bus system (loading level=150%)

As stated before, α_0 for the first ANR iteration is set to be 1 for the sake of simplicity. However, it has been pointed out in [58] that $\alpha_0 = 1$ may not be the best choice.

For example, Figure 2-4 shows the relationships between α_0 and the iteration counts for the ANR[1] scheme on two test systems.

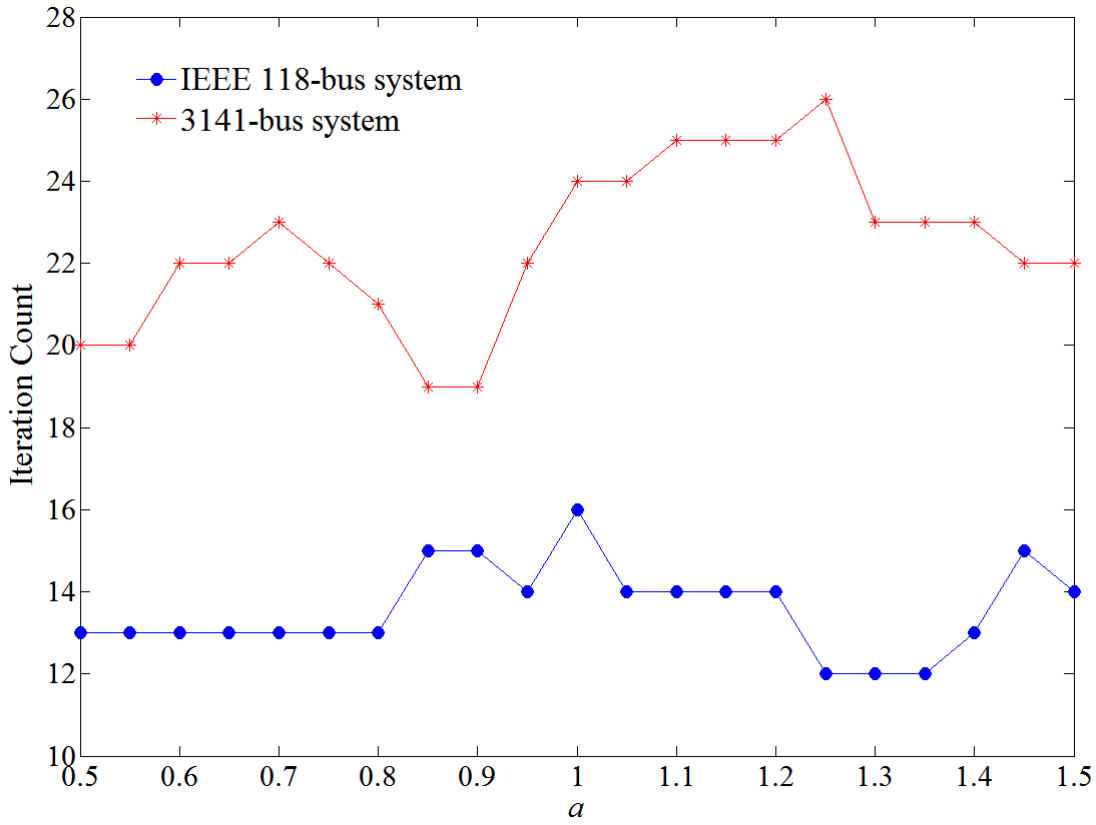

Figure 2-4 The ANR[1] iteration counts with different α_0 values on the IEEE 118-bus system (loading level: 300%) and on the 3141-bus system (loading level: 150%)

It can be seen that the total iteration count varies as the initial value of α_0 changes. It has been noticed that the number of iterations is not the minimal when $\alpha_0 = 1$. However, there seems to be no universal scheme at present to select the best value for α_0 for all the test systems. This is due to the irregular variation patterns of the iterations using different values of α_0 as shown in Figure 2-4.

2.5 Chapter Summary

In this chapter, the possibility of solving the AC power flow problem by the MRV Newton-like methods has been investigated. Based on this, the ANR power flow algorithm has been

proposed, where the constant Jacobian matrix is employed and the power mismatch vector is multiplied by a special factor.

In case studies, the ANR power flow shows super-linear convergence characteristics and achieves an advantage in time efficiency up to about 50% over the conventional NR power flow.

On the other hand, numerical results have indicated that it would be better to introduce the ANR iterations after at least one or two conventional NR iterations if only a poor start is available or under a heavy loading condition.

Another feature of the ANR power flow is that its convergence can be detected by monitoring the value of the factor α_k. In addition, the start value of α, i.e. α_0 for the first ANR iteration, is usually set to 1 for the sake of simplicity. However, this might not be the best choice. How to select the start value of α should be further researched.

CHAPTER 3 PROBABILITY MODELS OF UNCERTAINTIES IN POWER SYSTEMS

3.1 Introduction

In deterministic analysis of power systems, system inputs such as substation feeder loads and power plant generation are generally expressed as constant values. However, there are uncertain factors, such as sudden variation of loads, fluctuation of renewable generation, unexpected system component fault and so on, which could incessantly influence the operation of power systems. In order to incorporate such uncertainties, deterministic analysis has to deal with the possible combinations of different values of system inputs, but this way is limited by the computational complexity resulting from the system scale.

In contrast to deterministic analysis, stochastic analysis of power systems views uncertain factors as random variables. Compared to constant values and their combination, random variables offer not only numerical information, but also corresponding probability information through its probability distribution, such as possibility of occurrence, variation range, bias proportion, intensive degree and so on.

This chapter introduces the models of uncertain system inputs for stochastic analysis of power systems, which covers conventional loads and generators, as well as fast developing wind farms and newly emerged electric vehicles. Especially, a new methodology of modelling the overall charging demand of electric vehicles is proposed, which takes main factors that determine the charging behaviour of electric vehicles into consideration. Moreover, two

typical charging demand models are established through this methodology, i.e. the electric vehicle charging station and the local resident community respectively.

3.2 Load and Generator

3.2.1 Load

In deterministic analysis, bus loads are generally considered as constant or to scattered in several different levels. However, loads in reality could be influenced by a lot of factors so that they are in essence uncertain over a certain period. For example, from a short-term perspective, weather change and production activity, etc. could lead to unexpected fluctuation of loads; from a long-term perspective, population size, economic situation etc. could affect the accuracy of load forecasting. On the other hand, due to the inherent uncertain errors of measuring and monitoring instruments, loads could be distorted in the system analysis.

If a single load is modelled as a random variable and assumed to be uncorrelated with other loads, then the load on the feeder at a substation is the sum of a large number of uncorrelated random variables. According to the Central Limit Theorem [131], i.e. the sum of a sufficiently large number of uncorrelated random variables approximately obeys the Gaussian distribution. Therefore, a bus load in the stochastic analysis of the power system is generally modelled as a Gaussian random variable.

On the other hand, some bus loads in the power system could be discrete only. In this situation, discrete distributions could be employed to model such loads. Usually these discrete distributions have finite items so if there are more than one discrete load at a certain bus, the distribution of the total loads can be obtained through convolution [132].

3.2.2 Generator

A generator in the power system is not always available due to scheduled maintenance or accidental outage or the operation reasons. Therefore, the Forced Outage Rate (FOR) is introduced into power system analysis to describe the availability of a generator.

If we employ discrete values 0 and 1 to denote the status of a single generator, where 0 means it is not available while 1 means the opposite, then it can be viewed as a random variable of the Bernoulli distribution [133]. That is, FOR is the probability of 0 and 1−FOR is that of 1.

In a power plant, there are usually two or more generators of the same type, so they have the same FOR. Moreover, because each generator can operate individually, it can be assumed that these generators are uncorrelated with each other. Therefore, the power output of a power plant is the sum of several uncorrelated Bernoulli random variables, i.e. the Binomial distribution [133]. Therefore, the bus generation in the stochastic analysis of the power system is generally modelled as a Binomial random variable.

On the other hand, if the FORs of generators are different, the probability distribution of bus generation can be obtained through convolution [132].

3.3 Wind Farm

3.3.1 Power Output of Wind Generator

A wind generator captures the kinetic power of the wind through its wind turbine, conducts wind power to its rotor as mechanical torque and generates electric power. The amount of its power output P is mainly determined by several factors such as air density, wind speed, swept area of blades etc. Their relationship can be given as follows [134]:

$$P = 0.5AC_P\rho v^3 \tag{3.1}$$

where ρ is air density at the installation site;

v is the wind speed at the hub height;

A is the swept area of the blades;

C_p is the power efficiency coefficient.

However, a wind generator only operates within a certain range of wind speed, which is typically defined by its cut-in wind speed v_{ci}, rated wind speed v_r, and cut-off wind speed v_{co}, e.g. as the following figure shows:

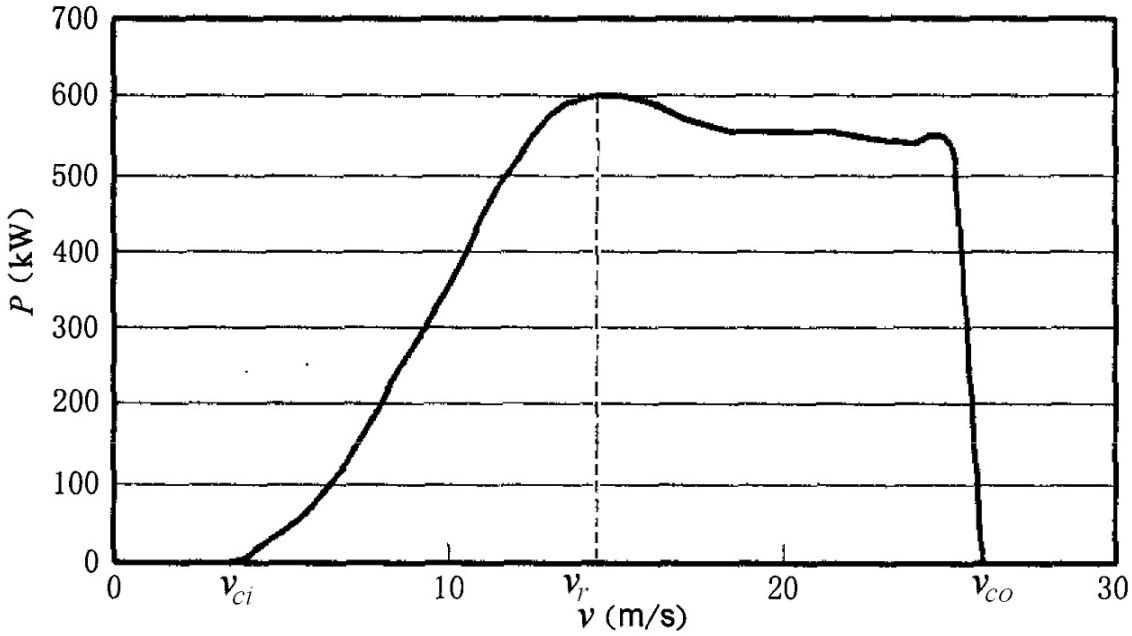

Figure 3-1 Typical power curve of a wind generator

The above figure depicts the power output curve of a typical 600kW rated wind generator with respect to wind speed. This could generally be fitted from the experimental data offered by its manufacturer.

It can be seen that the trapezoidal curve of its real power output P is divided into several segments by wind speed v. Thus, P is also approximately expressed as a piecewise function as follows [135]

$$P = \begin{cases} 0 & (v < v_{ci}, v > v_{co}) \\ \dfrac{v^3 - v_{ci}^3}{v_r^3 - v_{ci}^3} P_r & (v_{ci} \le v < v_r) \\ P_r & (v_r \le v \le v_{co}) \end{cases} \tag{3.2}$$

where P_r is the rated power of the wind generator.

3.3.2 Randomness of Wind Speed

According to Equations (3.1) and (3.2), wind speed directly determines the power output of a wind generator, so it is necessary to study its randomness over a certain period of time. Because topography, orientation, weather, altitude etc. could all influence wind speed at the hub height of a wind turbine, the modelling of wind speed is generally based on statistical analysis.

Different probability distributions have been employed to fit the statistical distribution of wind speed, such as the chi-squared distribution [136], the Rayleigh distribution [137]-[138], the lognormal distribution [139], and the Weibull distribution [139]-[142], among which the Weibull distribution is currently the most widely used.

According to its formulation of the Weibull distribution in Appendix I, its scale parameter λ reflects the mean value of wind speed, while its shape parameter k reflects the shape of wind speed distribution. Under the hypothesis that wind speed obeys the Weibull distribution, these two parameters can be obtained through maximum likelihood estimation [143] according to the measured data at the installation site.

As an example, Figure 3-2 shows the Weibull distribution fitting of yearly wind speed according to the measured data reported in [144], where λ = 7.6085 and k = 1.9108. Accordingly, the mean value of wind speed is 6.7503m/s and its standard variation reaches 3.6765m/s, which indicates a wide variation.

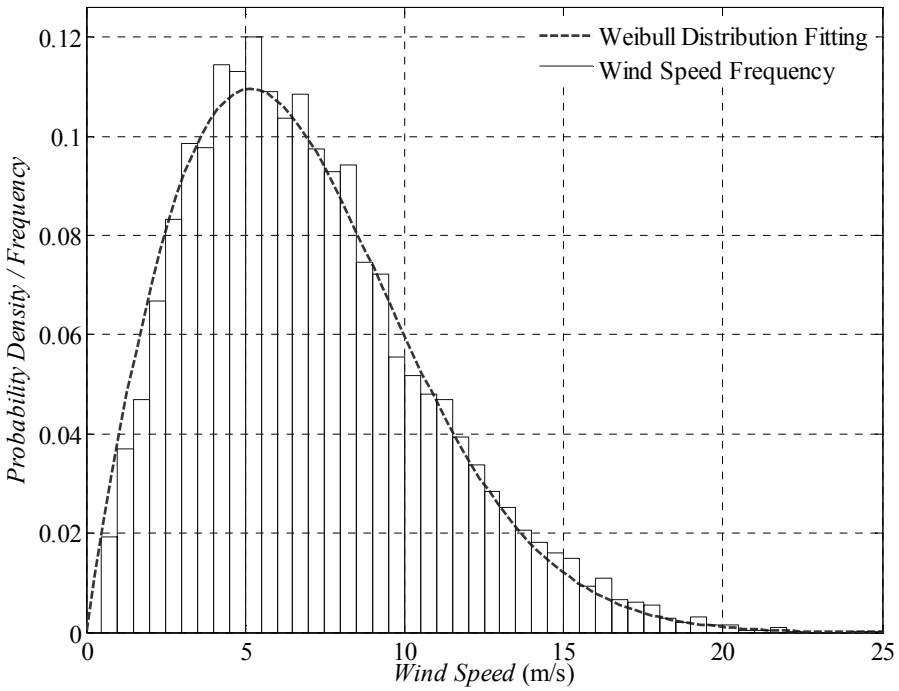

Figure 3-2 Weibull distribution of yearly wind speed

By the way, when the time period of interest is very short, e.g. hourly, it can be assumed that wind speed approximately obeys the Gaussian distribution [145].

3.3.3 Generation of Wind Farm

A wind farm is a group of wind turbine generators installed at the same site onshore or offshore to produce electric power. A large wind farm may consist of several hundred individual wind turbines, and cover an extended area of hundreds of square miles.

Because a wind turbine extracts kinetic energy from the wind, it always casts a wind shade in the downwind direction. As a result, there is a wake behind the wind turbine, i.e. a long trail of wind which is quite turbulent and slowed down, when compared to the wind arriving in the front of the wind turbine. This is the so called wake effect, which is demonstrated as follows:

Figure 3-3 Wake effect demonstration (Source: Riso National Laboratory, Denmark)

In a wind farm, wake effect leads to adverse interaction among wind turbines, where turbulent air flow could damage their machinery construction, and slowed wind speed decreases their electric power production. Therefore, wind turbines in a wind farm have to be spaced in a certain distance to avoid too much turbulent and slow wake. However, the impact of wake effect is still inevitable due to fixed installation layout and varying wind direction [146].

Wake effect results in different operation status of wind turbines, which along with other factors, such as varying wind speed, time-lags and nonlinear wind generators, makes the total power output of the wind farm very complicated [147]-[149]. It is not the purpose of this thesis to model the impact of wake effect, therefore a statistical model described in [150] is employed, where the total power output of a wind farm is assumed to obey the Beta

distribution. Such an assumption is based on the duration curves of some wind farms drawn from the measured data and takes prediction errors into account as well.

The bounded Beta distribution reflects the wind farm power output varying between zero and its rated power, and heuristic data given in [151]-[153] supports this assumption, although this is still an open field for research.

3.4 Electric Vehicle

3.4.1 Main Factors of Electric Vehicle Charging

The charging behaviour of electric vehicles is determined by different factors, such as the number of vehicles being charged, their charging voltage and current levels, power battery start/end status and capacity, and charging time duration etc. All these factors tend to be uncertain if all the electric vehicles within a certain region are considered, so from an overall point of view their total charging demand is uncertain as well.

The following subsections will present a new methodology of modelling the total charging demand of electric vehicles in a certain region. Plug-in hybrid electric vehicles (PHEVs) are chosen during the modelling process, because currently they have the best market prospect and have already achieved a considerable quantity scale.

3.4.2 Charging Demand of Single Electric Vehicle

The energy consumption for charging a PHEV is developed based on the probabilistic model proposed in [79], so that the main factors that determine the PHEV charging behaviour can be taken into consideration, such as its battery capacity, operating status, and daily driving range and so on.

Firstly, in order to describe the operating status of a PHEV, a key parameter k_{EV} is defined as

$$k_{EV} = \frac{E_{Bat}}{E_{Eng} + E_{Bat}} \tag{3.3}$$

where E_{Eng} is the total energy over a certain time period input into the vehicle engine and electric drive controller;

E_{Bat} is the energy delivered at the same time by the onboard battery to the electric drive controller.

Obviously, k_{EV} represents the fraction of the total energy input supplied by the battery. For a charge-sustaining electric vehicle, since no energy is drawn from the battery, $k_{EV} = 0$; For a zero-emission electric vehicle (ZEV), which is purely driven by the battery, $k_{EV} = 1$; For a PHEV, the actual value of k_{EV} is somewhere between 0 and 1.

Secondly, another key parameter of a PHEV is its total battery capacity C_{Bat}. The control strategy of a PHEV is assumed to adjust k_{EV}, i.e. its operating status, according to its C_{Bat} [154], so k_{EV} and C_{Bat} are correlated and modelled as the bivariate Gaussian distribution:

$$\begin{bmatrix} k_{EV} \\ C_{Bat} \end{bmatrix} = \begin{bmatrix} \mu_{k_{EV}} \\ \mu_{C_{Bat}} \end{bmatrix} + \boldsymbol{L} \cdot \begin{bmatrix} N_1 \\ N_2 \end{bmatrix} \tag{3.4}$$

where $\mu_{k_{EV}}$ is the mean value of k_{EV};

$\mu_{C_{Bat}}$ is the mean value of C_{Bat};

$\boldsymbol{L}$ is the Cholesky decomposition of their covariance matrix $\boldsymbol{\Sigma}$, i.e. $\boldsymbol{\Sigma} = \boldsymbol{L} \cdot \boldsymbol{L}^{\mathrm{T}}$;

N_1 and N_2 are two uncorrelated standard Gaussian variates.

Thirdly, the performance of a PHEV can be assessed by its energy consumption per mile driven, denoted as E_m, which is approximately expressed as a monomial function of k_{EV}:

$$E_m = A_E \cdot (k_{EV})^{B_E} \tag{3.5}$$

where the constant coefficients A_E and B_E depend on the PHEV type.

Fourthly, according to statistical data on the PHEV driving pattern given in [155], the daily driven miles of a PHEV, denoted as M_d, tends to follow the lognormal distribution:

$$M_d = e^{(\mu_m + \sigma_m \cdot N)} \tag{3.6}$$

where N is a standard Gaussian variate.

According to Appendix I, the parameters μ_m and σ_m can be calculated from the mean and standard variation of M_d, denoted as μ_{M_d} and σ_{M_d} respectively:

$$\begin{cases} \mu_m = \ln\left(\mu_{M_d}^2 \Big/ \sqrt{\mu_{M_d}^2 + \sigma_{M_d}^2}\right) \\ \sigma_m = \sqrt{\ln\left(1 + \sigma_{M_d}^2 \Big/ \mu_{M_d}^2\right)} \end{cases} \tag{3.7}$$

Finally, the daily recharge energy of a single PHEV, denoted as D_E, can be defined as follows

$$D_E = \begin{cases} C_{Bat} & M_d \geq M_E \\ M_d \cdot E_m & M_d < M_E \end{cases} \tag{3.8}$$

where constant M_E is the maximum driving distance of a PHEV in all electric driven mode, i.e.

$$M_E = C_{Bat} / E_m = C_{Bat} / \left(A_E \cdot k_{EV}^{B_E}\right) \tag{3.9}$$

3.4.3 Charging Demand of Multiple Electric Vehicles

For multiple PHEVs, queuing theory [76] can be employed to describe their overall charging process. For different situations of PHEV charging, different queue models are selected. In this section, two typical scenarios of PHEV charging are presented, i.e. charging PHEVs at an electric vehicle charging station and in a local residential community respectively.

PHEVs at an electric vehicle charging station can be considered as queuing customers to be served in an *M*/*M*/*c* queue, where the first *M* denotes the inter-arrival time of customers obeying the exponential distribution with mean T_λ ($T_\lambda > 0$), the second *M* denotes the service time of a customer for a customer obeying the exponential distribution with mean T_μ ($T_\mu > 0$), and *c* denotes the maximum customer number being served at the same time.

It should be explained that the exponential distribution is employed here because the PHEVs are assumed to be uncorrelated in their arrival and charging duration, i.e. both their arrival and charging are the Poisson process [156]. On the other hand, the number of waiting customers is assumed to be infinite for simplicity.

In terms of queuing theory, the number of PHEVs being charged at the same time in an *M*/*M*/*c* queue, denoted as *n*, follows a discrete distribution as follows

$$p_n = \begin{cases} \left(\sum_{i=0}^{c-1} \frac{(c\rho)^i}{i!} + \frac{(c\rho)^c}{c!} \cdot \frac{1}{1-\rho} \right)^{-1} & n = 0 \\ \frac{(c\rho)^n}{n!} \cdot p_0 & n = 1, 2, \cdots, c \end{cases} \tag{3.10}$$

where ρ is the so called occupation rate per server defined as follows

$$\rho = \frac{T_\mu}{cT_\lambda} \tag{3.11}$$

It should be noted that it is generally required that the occupation rate $\rho < 1$, so that the length of the PEHV queue doesn't explode.

As for the PHEVs in a local residential community, the $M/M/c/k/N_{\max}$ ($c \le k \le N_{\max}$) queue is employed to describe their overall charging process, where k is the maximum number of customers being served or waiting in the queue, and $N_{\max}$ is the maximum number of possible customers. Similarly, it is also assumed that the arrival and charging patterns of PHEVs are the Poisson process.

The difference between a charging station and a residential community is: in the latter scenario, the charging slots are generally privately owned or shared only by the local residents, so the number of possible customers to be served is limited, compared to the first scenario where the number of possible customers could be unlimited. Such a difference leads to different queue models to be applied.

Accordingly, the number of PHEVs being charged at the same time in an $M/M/c/k/N_{\max}$ queue follows another discrete distribution as follows

$$p_n = \begin{cases} \left(\sum_{i=0}^{c} \binom{N_{\max}}{i} \cdot (c\rho)^i + \sum_{i=c+1}^{k} \frac{N_{\max}! \cdot (c\rho)^i}{(N_{\max}-i)! \cdot c! \cdot c^{i-c}} \right)^{-1} & n = 0 \\ (c\rho)^n \cdot \binom{N_{\max}}{n} \cdot p_0 & n = 1, 2, \cdots, c \end{cases} \tag{3.12}$$

In both the above queue models, the service time T for charging a PHEV is assumed to obey the exponential distribution with mean T_μ, i.e.

$$T = -T_{\mu} \cdot \ln(U) \tag{3.13}$$

where U is a random variate of the continuous uniform distribution within (0, 1).

However, it is not reasonable that a PHEV is being charged for a very short time, and the charging time also has an upper limit due to its battery capacity or service regulations, so T is truncated within a certain range $[T_{\min}, T_{\max}]$. Therefore, T becomes

$$T = \begin{cases} T_{\min} & T \le T_{\min} \\ -T_{\mu} \cdot \ln(U) & T_{\min} < T < T_{\max} \\ T_{\max} & T \ge T_{\max} \end{cases} \tag{3.14}$$

On the other hand, it is reported in [157] that currently there mainly exist 3 charging power levels for PHEVs. It is reasonable to assume that an electric vehicle charging station prefers a higher charging power level so that the service time T could be reduced by supplying higher charging power, e.g. level 3. In contrast, the charging slots distributed in a local residential community are limited by the distribution capacity, so their charging power level is usually limited to level 1. Therefore, a level 3 (400V/63A) is selected for the charging station and a level 1 (230V/16A) for the residential community.

Once the charging power level is determined, the charging voltage V and maximum charging current $I_{\max}$ are known. Then the average charging current of a PHEV can be calculated by

$$I = \min\left\{\frac{D_E}{V \cdot T}, I_{\max}\right\} \tag{3.15}$$

Finally, for all the n PHEVs being charged at an electric vehicle charging station or in a local residential community, their total charging demand P is

$$P = \sum_{i=1}^{n} V \cdot I_i \tag{3.16}$$

where I_i is the charging current of the i-th PHEV obtained from Equation (3.15).

3.4.4 Different Categories of Electric Vehicles

In order to consider the difference in PHEV parameters, such as k_{EV}, C_{Bat}, E_m and M_E, PHEVs are divided into 4 classes in this section, according to their possible k_{EV} and C_{Bat}:

Table 3-1 C_{Bat} Range of Each PHEV Class

Class	Min C_{Bat} (kWh)	Max C_{Bat} (kWh)
Micro car	8	12
Economy car	10	14
Mid-size car	14	18
Light truck/SUV	19	23

Moreover, their market share is assumed to be given in Table 3-2:

Table 3-2 Market Share of Each PHEV Class

Class	Percentage (100%)
Micro car	0.2
Economy car	0.3
Mid-size car	0.3
Light truck/SUV	0.2

Because the market share can be viewed as a discrete distribution, the class of a PHEV can be randomly selected according to its market share.

3.4.5 Random Simulation of the Overall Charging Demand of Electric Vehicles

After establishing the distributions and relations of the main factors that determine the charging behaviour of PHEVs, a random simulation could be carried out to obtain their total charging demand samples. The procedure of this random simulation is outlined as follows:

1. Randomly generate the number of PHEVs being charged at the same time n, according to Equation (3.10) or (3.12). Then for each one among the n PHEVs, do the following Step 2~8:
2. Randomly select its class according to its market share in Table 3-2;
3. Randomly generate its parameters k_{EV} and C_{Bat} according to Equation (3.4);
4. Calculate its energy consumption per mile E_m according to Equation (3.5);
5. Randomly generate its daily driven miles M_d according to Equations (3.6) and (3.7);
6. Calculate its recharge energy D_E according to Equation (3.8);
7. Randomly generate its charging time T according to Equation (3.14);
8. Calculate its charging current I according to Equation (3.15);
9. Accumulate the total charging demand P according to Equation (3.16).

The above procedure is repeatedly executed until enough statistical samples are generated for further statistical analysis.

3.4.6 Distribution Fitting of the Overall Charging Demand of Electric Vehicles

In this section, the proposed methodology is applied to model the total charging demand of PHEVs at a charging station and in a residential community with specified parameters.

By referring to the experimental data in [79] and [158], the constants A_E and B_E in Equation (3.5) of different PHEV classes are listed in Table 3-3:

Table 3-3 E_m Parameters of Each PHEV Class

Class	A_E (kWh/mile)	B_E
Micro car	0.3790	0.4541
Economy car	0.4288	0.4179
Mid-size car	0.5740	0.4040
Light truck/SUV	0.8180	0.4802

In order to approximate the statistical data on electric vehicle driving distance in [158], it is assumed that M_d has a mean μ_{M_d} = 40miles and a deviation σ_{M_d} = 20miles.

Because M_E of different PHEV classes could range widely, it is selected to be μ_{M_d} for simplicity. Thus the range of k_{EV} can be calculated from Equation (3.9):

$$k_{EV} = \sqrt[B_E]{C_{Bat} / (A_E \cdot M_E)} \tag{3.17}$$

By substituting Min C_{Bat} and Max C_{Bat} in Table 3-1 and μ_{M_d} into Equation (3.9), the ranges of k_{EV} are obtained as follows

Table 3-4 k_{EV} Range of Each PHEV Class

Class	Min k_{EV}	Max k_{EV}
Micro car	0.2447	0.5976
Economy car	0.2750	0.6151
Mid-size car	0.2939	0.5475
Light truck/SUV	0.3224	0.4800

As mentioned above, k_{EV} and C_{Bat} are modelled as the bivariate Gaussian distribution. The corresponding parameters are given as follows

$$\begin{aligned} \mu_{k_{EV}} &= \left(\mathrm{Min}k_{EV} + \mathrm{Max}k_{EV}\right)/2 \\ \mu_{C_{Bat}} &= \left(\mathrm{Min}C_{Bat} + \mathrm{Max}C_{Bat}\right)/2 \end{aligned} \tag{3.18}$$

$$\begin{aligned} \sigma_{k_{EV}} &= \left(\mathrm{Max}k_{EV} - \mathrm{Min}k_{EV}\right)/4 \\ \sigma_{C_{Bat}} &= \left(\mathrm{Max}C_{Bat} - \mathrm{Min}C_{Bat}\right)/4 \end{aligned} \tag{3.19}$$

$$\boldsymbol{\Sigma} = \begin{bmatrix} \sigma^2_{k_{EV}} & \rho_\Sigma \sigma_{k_{EV}} \sigma_{C_{Bat}} \\ \rho_\Sigma \sigma_{k_{EV}} \sigma_{C_{Bat}} & \sigma^2_{C_{Bat}} \end{bmatrix} \tag{3.20}$$

where the correlation coefficient ρ_Σ is arbitrarily set to 0.8.

The queue model parameters and charging level are listed in Table 3-5, which are selected to simulate a busy period:

Table 3-5 Queue Model Parameters

Queue Model / Parameter	*M*/*M*/*c*	*M*/*M*/*c*/*k*/$N_{\max}$
T_λ (min.)	10	30
T_μ (min.)	60	240
c	30	100
k	–	100
$N_{\max}$	–	100
$T_{\min}$ (min.)	10	120
$T_{\max}$ (min.)	120	360
Voltage (V)	400	230
$I_{\max}$ (A)	63	16

As for an electric vehicle charging station, 10000 samples of total charging demand is generated, and their histogram is depicted in Figure 3-4. The shape of this histogram changes little when the number of samples increases, so the sample capacity is adequate.

It is hypothesized that the recharge power obeys the Weibull distribution, and through Maximum likelihood estimation, its parameters are obtained as $\lambda = 0.192329$ and $k = 1.87103$ with a confidence degree $1-\alpha = 95\%$. For comparison, the fitted Weibull probability density curve is also plotted in Figure 3-4.

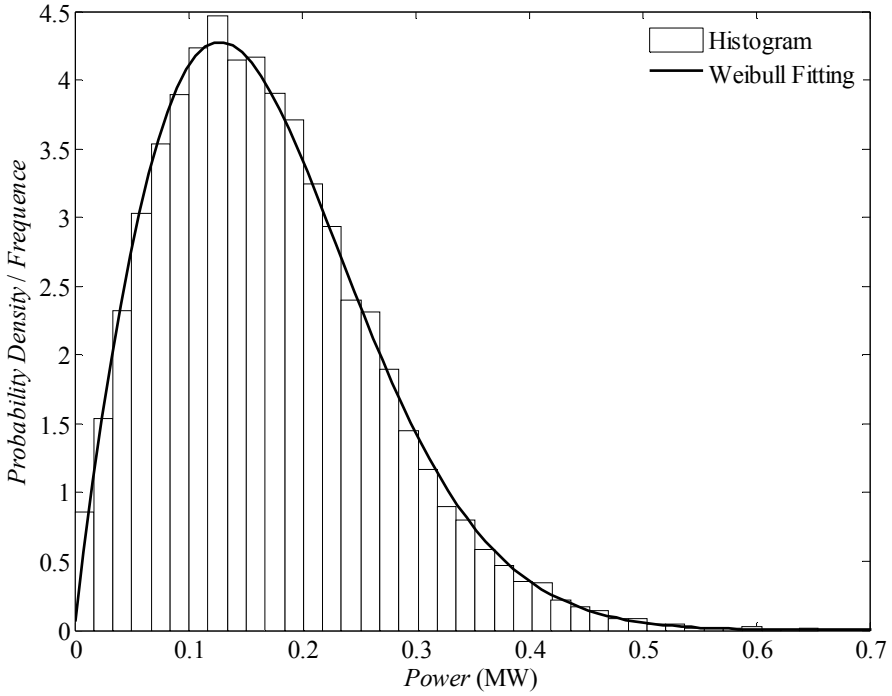

Figure 3-4 Sample histogram and probability density fitting (charging station)

In order to validate the above hypothesis, Kolmogorov-Smirnov goodness-of-fit test (K-S test) [159] with a significance level $\alpha = 5\%$ is carried out: K-S test statistics is 0.007413, much less than its cut-off value 0.013564, so the above hypothesis is accepted, i.e. the total charging demand of an electric vehicle charging station is identified as a Weibull distributed variate.

For comparison, the empirical cumulative distribution curve of the recharge power samples and the fitted Weibull cumulative distribution function are plotted in Figure 3-5.

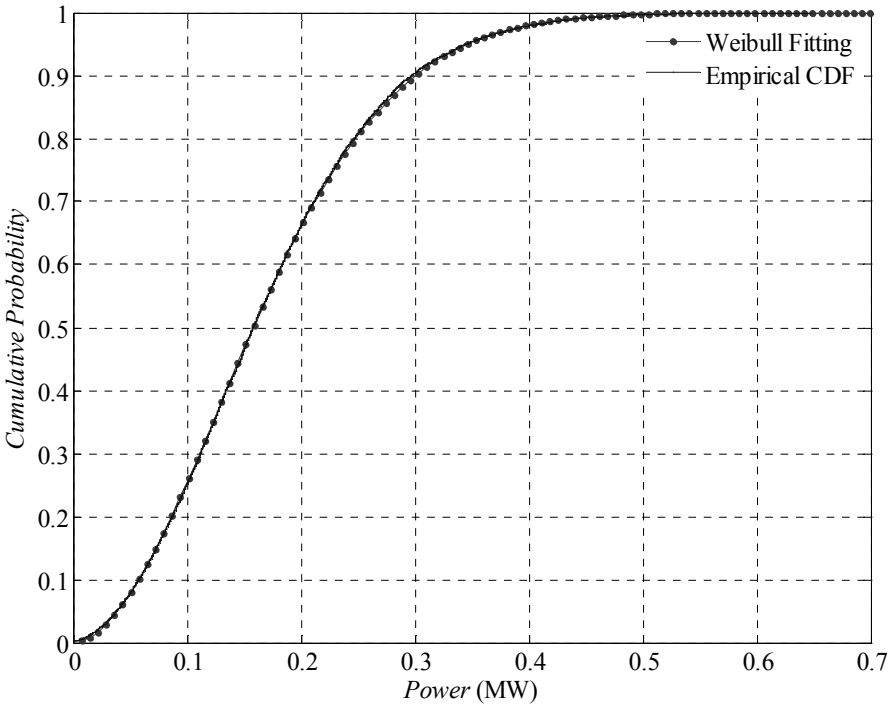

Figure 3-5 K-S test for cumulative distribution fitting (charging station)

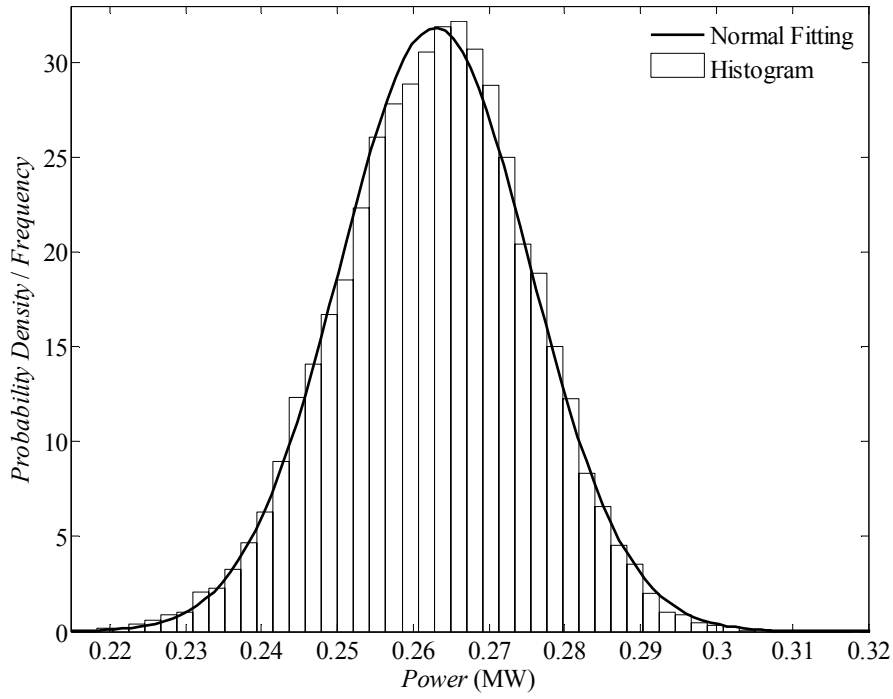

Figure 3-6 Sample histogram and probability density fitting (residential community)

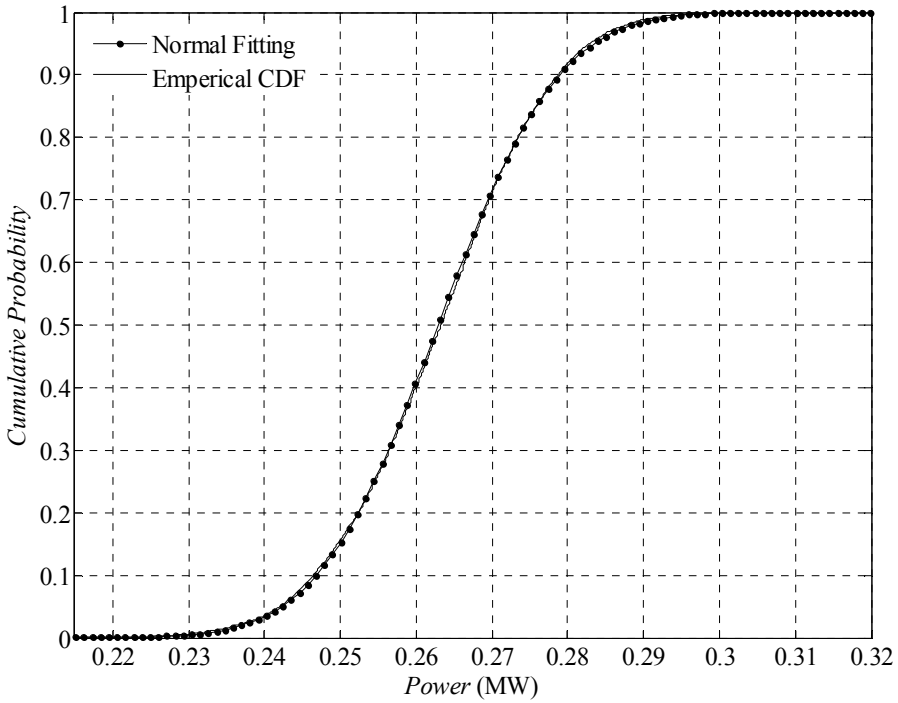

Figure 3-7 K-S test for cumulative distribution fitting (residential community)

In a similar way, the total charging demand of PHEVs in a local residential community is identified to obey the Gaussian distribution with a significance level α = 5%, as shown in Figure 3-6 and Figure 3-7.

3.5 Correlation between Uncertainties

It has been confirmed for years in [86] and [89] that there is a certain degree of correlation between bus power injections, either loads or generation sources, due to various reasons.

For example, a group of loads existing in the same area tend to increase and decrease in a like manner due to environmental or social factors. Similarly, renewable energy sources are spatially correlated within a given geographical area in a very significant manner often due to the same physical phenomena [160]-[161].

It is necessary to take such correlation into account during the analysis of power systems. Otherwise it would lead to negative effect on analysis results. Conventional deterministic analysis cannot describe nonlinear correlation among loads or generation sources; while in stochastic analysis, linear or nonlinear correlation can be measured by covariance or correlation coefficients.

It should be pointed out that there are several correlation coefficients of different sensitivity to the nonlinear relationship [162], but distinction in depth between them are out of the focus of this research. The most common Pearson's correlation coefficient defined in Section 1.2 is employed to describe the correlation in power systems.

3.6 Chapter Summary

This chapter introduces the probabilistic models of power system inputs, such as substation loads, power plants, and wind farms. Especially, a methodology of modelling the charging demand of electric vehicles is proposed. Moreover, the representation of the correlation between these inputs is also addressed. This lays a foundation of further stochastic analysis and optimization of power systems, which will be addressed in next chapters.

CHAPTER 4 ANALYTICAL PROBABILISTIC POWER FLOW CALCULATIONS

4.1 Introduction

Power flow calculations are also fundamental to stochastic analysis of power systems. Nevertheless, besides the solution of power flow equations, power flow calculations in stochastic analysis of power systems need to obtain the probability distributions of system outputs, state variables or reliability indices of interest, e.g. bus voltages or branch flows, through given probability distributions of system inputs. This is the so-called Probabilistic Power Flow (PPF) or sometimes also called Stochastic Power Flow.

Because of the nonlinearity of AC power flow model, it is difficult to directly obtain the analytic expression of the probability distributions of system outputs or state variables. In order to overcome this difficulty, a lot of alternative methods of PPF calculations have been developed over last 30 years. Currently, there are three main PPF methods, i.e. Monte Carlo Simulation (MCS), Point Estimate Method (PEM), as well as Cumulant Method (CM). Note that, MCS is based on principles of statistics, so it is sometimes not classified as one of PPF methods in a narrow term.

This chapter will first introduce the features of these three PPF methods, and then especially gives more details on CM. Moreover, a new technique will be proposed in this chapter to improve CM so that it is able to consider the correlation between random system inputs. In case studies, the accuracy and efficiency of these three PPF methods will be compared. On the other hand, the modelling methodology of the overall charging demand of electric vehicles

proposed in last chapter will also be validated through a PPF case study. Moreover, another case study will be given to show the effectiveness of the proposed technique in dealing with the correlation between random system inputs.

4.2 Main Probabilistic Power Flow Methods

4.2.1 Monte Carlo Simulation

Monte Carlo simulation (MCS) [82], which is based on the Law of Big Numbers [132], is the first simulation method addressing the uncertainties in power systems, and it has been used in the reliability assessment of power systems for many years.

In MCS, uncertain system inputs modelled as probability distributions are sampled first, and then deterministic power flow is calculated with each group of these samples. The probability distribution or numerical characteristics of a system output are obtained through statistical analysis on all the values generated by the system with the samples of system inputs. MCS generally shows strong applicability: It is not sensitive to the system scale, and it can consider internal changes, e.g. network contingency, and the correlation between system inputs.

MCS essentially converges in probability and the error of its statistical results is determined by their variance, confidence level and sample capacity [163]. In MCS, random samples of each system input are independent, identically distributed (i.i.d.), then their corresponding values of a system output are i.i.d. as well. According to the Central Limit Theorem [131], there is

$$\lim_{N\to\infty} \Pr\left\{\left|\frac{\overline{\mu}-\mu}{\sigma/\sqrt{N}} < x\right|\right\} = \frac{1}{\sqrt{2\pi}}\int_{-\infty}^{\infty} e^{-x^2/2}dx \tag{4.1}$$

where N is the sample capacity, i.e. the number of simulations;

$\overline{\mu}$ is the sample mean of the system output;

μ is the real mean of the system output;

σ is the real standard deviation of the system output.

Given a confidence level α, then the error of $\overline{\mu}$ is approximately expressed as

$$\lim_{N\to\infty} \Pr\left\{\left|\overline{\mu}-\mu\right| < \frac{x_\alpha \sigma}{\sqrt{N}}\right\} \approx \frac{2}{\sqrt{2\pi}} \int_0^{x_\alpha} e^{-x^2/2} dx \tag{4.2}$$

where N is the sample capacity, i.e. the number of simulations;

$\overline{\mu}$ is the sample mean of the system output;

μ is the real mean of the system output;

σ is the real standard deviation of the system output.

Apparently, the accuracy of MCS is proportional to the square root of the number of simulations [164], which means that if the decimal precision of MCS increases by one place, its number of simulations has to increase by 100 times. Therefore, a large number of simulations are required for MCS to obtain meaningful results. In practice, the sample variance of the system output is employed as a criterion of the convergence of MCS. That is, if the value of the sample variance changes little in comparison to that of last simulation, then it is considered that MCS is converged under the specified tolerance [82].

For its application in PPF calculations, MCS could be really time-consuming. In order to overcome this drawback, various variance reduction techniques, from sampling to clustering, have been applied to improve the computational efficiency of MCS [83], but basically tens of thousands of simulations are still needed in order to obtain meaningful results. High

computational cost restricts MCS mainly in long-term expansion planning or as a benchmark for other PPF methods.

4.2.2 Point Estimate Method

Point estimate method (PEM) [100]-[102] is currently the representative of approximate methods for PPF calculations. PEM extracts a few estimate points with corresponding weights from the probability distribution of each system input, and then calculates power flow at each of these points so that the raw moments of the system outputs of interest are accumulatively obtained. Through its raw moments, the probability distributions of a system output can be fitted by the methods described in Section 2.

PEM retains the nonlinear power flow model so that better accuracy can be achieved [165]. Moreover, it successfully reduces the number of power flow calculations to be linearly proportional to the number of random system inputs [101]. However, further research publications have revealed some drawbacks of PEM [166]-[169]: For some bounded non-Gaussian distributions, e.g. the lognormal distribution and the exponential distribution, estimate points could be located outside of their domain when the standard deviation is relatively large; Moreover, PEM is not able to deal with system internal changes, e.g. network contingency; On the other hand, the computational complexity of PEM is limited by system scale, i.e. the number of stochastic system inputs, which could make PEM lose advantage over MCS when it is applied to very large power systems.

4.2.3 Cumulant Method

Cumulant method (CM) [94]-[99] is currently the representative of analytical methods for PPF calculations. CM utilizes the properties of cumulants and maps the cumulants of system

outputs of interest as the linear combination of the cumulants of stochastic system inputs through a linearized power flow model.

In contrast to MCS and PEM, CM shows satisfactory precision but achieves much better computational efficiency [165], because it generally conducts power flow calculations once. Moreover, CM has been improved to take network contingency into account, through equivalent power compensation to branch outage [95] or calculating the conditional probability of network configuration [96].

However, in order to utilize the properties of cumulants, an assumption of independence between random system inputs has to be made in CM. As pointed out in Section 0, there could be correlation between power system inputs, and it could lead to error if such correlation was neglected. Therefore, in the remaining parts of this chapter, a new technique that removes this unrealistic assumption from CM will be proposed, along with a detailed description of CM.

4.3 Probabilistic Power Flow Considering Correlation

4.3.1 Linearized Power Flow Model

The bus power and branch flow equations can be formulated as

$$\left.\begin{aligned} \boldsymbol{S} &= \boldsymbol{F}(\boldsymbol{V},\boldsymbol{Y}) \\ \boldsymbol{S}_b &= \boldsymbol{H}(\boldsymbol{V},\boldsymbol{Y}) \end{aligned}\right\} \tag{4.3}$$

where $\boldsymbol{S}$ is the vector of bus power injections;

$\boldsymbol{S}_b$ is the vector of branch flows;

$\boldsymbol{V}$ is the vector of bus voltage phasors;

$\boldsymbol{Y}$ is the network admittance matrix.

Assuming that the original system operating point is $\boldsymbol{V} = \boldsymbol{V}_0$, $\boldsymbol{Y} = \boldsymbol{Y}_0$, so that $\boldsymbol{S} = \boldsymbol{S}_0$ and $\boldsymbol{S}_b = \boldsymbol{S}_{b0}$. When a small bus power injection incremental $\Delta\boldsymbol{S}$ occurs, due to the voltage change $\Delta\boldsymbol{V}$ the Taylor series expansion of Equation (4.3) in the neighbourhood of $(\boldsymbol{V}_0, \boldsymbol{Y}_0)$ is

$$\begin{aligned} \boldsymbol{S} &= \boldsymbol{S}_0 + \Delta\boldsymbol{S} = \boldsymbol{F}(\boldsymbol{V}_0 + \Delta\boldsymbol{V}, \boldsymbol{Y}_0) \\ &= \boldsymbol{F}(\boldsymbol{V}_0, \boldsymbol{Y}_0) + \partial\boldsymbol{F}(\boldsymbol{V}, \boldsymbol{Y}) / \partial\boldsymbol{V}\big|_{(\boldsymbol{V}_0, \boldsymbol{Y}_0)} \Delta\boldsymbol{V} + o[(\Delta\boldsymbol{V})^n] \\ \boldsymbol{S}_b &= \boldsymbol{S}_{b0} + \Delta\boldsymbol{S}_b = \boldsymbol{H}(\boldsymbol{V}_0 + \Delta\boldsymbol{V}, \boldsymbol{Y}_0) \\ &= \boldsymbol{H}(\boldsymbol{V}_0, \boldsymbol{Y}_0) + \partial\boldsymbol{H}(\boldsymbol{V}, \boldsymbol{Y}) / \partial\boldsymbol{V}\big|_{(\boldsymbol{V}_0, \boldsymbol{Y}_0)} \Delta\boldsymbol{V} + o[(\Delta\boldsymbol{V})^n] \end{aligned} \tag{4.4}$$

where $o[(\Delta\boldsymbol{V})^n]$ denotes the high order items of bus voltage incremental $\Delta\boldsymbol{V}$.

Substitute $\boldsymbol{S}_0 = \boldsymbol{F}(\boldsymbol{V}_0, \boldsymbol{Y}_0)$ and $\boldsymbol{S}_{b0} = \boldsymbol{H}(\boldsymbol{V}_0, \boldsymbol{Y}_0)$ into Equation (4.4) and omit the high order items, then there is

$$\left.\begin{aligned} \Delta\boldsymbol{S} &= \partial\boldsymbol{F}(\boldsymbol{V}, \boldsymbol{Y}) / \partial\boldsymbol{V}\big|_{(\boldsymbol{V}_0, \boldsymbol{Y}_0)} \Delta\boldsymbol{V} = \boldsymbol{J}_0 \Delta\boldsymbol{V} \\ \Delta\boldsymbol{S}_b &= \partial\boldsymbol{H}(\boldsymbol{V}, \boldsymbol{Y}) / \partial\boldsymbol{V}\big|_{(\boldsymbol{V}_0, \boldsymbol{Y}_0)} \Delta\boldsymbol{V} = \boldsymbol{G}_0 \Delta\boldsymbol{V} \end{aligned}\right\} \tag{4.5}$$

where $\boldsymbol{J}_0 = \partial\boldsymbol{F}(\boldsymbol{V}, \boldsymbol{Y}) / \partial\boldsymbol{V}\big|_{(\boldsymbol{V}_0, \boldsymbol{Y}_0)}$;

$\boldsymbol{G}_0 = \partial\boldsymbol{H}(\boldsymbol{V}, \boldsymbol{Y}) / \partial\boldsymbol{V}\big|_{(\boldsymbol{V}_0, \boldsymbol{Y}_0)}$.

Equation (4.5) is the so-called linearized power flow equations. Note that, $\boldsymbol{J}_0$ is actually the Jacobian matrix when power flow calculations converge.

Accordingly, the linear relationship between $\Delta\boldsymbol{S}$, $\Delta\boldsymbol{V}$ and branch flow incremental $\Delta\boldsymbol{S}_b$ can be formulated as

$$\left.\begin{aligned}\Delta \boldsymbol{V} &= \boldsymbol{J}_0^{-1}\Delta \boldsymbol{S} \\ \Delta \boldsymbol{S}_b &= \boldsymbol{G}_0\Delta \boldsymbol{V} = [\boldsymbol{G}_0\boldsymbol{J}_0^{-1}]\Delta \boldsymbol{S}\end{aligned}\right\} \tag{4.6}$$

4.3.2 Cumulant Based Probabilistic Power Flow

According to Equation (4.6), the incrementals of bus voltage and branch flow are represented as the linear combination of that of bus power injections, i.e. stochastic system inputs in PPF. According to *Property* 1 and *Property* 2 of cumulants in Section 1.1, the m-th ($m \geq 2$) order cumulant of $\Delta \boldsymbol{V}$ and $\Delta \boldsymbol{S}_b$ can be also formulated as the linear combination of that of $\Delta \boldsymbol{S}$ as follows

$$\left.\begin{aligned}\boldsymbol{\kappa}_m^{\Delta V} &= \left[\boldsymbol{J}_0^{-1}\right]^{(m)}\boldsymbol{\kappa}_m^{\Delta S} \\ \boldsymbol{\kappa}_m^{\Delta S_b} &= \boldsymbol{G}_0{}^{(m)}\boldsymbol{\kappa}_m^{\Delta V}\end{aligned}\right\} \quad (m \geq 2) \tag{4.7}$$

where $\boldsymbol{\kappa}_m^{\Delta S}$ is the m-th order cumulant of $\Delta \boldsymbol{S}$;

$\boldsymbol{\kappa}_m^{\Delta V}$ is the m-th order cumulant of $\Delta \boldsymbol{V}$;

$\boldsymbol{\kappa}_m^{\Delta S_b}$ is the m-th order cumulants of $\Delta \boldsymbol{S}_b$;

(m) denotes m-th power of each element in a matrix.

On the other hand, according to *Property* 1 of cumulants in Section 1.1, the m-th ($m \geq 2$) order cumulant of $\boldsymbol{S}$ is the same as that of its incremental $\Delta \boldsymbol{S}$ because $\boldsymbol{S} = \boldsymbol{S}_0 + \Delta \boldsymbol{S}$. The same conclusion also holds for $\boldsymbol{V}$ and $\boldsymbol{S}_b$. Therefore, Equation (4.7) can be rewritten as

$$\left.\begin{aligned}\boldsymbol{\kappa}_m^{V} &= \left[\boldsymbol{J}_0^{-1}\right]^{(m)}\boldsymbol{\kappa}_m^{S} \\ \boldsymbol{\kappa}_m^{S_b} &= \boldsymbol{G}_0{}^{(m)}\boldsymbol{\kappa}_m^{V}\end{aligned}\right\} \quad (m \geq 2) \tag{4.8}$$

where $\boldsymbol{\kappa}_m^{S}$ is the m-th order cumulant of $\boldsymbol{S}$;

$\boldsymbol{\kappa}_m^V$ is the m-th order cumulant of $\boldsymbol{V}$;

$\boldsymbol{\kappa}_m^{S_b}$ is the m-th order cumulants of $\boldsymbol{S}_b$;

(m) denotes m-th power of each element in the matrix.

On the assumption that stochastic system inputs are mutually uncorrelated, the unknown high order cumulants of bus voltages and branch flows can be obtained from that of stochastic system inputs according to Equation (4.8).

As for their first order cumulants, i.e. their expected values, it is assumed that

$$\left.\begin{aligned} \overline{\boldsymbol{S}} &= \boldsymbol{F}(\overline{\boldsymbol{V}}, \boldsymbol{Y}) \\ \overline{\boldsymbol{S}}_b &= \boldsymbol{H}(\overline{\boldsymbol{V}}, \boldsymbol{Y}) \end{aligned}\right\} \tag{4.9}$$

where $\overline{\boldsymbol{S}} = \boldsymbol{\kappa}_1^S$ is the expected value of $\boldsymbol{S}$;

$\overline{\boldsymbol{V}} = \boldsymbol{\kappa}_1^V$ is the expected value of $\boldsymbol{V}$;

$\overline{\boldsymbol{S}}_b = \boldsymbol{\kappa}_1^{S_b}$ is the expected value of $\boldsymbol{S}_b$.

Equation (4.9) is actually the power flow equations in Equation (4.3) with $\boldsymbol{S} = \overline{\boldsymbol{S}}$. Therefore, the expected values of $\boldsymbol{V}$ and $\boldsymbol{S}_b$ could be obtained through deterministic power flow calculations once.

It should be pointed out that though the equality in Equation (4.9) doesn't strictly hold in mathematics, the error in most cases is very small even the variation of stochastic system inputs is relatively wide [87]. However, if the variation of stochastic system inputs is too significant, PPF could be calculated at different levels with a multi-linearization scheme [88].

Above all, the procedures of CM for PPF calculations can be summarized as follows:

1. Solve deterministic power flow in Equation (4.9) to obtain $\boldsymbol{\kappa}_1^{\boldsymbol{V}}$ and $\boldsymbol{\kappa}_1^{\boldsymbol{S}_b}$.
2. Calculate $\boldsymbol{\kappa}_m^{\boldsymbol{S}}$ ($m \geq 2$) according to the probability distributions of $\boldsymbol{S}$. In Appendix, there are formulae to calculate the cumulants of several common probability distributions.
3. Calculate $\boldsymbol{\kappa}_m^{\boldsymbol{V}}$ and $\boldsymbol{\kappa}_m^{\boldsymbol{S}_b}$ ($m \geq 2$) according to Equation (4.8).
4. Fit the probability distributions of $\boldsymbol{V}$ or $\boldsymbol{S}_b$ by their cumulants $\boldsymbol{\kappa}_m^{\boldsymbol{V}}$ or $\boldsymbol{\kappa}_m^{\boldsymbol{S}_b}$ through polynomial or series approximation presented in Section 2.

Apparently, CM shows good computational efficiency because its main computational complexity only consists of deterministic load flow calculations: one sparse matrix inversion and two matrix-vector multiplications.

It should be pointed out that the linearization of power flow equations in Equation (4.4) requires a constant network configuration, thus branch random outage is not considered above. However, a branch outage can be simulated by fictitious power sources obeying the Bernoulli distribution at its two terminals as presented in [95]. This equivalence is also based on the linear relationship shown in Equation (4.6), so for a branch outage that causes a great impact, an extra deterministic power flow should be solved with this branch removed and convolution should be applied to obtain the final results. Another approach of dealing with branch outage was proposed in [96], where the conditional probability of the network configuration corresponding to a certain branch outage is calculated. PPF is calculated by CM under each possible network configuration and then the results are convolved with its corresponding conditional probability, so that final results are obtained. This approach is simpler compared to that in [95] but more number of deterministic power flow calculations is required.

4.3.3 Treatment of Correlation between System Inputs

Besides the assumption of a constant network configuration, another unrealistic assumption of CM is the independence between stochastic system inputs. In order to take the possible correlation between stochastic system inputs into consideration, CM will be improved by a technique proposed in this section. The proposed technique is based on 2 theorems proved in [170], so these theorems are introduced first.

Theorem 1: For random variables r_1 and r_2, their 2nd order cumulants, i.e. their variances, are $\kappa_2^{r_1}$ and $\kappa_2^{r_2}$ respectively, and their correlation coefficient is ρ_{r_1,r_2}, then the 2nd order cumulant of r_1+r_2 is

$$\kappa_2^{r_1+r_2} = \kappa_2^{r_1} + 2\rho_{r_1,r_2}\sqrt{\kappa_2^{r_1}\kappa_2^{r_2}} + \kappa_2^{r_2} \tag{4.10}$$

A method for approximating the higher order cumulants of r_1+r_2 is provided by *Theorem* 2:

Theorem 2: Given two positive numbers β_1 and β_2, the m-th order ($m \geq 3$) cumulant of r_1+r_2 can be approximated by

$$\kappa_m^{r_1+r_2} = C_m \kappa_m^{r_1} + D_m \kappa_m^{r_2} \tag{4.11}$$

where

$$\alpha_1 = \frac{\sqrt{\kappa_2^{r_1}}}{\beta_1}; \alpha_2 = \frac{\sqrt{\kappa_2^{r_2}}}{\beta_2}; \quad \theta = 0.5 \sin\left(-2\rho_{r_1,r_2} \frac{\beta_1 \beta_2}{\beta_1^2 + \beta_2^2} \right) \tag{4.12}$$

$$C_m = \frac{\left(\alpha_1 \cos^2\theta - \alpha_2 \cos\theta \sin\theta \right)^m + (-1)^m \left(\alpha_1 \sin^2\theta - \alpha_2 \cos\theta \sin\theta\right)^m}{\left(\alpha_1 \cos 2\theta\right)^m} \tag{4.13}$$

$$D_m = \frac{\left(\alpha_1 \cos\theta \sin\theta - \alpha_2 \sin^2\theta\right)^m + (-1)^m \left(\alpha_1 \cos\theta \sin\theta - \alpha_2 \cos^2\theta\right)^m}{\left(\alpha_2 \cos 2\theta\right)^m} \tag{4.14}$$

$$|\theta| < \frac{\pi}{4} \text{ for } \left|\rho_{r_1,r_2}\right| < 1 \tag{4.15}$$

The approximation accuracy can be assessed by the number

$$\varepsilon = \frac{\beta_1^2 \beta_2^2}{\beta_1^2 + \beta_2^2} \tag{4.16}$$

The smaller ε is, the better approximation is achieved.

For practical use, it is enough to choose the free parameters β_1 and β_2 as follows:

$$\begin{cases} \beta_1 = 10, \beta_2 = 0.1 \text{ when } \kappa_2^{r_1} \le \kappa_2^{r_2} \\ \beta_1 = 0.1, \beta_2 = 10 \text{ when } \kappa_2^{r_1} > \kappa_2^{r_2} \end{cases} \tag{4.17}$$

For example, in the particular case $r_1 = r_2$, it is valid that

$$r_1 = r_2 \Rightarrow r_1 + r_2 = 2r_1 \Rightarrow \kappa_m^{r_1+r_2} = 2^m \kappa_m^{r_1}$$

$$\rho_{r_1,r_2} = 1 \Rightarrow \theta = -0.01, \alpha_1 = 0.1\sqrt{\kappa_2^{r_1}}, \alpha_2 = 10\sqrt{\kappa_2^{r_2}}$$

$$\Rightarrow \begin{cases} C_m = 1 \\ D_m = (-1)^m + 2^m \end{cases} \tag{4.18}$$

$$\Rightarrow \kappa_m^{r_1+r_2} = C_m \kappa_m^{r_1} + D_m \kappa_m^{r_2} = (C_m + D_m)\kappa_m^{r_1} \quad (m \geq 3)$$

Therefore, the relative error of this approximation is

$$err = \left| \frac{C_m + D_m - 2^m}{2^m} \right| \times 100\% = \begin{cases} 0\% & \text{for } m \text{ is odd} \\ \dfrac{100\%}{2^{m-1}} & \text{for } m \text{ is even} \end{cases} \tag{4.19}$$

Obviously, the cumulants of higher order are obtained with higher accuracy.

According to *Theorem 1-2*, Equations (4.10) and (4.13) offer an approach to calculate the high order cumulants of any two correlated random variables' sum. However, if r_1 or r_2 are further correlated with other random variables, the correlation coefficients between $r_1 + r_2$ and the other random variables should be updated, so there is the following lemma [170]:

Lemma: For random variables r_1, r_2 and r_3, their 2nd order cumulants are $\kappa_2^{r_1}$, $\kappa_2^{r_2}$ and $\kappa_2^{r_3}$, and their correlation coefficients are ρ_{r_1,r_2}, ρ_{r_1,r_3} and ρ_{r_2,r_3}, then the correlation coefficient between $r_2' = r_1 + r_2$ and r_3 is

$$\rho_{r_2',r_3} = \left(\rho_{r_1,r_3} \sqrt{\kappa_2^{r_1}} + \rho_{r_2,r_3} \sqrt{\kappa_2^{r_2}} \right) \Big/ \sqrt{\kappa_2^{r_2'}} \tag{4.20}$$

where $\kappa_2^{r_2'}$ can be obtained according to Equation (4.10).

For a random vector $\boldsymbol{r}$, *Lemma* can be employed to iteratively update the correlation coefficient between $r_i' = r_{i-1} + r_i$ ($i = 2, 3, 4, \ldots$) and other remaining components r_j ($j > i$):

$$\rho_{r_i',r_j} = \left(\rho_{r_{i-1}',r_j} \cdot \sqrt{\kappa_2^{r_{i-1}'}} + \rho_{r_i,r_j} \cdot \sqrt{\kappa_2^{r_i}}\right) \Big/ \sqrt{\kappa_2^{r_i'}} \tag{4.21}$$

Now look at the treatment of correlation in CM. It should be pointed out that the 1st order cumulant, i.e. the expected value, is not affected by any correlation [170], thus only higher order cumulants are necessary to be discussed here.

When correlation in stochastic vector $\boldsymbol{S}$ should be considered, the incremental of the i-th bus voltage in Equation (4.6) can be separated into two parts:

$$\begin{cases} \Delta V_i = \sum_j s_{ij} \cdot \Delta S_j = \Delta V_{i,1} + \Delta V_{i,2} \\ \Delta V_{i,1} = \sum_{j \in \Omega_1} s_{ij} \cdot \Delta S_j \\ \Delta V_{i,2} = \sum_{j \in \Omega_2} s_{ij} \cdot \Delta S_j \end{cases} \tag{4.22}$$

where Ω_1 is the set of uncorrelated components in $\boldsymbol{S}$;

Ω_2 is the set of correlated components in $\boldsymbol{S}$;

s_{ij} is the element at the i-th row and the j-th column in $\boldsymbol{J}^{-1}$.

Because $\Delta V_{i,1}$ is the linear combination of uncorrelated ΔS_j ($j \in \Omega_1$), Equations (4.7) and (4.8) is still applicable to the high order cumulants of $\Delta V_{i,1}$ and ΔS_j ($j \in \Omega_1$), i.e.

$$\kappa_m^{\Delta V_{i,1}} = \sum_{j \in \Omega_1} s_{ij}^m \cdot \kappa_m^{\Delta S_j} = \sum_{j \in \Omega_1} s_{ij}^m \cdot \kappa_m^{S_j} \quad (m \geq 2) \tag{4.23}$$

As for $\Delta V_{i,2}$, let $\Delta S_j' = s_{ij} \cdot \Delta S_j$ ($j \in \Omega_2$), then

$$\Delta V_{i,2} = \sum_{j \in \Omega_2} \Delta S_j^{'} \tag{4.24}$$

The cumulants of $\Delta S_j^{'}$ ($j \in \Omega_2$) can be easily obtained from that of S_j according to *Property 1* of cumulants. Moreover, according to the correlation coefficient's definition as well as *Property 1* of cumulants, there is

$$\begin{aligned}
\rho_{\Delta S_j^{'}, \Delta S_k^{'}} &= \operatorname{cov}(\Delta S_j^{'}, \Delta S_k^{'}) \Big/ \sqrt{\kappa_2^{\Delta S_j^{'}} \kappa_2^{\Delta S_k^{'}}} \\
&= E[(s_{ij} \Delta S_j)(s_{ik} \Delta S_k)] \Big/ \sqrt{\kappa_2^{s_{ij} \Delta S_j} \kappa_2^{s_{ik} \Delta S_k}} \\
&= s_{ij} s_{ik} \cdot \operatorname{cov}(\Delta S_j, \Delta S_k) \Big/ \sqrt{s_{ij}^2 s_{ik}^2 \kappa_2^{\Delta S_j} \kappa_2^{\Delta S_k}} \\
&= E[(S_j - \overline{S}_j)(S_k - \overline{S}_k)] \Big/ \sqrt{\kappa_2^{\Delta S_j} \kappa_2^{\Delta S_k}} \\
&= \operatorname{cov}(S_j, S_k) \Big/ \sqrt{\kappa_2^{S_j} \kappa_2^{S_k}} \\
&= \rho_{S_j, S_k}
\end{aligned} \tag{4.25}$$

which indicates that the correlation in stochastic vector $\boldsymbol{S}$ is identical the correlation of its incremental $\boldsymbol{\Delta S}$.

Therefore, *Theorem 1-2* can be applied to Equation (4.24) to calculate the m-th order ($m \geq 2$) cumulants of $\Delta S_j^{''} = \Delta S_{j\text{-}1}^{'} + \Delta S_j^{'}$ ($j \in \Omega_2$):

$$\begin{cases}
\kappa_2^{\Delta S_j^{''}} = \kappa_2^{\Delta S_{j-1}^{'}} + 2\rho_{S_{j-1}, S_j} \sqrt{\kappa_2^{\Delta S_{j-1}^{'}} \kappa_2^{\Delta S_j^{'}}} + \kappa_2^{\Delta S_j^{'}} \\
\kappa_m^{\Delta S_j^{''}} = C_m \kappa_m^{\Delta S_{j-1}^{'}} + D_m \kappa_m^{\Delta S_j^{'}} \quad (m \geq 3)
\end{cases} \tag{4.26}$$

and then *Lemma* is used to update the correlation coefficients between $\Delta S_j^{''}$ and the remaining components $\Delta S_k^{'}$ ($k \in \Omega_2$, $k > j$):

$$\rho_{S_j'',S_k'} = \left(\rho_{S_{j-1}'',S_k'} \sqrt{\kappa_2^{S_{j-1}''}} + \rho_{S_j',S_k'} \sqrt{\kappa_2^{S_j'}} \right) \Big/ \sqrt{\kappa_2^{S_j''}} \tag{4.27}$$

The cumulants of $\Delta V_{i,2}$ can be iteratively calculated through Equations (4.26) and (4.27).

On the other hand, because $\Delta V_{i,1}$ and $\Delta V_{i,2}$ are uncorrelated, the m-th ($m \geq 2$) order cumulants of V_i are finally obtained as

$$\kappa_m^{V_i} = \kappa_m^{\Delta V_i} = \kappa_m^{\Delta V_{i,1}} + \kappa_m^{\Delta V_{i,2}} \tag{4.28}$$

Once the cumulants of $\boldsymbol{V}$ is ready, the cumulants of $\boldsymbol{S}_b$ can be calculated according to Equation (4.8).

4.4 Case Studies

4.4.1 Comparison of Probabilistic Power Flow Methods

Two cases are presented in this section to compare the performance of CM, PEM (the most common 3-point scheme [101]) and MCS (as a benchmark). PPF calculations were conducted on IEEE 14-bus and 118-bus test systems. Up to 6th order cumulants are adopted for Gram-Charlier series to fit the probability distributions of system outputs. The number of MCS is selected to be 10000 for simplicity, which is big enough to grantee its convergence for these two systems.

The probabilistic data of the IEEE 14-bus system include 1 discrete load, 10 Gaussian loads and 12 generators, which are listed in Table 4-1:

Table 4-1 Probabilistic Data of the IEEE 14-Bus Test System

(a) Generator Data

Bus	Unit Capacity (MW)	Unit Number	FOR	Mean Real Output (MW)
1	2.5	10	0.08	23.00
2	22	2	0.09	40.04

(b) Discrete Load Data

Real (MW)	13.4	19.5	30.2	34.8	37.3
Probability	0.10	0.15	0.30	0.25	0.20
Reactive (Mvar)	7.5	11.0	17.0	19.6	21.0
Probability	0.10	0.15	0.30	0.25	0.20

(c) Gaussian Load Data

Bus	Real		Reactive	
	μ (MW)	σ/μ (100%)	μ (Mvar)	σ/μ (100%)
1	0.0	0.0	0.0	0.0
2	21.74	0.09	12.7	0.092
3	94.20	0.10	19.0	0.105
4	47.80	0.11	-3.9	0.097
5	7.60	0.05	1.6	0.05
6	11.20	0.06	7.5	0.063
7	0.0	0.0	0.0	0.0
8	0.0	0.0	0.0	0.0
9	0.0	0.0	0.0	0.0
10	9.0	0.10	5.8	0.10
11	3.5	0.095	1.8	0.095
12	6.1	0.076	1.6	0.086
13	13.5	0.105	5.8	0.095
14	14.9	0.086	5.0	0.086

The mean (μ) and standard deviation (σ) results of some buses and branches are listed in Table 4-2:

Table 4-2 Mean and Standard Deviation of the IEEE 14-Bus Test System

PPF Method		V_{11} (p.u.)	δ_{11} (deg)	P_1 (p.u.)	Q_1 (p.u.)	$P_{6\text{-}12}$ (p.u.)	$Q_{6\text{-}12}$ (p.u.)
CM	μ	1.0569	-14.791	2.264	-0.1755	0.0779	0.0250
	σ	0.0029	0.9706	0.1626	0.0313	0.0047	0.0020

PEM	μ	1.0568	-14.850	2.268	-0.1757	0.0779	0.0250
	σ	0.0031	0.9719	0.1629	0.0312	0.0044	0.0018
MCS	μ	1.0569	-14.879	2.268	-0.1758	0.0780	0.0249
	σ	0.0031	0.9737	0.1628	0.0311	0.0044	0.0018

It can be seen that both CM and PEM provide good results compared with MCS. For illustrative purpose, the cumulative distribution function of V_{11} and the probability density function of $P_{6\text{-}12}$ obtained by different methods are plotted in Figure 4-1 and Figure 4-2 respectively.

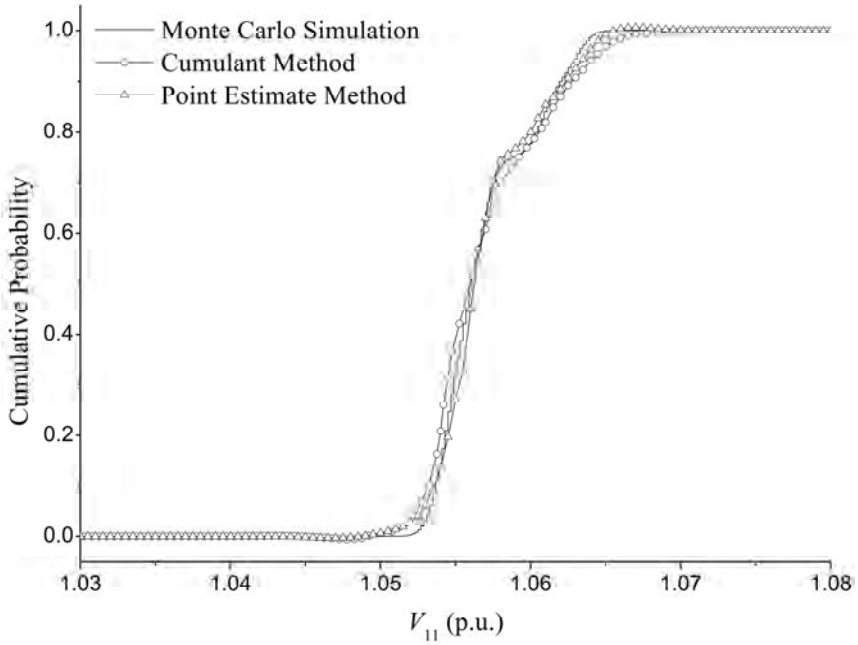

Figure 4-1 Cumulative distribution function of V_{11}

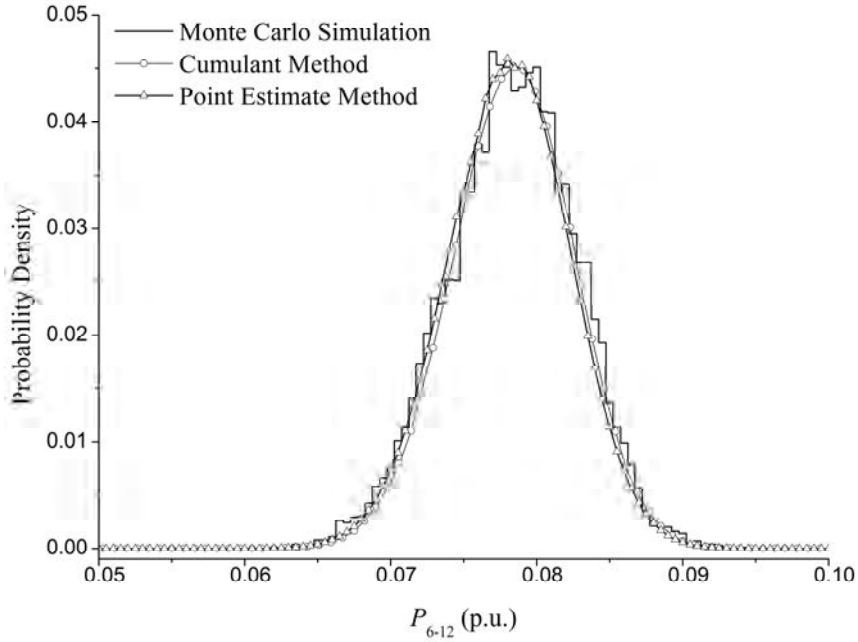

Figure 4-2 Probability density function of $P_{6\text{-}12}$

As for the IEEE 118-bus test system, it is assumed that each generator bus has 5 units with the same capacity and a FOR of 0.08. Units are modelled as uncorrelated Bernoulli distributions, and their mean values are set to be that of the base case. Loads are modelled as uncorrelated Gaussian distributions with mean values equal to that of the base case. In order to show the impact of uncertainty level on the accuracy, the variation coefficient σ/μ of each load is selected to be 5% and 15%.

Table 4-3 shows the mean (μ) and standard deviation (σ) results of some buses and branches with a load variation coefficient of 5%. Similarly, CM and PEM show good accuracy again.

Table 4-3 Mean and Standard Deviation of the IEEE 118-Bus Test System

PPF Method		V_{47} (p.u.)	δ_{11} (deg)	P_{100} (p.u.)	Q_{54} (p.u.)	$P_{65\text{-}68}$ (p.u.)	$Q_{65\text{-}8}$ (p.u.)
CM	μ	1.0171	-16.994	2.150	-0.2810	0.00142	-0.2243
	σ	1.94e-4	1.0179	0.0412	0.01932	0.00201	0.01904
PEM	μ	1.0171	-17.805	2.145	-0.2810	0.00130	-0.2230
	σ	1.94e-4	1.0219	0.0398	0.01983	0.00166	0.01408

MCS	μ	1.0170	-17.036	2.140	-0.2805	0.00134	-0.2234
	σ	1.94e-4	1.0946	0.0405	0.01976	0.00171	0.01335

Table 4-4 shows the average relative error of mean and standard deviation results corresponding to different load variation coefficients:

Table 4-4 Average Error of the IEEE 118-Bus System at Different Load Variation Levels

(d) Variation coefficient of loads: 5%

PPF Method		V_i	δ_i	P_i	Q_i	P_{ij}	Q_{ij}
CM (100%)	ε_μ^*	0.002	0.112	0.201	0.135	0.931	0.248
	ε_σ^*	3.259	0.578	0.811	4.401	0.725	2.312
PEM (100%)	ε_μ^*	0.002	0.103	0.186	0.120	0.828	0.193
	ε_σ^*	3.257	0.563	0.772	4.121	0.659	2.024

(e) Variation coefficient of loads: 15%

PPF Method		V_i	δ_i	P_i	Q_i	P_{ij}	Q_{ij}
CM (%)	ε_μ^*	0.021	0.209	0.301	0.216	1.489	0.524
	ε_σ^*	4.004	0.672	0.986	5.013	1.014	3.183
PEM (%)	ε_μ^*	0.004	0.148	0.217	0.141	0.902	0.242
	ε_σ^*	3.593	0.602	0.834	4.481	0.719	2.201

Evidently, as the variation of system inputs becomes larger, the average error of CM and PEM increases. This phenomenon seems to be more obvious for CM resulting from its linearized power flow equations; In contrast, PEM retains the non-linearity of power flow equations, so it is influenced less by the variation range of system inputs in comparison to CM. However, such a difference is not significant. It has been pointed out in [171] that when the variation coefficient of most stochastic system inputs is less than 20%, the linearization of power flow equations is not the main error source in CM.

On the other hand, the computational efficiency is also tested. All PPF methods were implemented in C++ and ran on a desktop PC with a Core Duo 2 2.4GHz CPU and 2GB DDR2-800 RAM. Timing results are listed as follows

Table 4-5 Computation Time Comparison (in Seconds)

Method / System	CM	PEM	MCS
14-bus	0.005	0.062	18.051
118-bus	0.023	3.847	193.28

As seen from Table 4-5, CM shows the best computational efficiency, because deterministic power flow is solved only once; then PEM follows, whose number of deterministic power flow solution is proportional to the number of stochastic system inputs; In contrast, the computational disadvantage of MCS is apparent.

4.4.2 Validation of Electric Vehicle Charging Demand Model

In last subsection, the accuracy of CM has been verified through two case studies in comparison with PEM and MCS. In this section, CM will be further employed in PPF calculations to validate the modelling methodology of electric vehicle overall charging demand proposed in Section 3.4.

Case studies were carried out on a modified IEEE 30-bus test system. This regional transmission system is connected with two UKGDS-EHV5 urban distribution systems [172] at bus 7 and 8 respectively, replacing their original loads. The grid topology of the UKGDS-EHV5 system is shown in Figure 4-3:

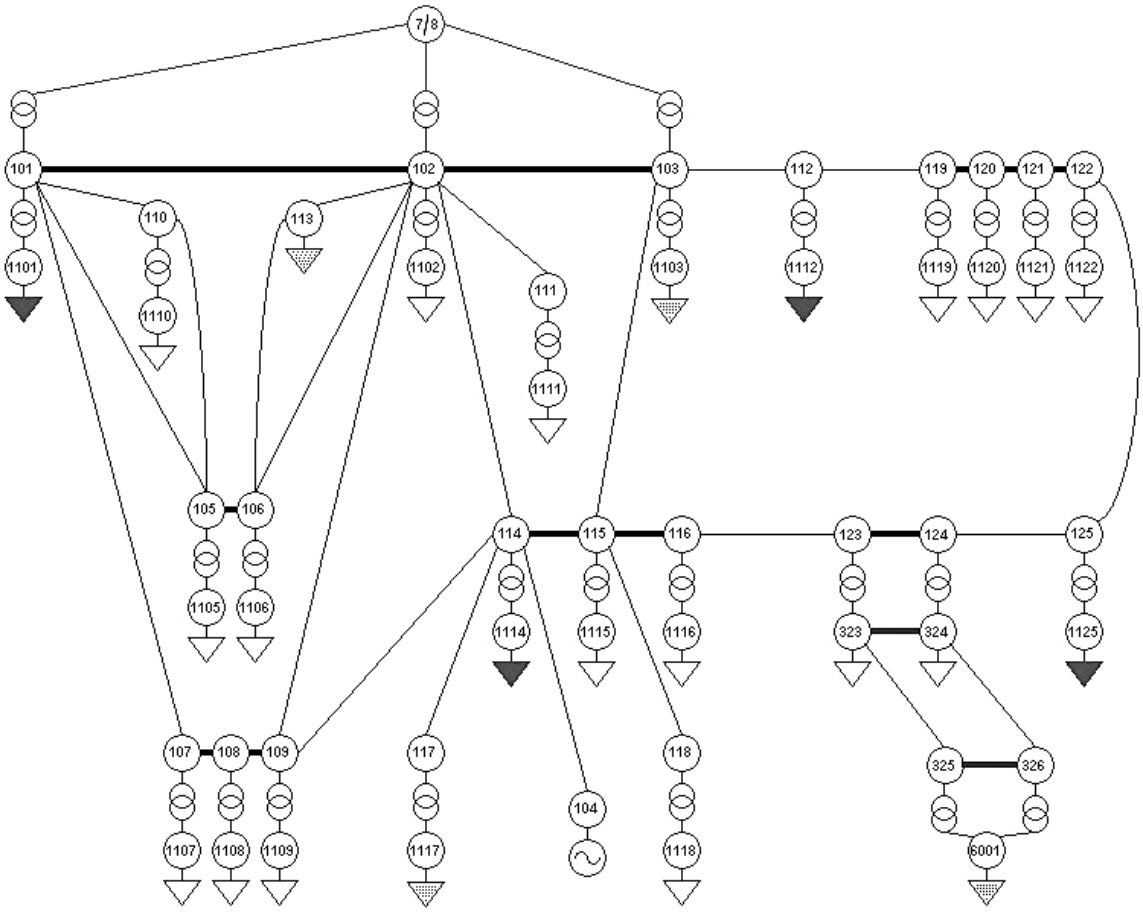

Figure 4-3 UKGDS-EHV5 urban distribution system

As shown in Figure 4-3, electric vehicle charging demands are attached at several load buses in the UKGDS-EHV5 system: A dot arrow represents the overall charging demand of electric vehicles in a residential community, which are modelled as the Gaussian distribution with the following parameters:

Table 4-6 Gaussian Charging Demand Parameters

Bus ID	Gaussian Parameter		Power Factor
	μ_P (MW)	σ_P/μ_P	
113	20.0	15%	0.97014
1103	9.7689	10%	0.94551
1117	11.0227	10%	0.94551
6001	16.2325	15%	0.97918

A solid arrow represents the overall charging demand of an electric vehicle charging station. Two sizes of charging stations are included here: the two at bus 1101 and 1114 have c = 30 while the other two have c = 17. Their charging demands are modelled as the Weibull distributions with the following parameters:

Table 4-7 Weibull Charging Demand Parameters

Bus ID	Weibull Parameter		Mean Power (MW)	Power Factor
	a_P	b_P		
1101	0.192329	1.87103	17.076	0.95
1112	0.11045	2.33015	9.7865	0.95
1114	0.192329	1.87103	17.076	0.95
1125	0.11045	2.33015	9.7865	0.95

Note that, the power factors in above two tables are lead.

The results of PPF calculations by CM were compared with that of MCS, whose charging demand samples were directly generated by the procedure described in Subsection 3.4.5 instead of sampling the fitted distributions. The sample capacity N_S = 10000, which is big enough for the convergence of MSC here.

All programs were implemented in C++ and ran on a desktop PC with a 2.53GHz Core 2 Duo CPU, 2GB DDR2-800 RAM. The programs took 0.107s for PPF and 225.86s for MCS respectively.

Table 4-8 shows the relative error of mean μ, variance σ_2, skewness γ_1 and kurtosis γ_2 of bus voltages and branch power flows, respectively.

Table 4-8 Average and Maximum Relative Error

Numerical Characteristic	Avg. ε (100%)	Max ε (100%)
μ_V	0.211	0.401
$\sigma_{2,V}$	1.136	3.521
$\gamma_{1,V}$	2.769	5.786
$\gamma_{2,V}$	4.361	10.08
μ_S	0.981	2.134
$\sigma_{2,S}$	2.115	4.691
$\gamma_{1,S}$	6.083	8.437
$\gamma_{2,S}$	10.747	17.318

As shown in Table 4-8, the error increases as the order of numerical characteristic increases. Nevertheless, the overall accuracy is still satisfactory, which indicates that it is feasible to substitute the overall charging demand of substantial electric vehicles with a single probability distribution through the proposed modelling methodology in Section 3.4.

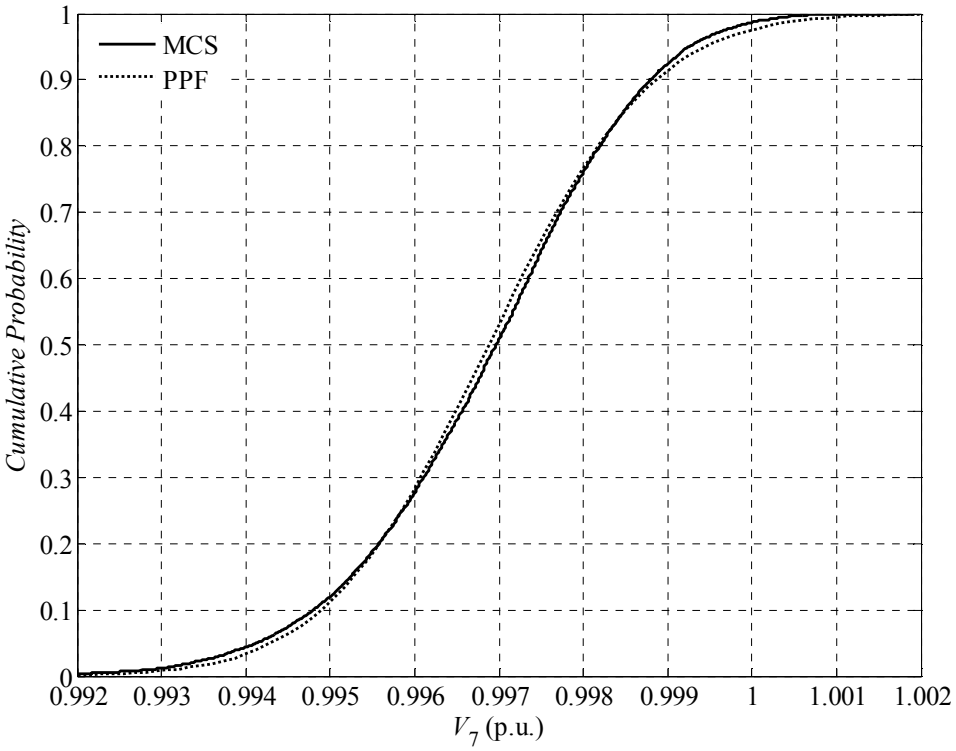

Figure 4-4 Cumulative distribution function of V_7

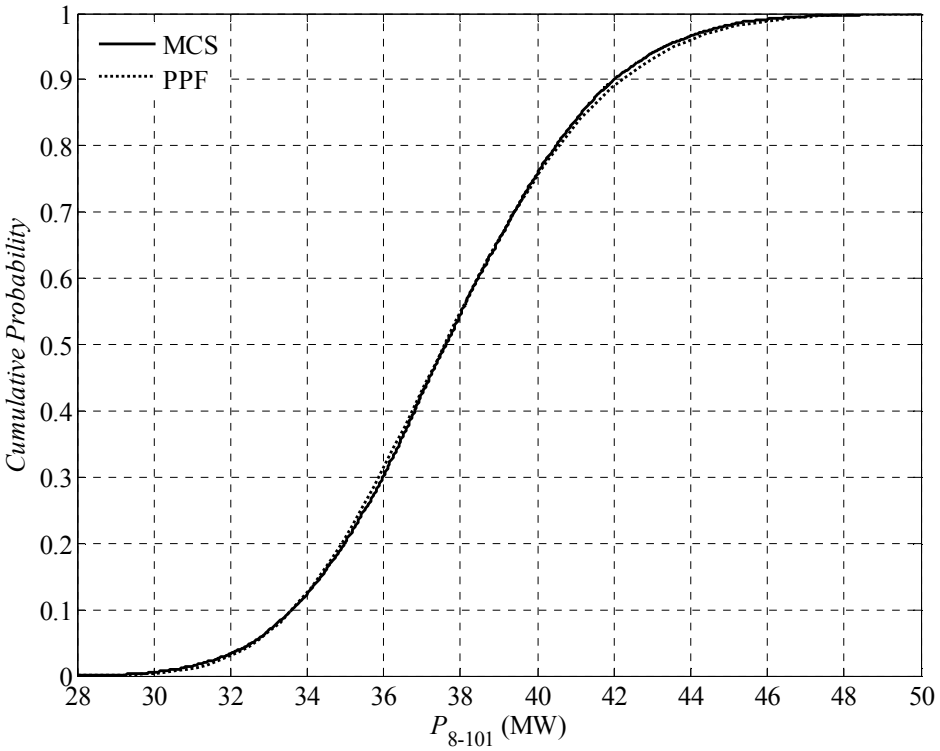

Figure 4-5 Cumulative distribution function of $P_{8\text{-}101}$

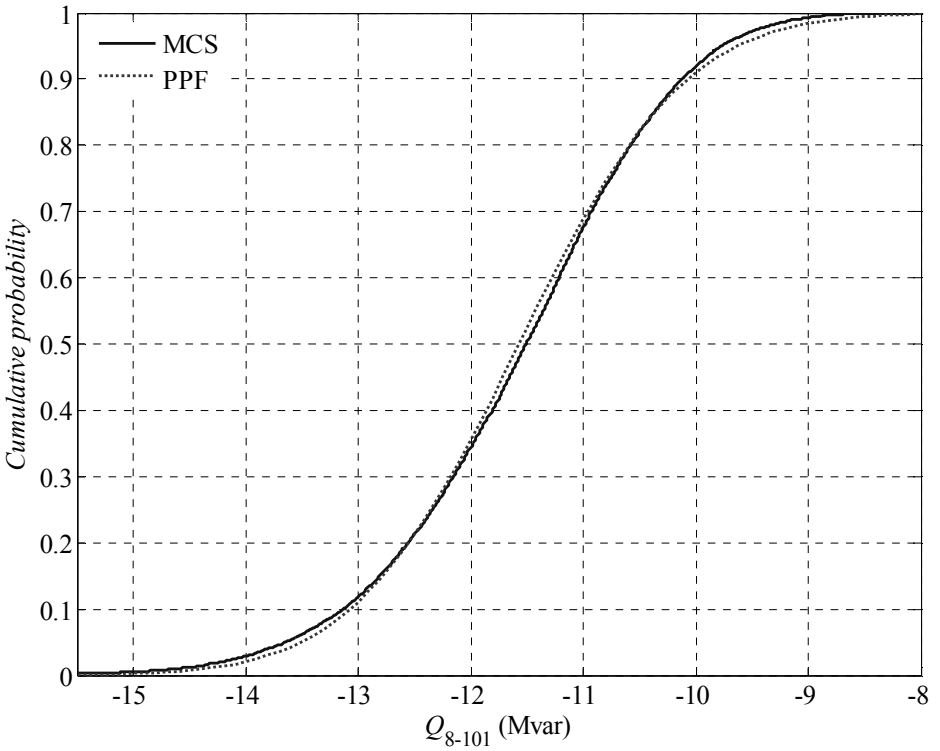

Figure 4-6 Cumulative distribution function of $Q_{8\text{-}101}$

For illustration purpose, the cumulative distribution functions of some bus voltages and branch power flows were plotted from Figure 4-4 to Figure 4-6. Up to 5th-order Cornish-Fisher series was employed to fit these curves, because it could perform better than the Gram-Charlier series when asymmetric probability distribution is included [97]-[99], e.g. the Weibull distribution in this case.

It can be seen that the empirical cumulative distribution curves obtained from MCS is approximated well by the results of PPF calculations, though the error increases a bit at the tail parts. Such error mainly results from both the PPF method itself and the proposed modelling methodology. In these three figures, the relative errors for the 90% quantile are 0.0060%, 0.4762% and 0.5929% respectively, while for the 10% quantile they are 0.0085%, 0.0499% and 0.3552%. The average relative errors for the 90% and 10% quantile of bus voltage magnitudes are 0.0071% and 0.0083% respectively, while the average relative errors of branch power flows are 2.315% and 2.984%. The average relative error of p% quantile is defined as

$$\frac{1}{N_{total}}\sum_{i=1}^{N_{total}}\left|\frac{q_{p\%,i}^{PPF}-q_{p\%,i}^{MCS}}{q_{p\%,i}^{MCS}}\right|\times 100\% \tag{4.29}$$

where $q_{p\%,i}^{PPF}$ is the p% quantile of bus i or branch i obtained from PPF;

$q_{p\%,i}^{MCS}$ is the p% quantile of bus i or branch i obtained from MCS;

N_{total} is the total number of buses or branches.

It should be noted that the voltage magnitude at connection bus 7 varies in a very small range, as shown in Figure 4-4. A similar phenomenon was observed at connection bus 8 as well. This is because the UKGDS-EHV5 system has abundant reactive power to support the bus

voltages by itself and feed the reactive power back to the IEEE 30-bus transmission system, e.g. Figure 4-6. In contrast, the charging demands drawn by the UKGDS system from the IEEE 30-bus system fluctuate widely, e.g. Figure 4-5 and Figure 4-6.

4.4.3 Impact of Correlation on Probabilistic Power Flow

In this subsection, the proposed technique in Section 4.3.3 will be applied in CM to calculate PPF in a modified IEEE 14-bus test system. This system includes 6 uncorrelated loads, 4 correlated loads, and 1 wind farm.

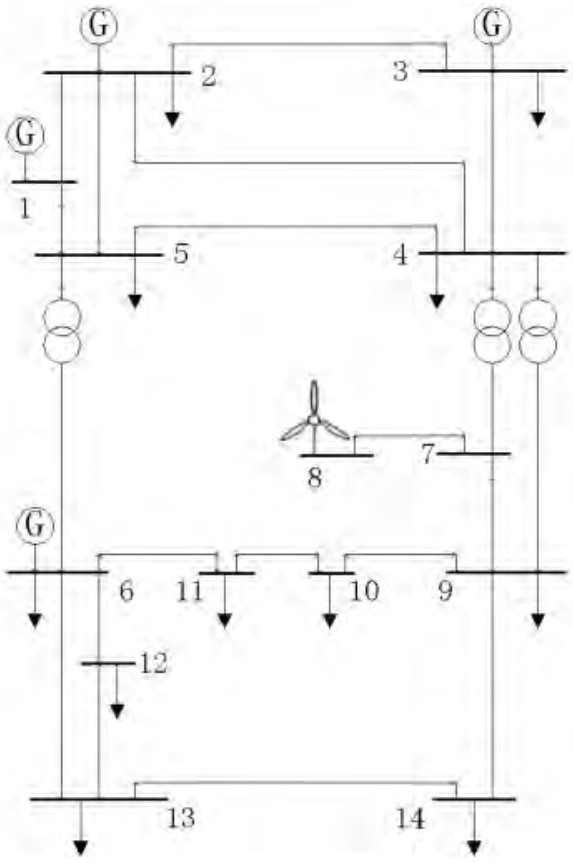

Figure 4-7 Modified IEEE 14-bus test system

The parameters of stochastic loads are given in Table 4-9 as follows

Table 4-9 Probabilistic Load Data in the IEEE 14-Bus Test System

(a) Gaussian Load Data

Bus ID	μ_P (MW)	σ_P/μ_P	μ_Q (Mvar)	σ_Q/μ_Q
2	21.7	0.18	12.7	0.184
5	7.6	0.10	1.6	0.10
6	11.2	0.12	7.5	0.126
10	9.0	0.20	1.6	0.20
11	3.5	0.19	1.8	0.19
12	6.1	0.152	1.6	0.172

(b) Lognormal Load Data

Bus ID	μ_P (MW)	σ_P/μ_P	μ_Q (Mvar)	σ_Q/μ_Q
3	94.2	0.20	19.0	0.21
4	47.8	0.22	-3.9	0.194
13	13.5	0.21	5.8	0.19
14	14.9	0.172	5.0	0.172

(c) Lognormal Load Correlation Coefficient

$$\begin{array}{c} \text{Bus ID} \\ 3 \\ 4 \\ 13 \\ 14 \end{array} \begin{array}{c} \begin{array}{cccc} 3 & 4 & 13 & 14 \end{array} \\ \begin{bmatrix} 1 & 0.24 & 0 & 0.18 \\ 0.24 & 1 & 0 & 0 \\ 0 & 0 & 1 & -0.09 \\ 0.18 & 0 & -0.09 & 1 \end{bmatrix} \end{array}$$

As shown in Figure 4-7, the wind farm is attached at bus 8, and its rated capacity is 80MW and its predicted power output is 20MW. According to Section 3.3, its power output is modelled as the Beta distribution with parameters a = 2 and b = 8. The probability density curve of the wind farm is plotted as follows

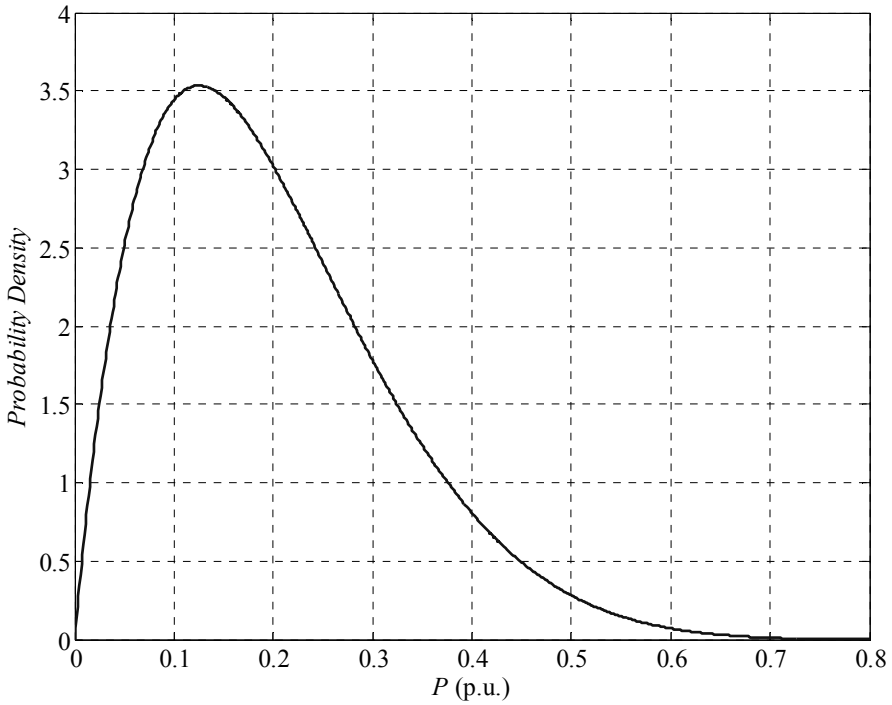

Figure 4-8 Probability density curve of wind farm power output at bus 8

The programs were implemented in MATLAB and run on a desktop PC with 2.4GHz Core 2 Duo CPU and 2GB DDR2-800 RAM.

MCS was also executed as a benchmark for accuracy. For the sake of simplicity, its sample capacity is set to be 10000, which is big enough for the convergence of simulations.

The samples of correlated loads are generated according to the way described in [173]:

The correlation coefficients of correlated lognormal loads are transformed through Nataf transformation [168] into that of correlated standard Gaussian variables; and then correlated standard Gaussian samples are generated from a multivariate Gaussian variable; finally these Gaussian samples are transformed through inverse Nataf transformation back into correlated lognormal samples.

The relative errors of mean, standard deviation, skewness and kurtosis obtained by CM in comparison with MCS are given in Table 4-10:

Table 4-10 Average Relative Error in Percentage

(a) Not Considering Correlation

Error	V_i	θ_i	P_i	Q_i	P_{ij}	Q_{ij}
ε_μ^* (%)	0.058	1.028	1.601	1.504	3.815	6.109
ε_σ^* (%)	2.032	2.127	3.038	4.791	6.201	9.253
ε_γ^* (%)	4.139	3.234	5.027	7.819	9.304	12.28
ε_κ^* (%)	6.215	7.261	9.314	11.23	15.52	18.03

(b) Considering Correlation

Error	V_i	θ_i	P_i	Q_i	P_{ij}	Q_{ij}
ε_μ^* (%)	0.028	0.241	0.371	0.248	1.521	1.097
ε_σ^* (%)	0.125	0.983	1.104	2.273	3.021	3.917
ε_γ^* (%)	1.217	1.098	2.064	2.981	3.508	4.668
ε_κ^* (%)	2.964	3.218	4.318	5.675	5.729	7.524

It can be seen that the proposed technique in Subsection 4.3.3 effectively helps CM to reduce errors when correlation is considered; while the errors of CM without consideration of correlation are obviously larger. For illustration purpose, the probability distribution curves of some bus voltage and branch flow are plotted in Figure 4-9 and Figure 4-10. Up to 5th-order Cornish-Fisher series was employed again to fit these curves.

As shown in these figures, the fitted curves with consideration of correlation give better approximation of the empirical distribution curves obtained from MCS, which indicates again the necessity of taking correlation into consideration during PPF calculations.

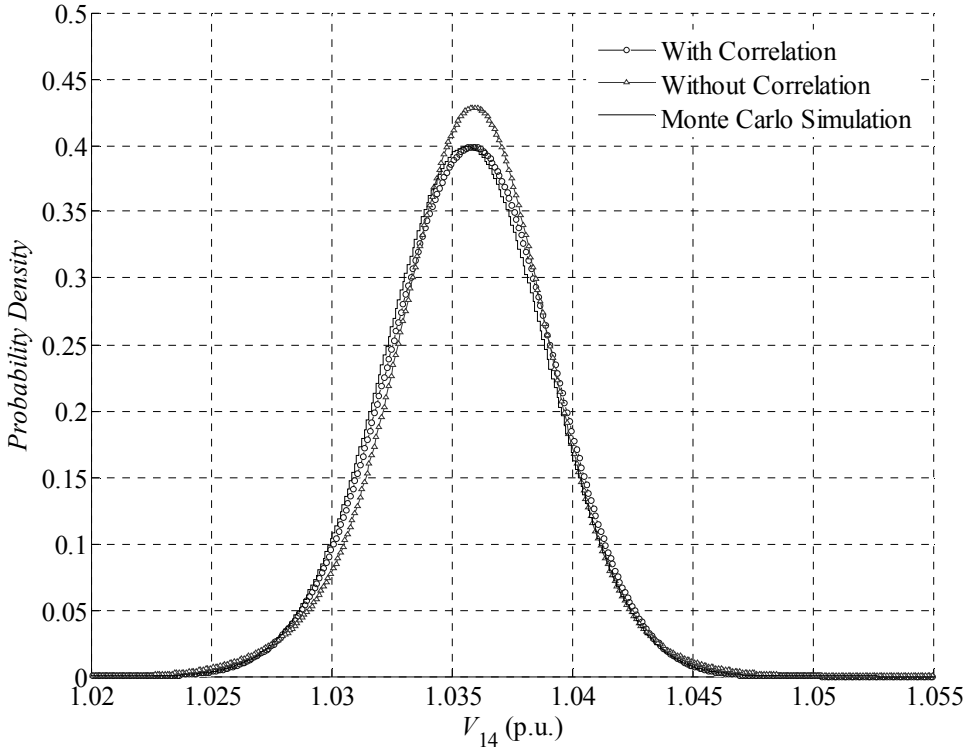

Figure 4-9 Probability density function of V_{14}

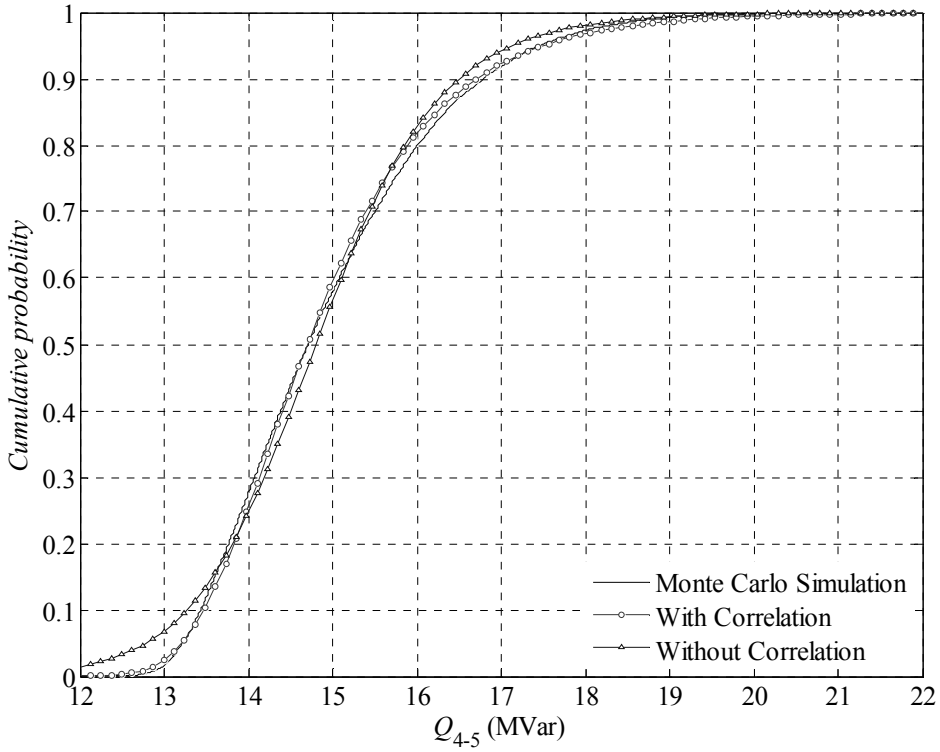

Figure 4-10 Cumulative distribution function of $Q_{4\text{-}5}$

As for the computational time, CM without consideration of correlation spent 0.032s, while CM with consideration of correlation spent 0.034s. In contrast, MCS spent 26.58s. Therefore, the proposed technique in Subsection 4.3.3 adds little burden to the computational efficiency of original CM.

4.5 Chapter Summary

This chapter first introduces the main features of three mainstream methods of PPF calculations, i.e. MCS, PEM and CM. Especially, a new technique is proposed in this chapter to improve CM so that it is able to take the correlation between stochastic system inputs into consideration.

In case studies, two cases are given to compare the accuracy and efficiency of these three PPF methods, and then the modelling methodology of overall charging demand of electric vehicles proposed in Section 3.4 are verified in another case study through PPF calculations by CM. Moreover, a case study is given to show the necessity of considering correlation in PPF calculations. The results validate the effectiveness of the proposed technique to treat correlation in CM.

CHAPTER 5 CHANCE-CONSTRAINED STOCHASTIC OPTIMAL POWER FLOW

5.1 Introduction

The AC optimal power flow (OPF) is essentially a nonlinear planning problem [105]. It is typically aimed at seeking a feasible power flow operating point by adjusting a set of control variables subject to certain physical, operational and policy constraints, so that the specified target can be optimal. Because it covers both economy and security of the power system, OPF has become an essential part of the power system toolbox and is widely used in the power industry.

Although a wide range of models have been developed over last decades, a classic optimal power flow is usually formulated as a deterministic optimization problem. Such deterministic optimal power flow (D-OPF) neither reveals the influences of the uncertainties such as load forecasting error or renewable generation fluctuation, nor provides information on the degree of importance or likelihood of constraint violations [106]. In contrast, stochastic optimal power (S-OPF) [115]-[119] describes these uncertainties as random distributions, and establishes a stochastic formulation of OPF, so that their influence can be incorporated into the OPF problem through chance constraints.

This chapter will present a heuristic approach to solve the chance-constrained S-OPF problem, considering Gaussian and non-Gaussian distributed system inputs, as well as the possible correlation between them. Such a solution approach starts from the result of a D-OPF problem obtained by the interior point method, and then converts all the chance constraints into

equivalent deterministic constraints through probabilistic power flow (PPF) calculations, and the satisfaction of these equivalent constraints are further verified. If some violation happens, the corresponding constraint bounds are adjusted according to a heuristic strategy and the D-OPF problem is solved again. This process is repetitively run until no constraint violation exists.

5.2 Mathematical Formulation

5.2.1 Deterministic Optimal Power Flow

A general D-OPF problem can be formulated as follows

$$\min_{\boldsymbol{u}} f(\boldsymbol{x},\boldsymbol{u}) \tag{5.1}$$

$$s.t. \quad g(\boldsymbol{x},\boldsymbol{u}) = \boldsymbol{0} \tag{5.2}$$

$$\boldsymbol{b}^{\min} \le \boldsymbol{b}(\boldsymbol{x},\boldsymbol{u}) \le \boldsymbol{b}^{\max} \tag{5.3}$$

$$\boldsymbol{u}^{\min} \le \boldsymbol{u} \le \boldsymbol{u}^{\max} \tag{5.4}$$

where:

1. $f : R^{n_1} \times R^{n_2} \to R$ is a scalar objective function to be minimized, which can be the generation cost, the real power network loss and so on.
2. $\boldsymbol{u} \in R^{n_1}$ is the vector of control variables to be adjusted in order to obtain the optimal objective function value. Control variables $\boldsymbol{u}$ in the power system usually consist of real power outputs and voltage magnitudes of generator buses, transformer tap ratios, capacities of shunt devices and so on. For simplicity, only real power outputs P_g and voltage magnitudes V_g at generator buses are considered in this chapter. As shown in Equation (5.4), control variables $\boldsymbol{u}$ could be also bounded due to certain physical limits or operational requirements, e.g. for the generator bus *i*,

$$\begin{cases} P_{g,i}^{\min} \le P_{g,i} \le P_{g,i}^{\max} \\ V_{g,i}^{\min} \le V_{g,i} \le V_{g,i}^{\max} \end{cases} \tag{5.5}$$

where i denotes generator bus i.

3. $\boldsymbol{x} \in R^{n_2}$ is the vector of dependent variables, which are determined by control variables $\boldsymbol{u}$. Dependent variables $\boldsymbol{x}$ in the power system typically include voltage magnitudes and angles at PQ buses, voltage angles and reactive power outputs at PV buses, real and reactive power outputs of slack buses, as well as branch power flows and so on.

4. $\boldsymbol{g}$ is the vector of equality constraint functions, and $\boldsymbol{g}(\boldsymbol{x}, \boldsymbol{u}) = \boldsymbol{0}$ denotes the power flow equations. The power flow model could be either AC or DC, depending on the requirement of the OPF problem. In this chapter, AC power flow model is employed, so Equation (5.2) in the polar coordinate form becomes

$$P_{g,i} - P_{d,i} - V_i \sum_j V_j [G_{ij} \cos(\theta_i - \theta_j) + B_{ij} \sin(\theta_i - \theta_j)] = 0 \tag{5.6}$$

$$Q_{g,i} - Q_{d,i} - V_i \sum_j V_j [G_{ij} \sin(\theta_i - \theta_j) - B_{ij} \cos(\theta_i - \theta_j)] = 0 \tag{5.7}$$

where $P_{g,i}$ is the specified real generation at bus i

$P_{d,i}$ is the specified real load at bus i

$Q_{g,i}$ is the specified reactive generation at bus i

$Q_{d,i}$ is the specified reactive load at bus i

G_{ij} is the conductance between bus i and j, i.e. the real part of Y_{ij}

B_{ij} is the susceptance between bus i and j, i.e. the imaginary part of Y_{ij}

5. $\boldsymbol{b}$ is the vector of inequality constraint functions with lower bound $\boldsymbol{b}^{\min}$ and upper bound $\boldsymbol{b}^{\max}$. Inequality constraints in the OPF problem typically include the limits of generator reactive capacities Q_g, branch current magnitudes $||I_{br}||$, and load bus voltage magnitudes V_d:

$$\begin{cases} Q_{g,i}^{\min} \le Q_{g,i} \le Q_{g,i}^{\max} \\ V_{d,j}^{\min} \le V_{d,j} \le V_{d,j}^{\max} \\ \left\| \widetilde{I}_{br,k} \right\| \le \widetilde{I}_{br,k}^{\max} \end{cases} \tag{5.8}$$

where i denotes generator bus i;

j denotes load bus j;

k denotes branch k.

5.2.2 Stochastic Optimal Power Flow

When uncertain system inputs are modelled as random variables, let $\boldsymbol{\xi}$ denote the stochastic vector of these system inputs. By explicitly incorporating $\boldsymbol{\xi}$ into the OPF formulation in Equations (5.1)-(5.4), we have

$$\min_{\boldsymbol{u}} f(\boldsymbol{x}, \boldsymbol{u}, \boldsymbol{\xi}) \tag{5.9}$$

$$s.t. \quad g(\boldsymbol{x}, \boldsymbol{u}, \boldsymbol{\xi}) = \boldsymbol{0} \tag{5.10}$$

$$\boldsymbol{b}^{\min} \le \boldsymbol{b}(\boldsymbol{x}, \boldsymbol{u}, \boldsymbol{\xi}) \le \boldsymbol{b}^{\max} \tag{5.11}$$

$$\boldsymbol{u}^{\min} \le \boldsymbol{u} \le \boldsymbol{u}^{\max} \tag{5.12}$$

In this chapter, the stochastic vector $\boldsymbol{\xi}$ includes uncertain loads and wind farm generation outputs.

According to Section 3.2.1, an uncertain load is typically modelled as the Gaussian distribution. According to Section 3.3.3, the uncertain generation output of a wind farm is modelled as the Beta distribution due to the bounded nature of wind generation. Moreover, the potential correlation between these random system inputs is also considered.

Due to the incorporation of stochastic system inputs $\boldsymbol{\xi}$, the objective function f in Equation (5.9) becomes a stochastic function, so it cannot be predicted what its minimization result would be. A natural idea is to employ the expected value of the objective function:

$$\min_{\boldsymbol{u}} \underset{\boldsymbol{\xi}}{E}\left[f(\boldsymbol{x},\boldsymbol{u},\boldsymbol{\xi})\right] \tag{5.13}$$

On the other hand, constraint functions $\boldsymbol{g}$ and $\boldsymbol{b}$ are stochastic functions as well. According to stochastic optimization theory [120], since $\boldsymbol{g}$ and $\boldsymbol{b}$ do not define a deterministic feasible set, it is desired that the corresponding constraints hold with a certain probability, i.e. becoming the so called chance constraints. However, the equality constraints in Equation (5.10), i.e. the power flow equations, should always be tenable to assure a feasible system operating point, so only inequality constraints in Equation (5.11) are changed into chance constraints:

$$\begin{cases} \Pr\{\boldsymbol{b}(\boldsymbol{x},\boldsymbol{u},\boldsymbol{\xi}) \le \boldsymbol{b}^{\max}\} \ge \boldsymbol{p}^{\max} \\ \Pr\{\boldsymbol{b}(\boldsymbol{x},\boldsymbol{u},\boldsymbol{\xi}) \ge \boldsymbol{b}^{\min}\} \ge \boldsymbol{p}^{\min} \end{cases} \tag{5.14}$$

where $\boldsymbol{p}^{\max}$ is the constraint probability value corresponding to the upper bound of $\boldsymbol{b}$

$\boldsymbol{p}^{\min}$ is the constraint probability value corresponding to the lower bound of $\boldsymbol{b}$.

By combining Equations (5.10), (5.12)-(5.14), the chance-constrained S-OPF formulation could be given as follows

$$\min_{\boldsymbol{u}} \underset{\boldsymbol{\xi}}{E}\left[f(\boldsymbol{x},\boldsymbol{u},\boldsymbol{\xi})\right] \tag{5.15}$$

$$s.t. \quad g(\boldsymbol{x},\boldsymbol{u},\boldsymbol{\xi}) = \boldsymbol{0} \tag{5.16}$$

$$\begin{cases} \Pr\{\boldsymbol{b}(\boldsymbol{x},\boldsymbol{u},\boldsymbol{\xi}) \le \boldsymbol{b}^{\max}\} \ge \boldsymbol{p}^{\max} \\ \Pr\{\boldsymbol{b}(\boldsymbol{x},\boldsymbol{u},\boldsymbol{\xi}) \ge \boldsymbol{b}^{\min}\} \ge \boldsymbol{p}^{\min} \end{cases} \tag{5.17}$$

$$\boldsymbol{u}^{\min} \le \boldsymbol{u} \le \boldsymbol{u}^{\max} \tag{5.18}$$

5.3 Heuristic Solution Approach

5.3.1 Overall Procedure

According to Equation (5.16), because $\boldsymbol{x}$ is an implicit non-linear function of $\boldsymbol{u}$ and $\boldsymbol{\xi}$, it is difficult to directly obtain the analytic expression of $\boldsymbol{x}$ or its derivatives with respect to $\boldsymbol{u}$ or $\boldsymbol{\xi}$, which makes the derivative-based classic methods of OPF solution, e.g. the category of Kuhn-Tucker methods [120], inapplicable. Therefore, a heuristic solution approach to the chance-constrained S-OPF problem described in Equations (5.15)-(5.18) is presented in this section. Its overall procedures can be described as follows:

1. Based on the assumption that the variation of $\boldsymbol{\xi}$ is not significant, the essential idea of the proposed heuristic solution approach is to search the optimal solution of the S-OPF problem in the neighbourhood of that of a corresponding D-OPF problem as follows:

$$\min_{\boldsymbol{u}} \ f(\boldsymbol{x}, \boldsymbol{u}, \bar{\boldsymbol{\xi}}) \tag{5.19}$$

$$s.t. \quad g(\boldsymbol{x}, \boldsymbol{u}, \bar{\boldsymbol{\xi}}) = \boldsymbol{0} \tag{5.20}$$

$$\boldsymbol{b}^{\min} \le \boldsymbol{b}(\boldsymbol{x}, \boldsymbol{u}, \bar{\boldsymbol{\xi}}) \le \boldsymbol{b}^{\max} \tag{5.21}$$

$$\boldsymbol{u}^{\min} \le \boldsymbol{u} \le \boldsymbol{u}^{\max} \tag{5.22}$$

   where $\bar{\xi} = E(\xi)$.

   Such a D-OPF problem can be solved by any derivative-based OPF methods, and the primal-dual interior point method described in [174] is adopted here to produce the values of control variables $\boldsymbol{u}^*$.

2. Once the solution of the above D-OPF problem is ready, PPF is calculated with $\boldsymbol{u} = \boldsymbol{u}^*$ to obtain the probability distributions of inequality constraint functions $\boldsymbol{b}$, so that the chance

constraints in Equation (5.17) can be verified. The CM method in Section 4.3 is employed here.

3. If a certain chance constraint in Equitation (5.17) is violated, corresponding constraint bounds $\boldsymbol{b}^{\max}$ or $\boldsymbol{b}^{\min}$ would be adjusted, and then the above D-OPF problem described in Equations (5.19)-(5.22) is solved again with the updated constraint bounds in Equation (5.21).

The above process is repetitively executed until there is no violation of any chance constraint. If this is achieved, the corresponding sequence of control variable values is considered convergent. Clearly, there will be some loss on optimality. Detailed analysis of conditions, which are sufficient for the convergence and deriving bounds on the loss on optimality, is left for further research work. However, the proposed approach will validated by application to two case-study power systems in Section 5.4.

More details on two key points, i.e. the verification of chance constraints and the adjustment of corresponding constraint bounds, will be addressed in next two subsections.

5.3.2 Equivalence of Chance Constraint

The typical chance constraints in Equation (5.17) can be given in more details as follows

$$\begin{cases} \Pr\{Q_{g,i} \le Q_{g,i}^{\max}\} \ge p_{Q_{g,i}}^{\max} \\ \Pr\{Q_{g,i} \ge Q_{g,i}^{\min}\} \ge p_{Q_{g,i}}^{\min} \\ \Pr\{V_{d,j} \le V_{d,j}^{\max}\} \ge p_{V_{d,j}}^{\max} \\ \Pr\{V_{d,j} \ge V_{d,j}^{\min}\} \ge p_{V_{d,j}}^{\min} \\ \Pr\{\left\|\widetilde{I}_{br,k}\right\| \le \widetilde{I}_{br,k}^{\max}\} \ge p_{I_{br,k}}^{\max} \end{cases} \tag{5.23}$$

where i denotes generator bus i;

j denotes load bus j;

k denotes branch k.

For simplicity, the above chance constraints are represented in a unified form as follows

$$\begin{cases} \Pr\{x_i \le x_i^{\max}\} \ge p_{x_i}^{\max} \\ \Pr\{x_i \ge x_i^{\min}\} \ge p_{x_i}^{\min} \end{cases} \tag{5.24}$$

where x_i denotes the i-th constrained dependent variable;

$p_{x_i}^{\max}$ is the constraint probability value corresponding to the upper bound of x_i;

$p_{x_i}^{\min}$ is the constraint probability value corresponding to the lower bound of x_i.

The cumulative distribution function of x_i, i.e.

$$P_{x_i}(x) = \Pr\{x_i \le x\} \tag{5.25}$$

can be usually approximated by substituting its cumulants obtained through PPF calculations into the Gram-Charlier series [116]. However, it has been identified in [97]-[99] that the Cornish-Fisher series performs better than the Gram-Charlier series does when non-Gaussian distributions, e.g. the random distribution of a wind farm generation output, are considered. Therefore, here up to 5th order Cornish-Fisher series are employed.

The Cornish-Fisher series provide an approximation of the quantile function of x_i through its cumulants. The quantile function is actually the inversion of the monotone increasing cumulative distribution function, so the chance constraints in Equation (5.24) can be converted into an equivalent form:

$$\begin{cases} Q_{x_i}(p_{x_i}^{\max}) \le x_i^{\max} \\ Q_{x_i}(1-p_{x_i}^{\min}) \ge x_i^{\min} \end{cases} \tag{5.26}$$

where $Q_{x_i}(p) = P_{x_i}^{-1}(p)$ is the quantile function of x_i.

Such an equivalent conversion of the chance constraints from Equation (5.24) to Equation (5.26) brings an extra benefit that the bounds of x_i are moved out to the right-hand side of the inequalities, which makes further adjustment to them easy if any constraint violation occurs.

5.3.3 Adjustment of Constraint Bound

A heuristic strategy is applied to adjust the constraint bounds in Equation (5.26) when a certain violation occurs:

1. If $Q_{x_i}(p_{x_i}^{\max}) > x_i^{\max}$, then

$$x_i^{\max} = x_i^{\max} \cdot \max\{1 - \frac{Q_{x_i}(p_{x_i}^{\max}) - x_i^{\max}}{x_i^{\max}}, 1-\alpha\} \tag{5.27}$$

2. If $Q_{x_i}(1-p_{x_i}^{\min}) > x_i^{\min}$, then

$$x_i^{\min} = x_i^{\min} \cdot \min\{1 + \frac{x_i^{\min} - Q_{x_i}(p_{x_i}^{\min})}{x_i^{\min}}, 1+\alpha\} \tag{5.28}$$

The essential thought of the above adjustment is to shrink the corresponding boundary of the feasible set according to the extent of bound violation. However, in some circumstances, large extend of bound violation could lead to unreasonable adjustment. Therefore, in order to avoid this, a limit value α is applied to Equations (5.27)-(5.28). For constrained variables V_d, Q_g and $||I_{br}||$ in Equation (5.23), α is set to be 5%, 10% and 20% respectively.

5.3.4 Flowchart of Heuristic Solution Approach

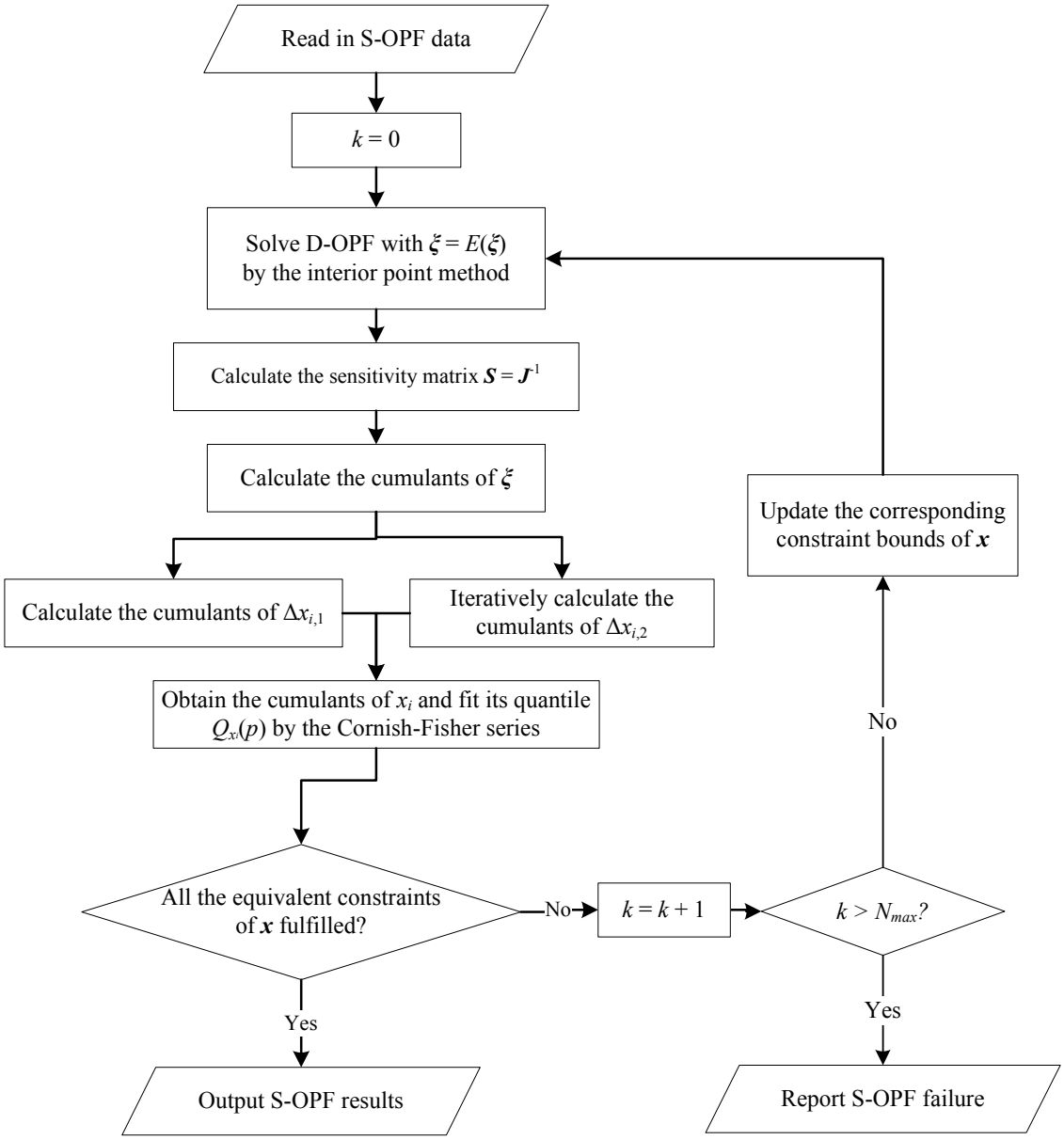

Figure 5-1 Computational procedure of the proposed S-OPF approach

The computational procedures of the proposed heuristic approach for chance-constrained S-OPF are concluded in the Figure 5-1, where k is the total iteration count, and N_{max} is the allowed maximum iteration count:

5.4 Case Studies

The proposed heuristic S-OPF approach was implemented in MATLAB v7.13 with the open source toolbox MATPOWER v4.1 [175]. All the tests were conducted on a desktop PC with a 2.53GHz Core 2 Duo CPU and 3GB DDR2-800 RAM.

The first test system is a 5-bus system [114] shown in Figure 5-2 as follows:

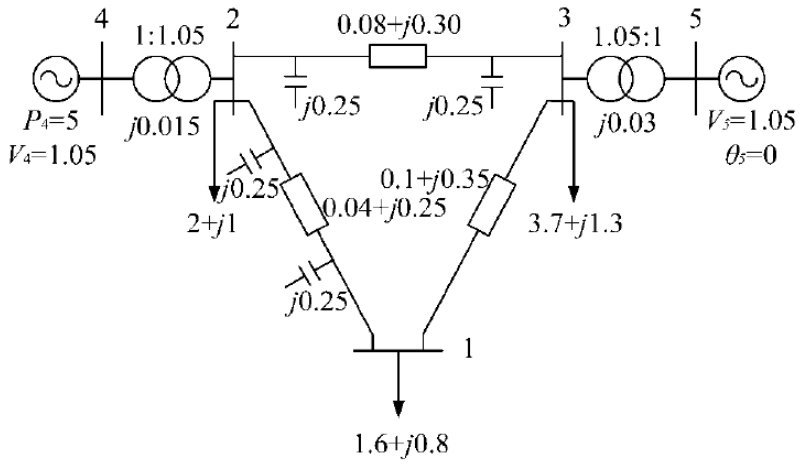

Figure 5-2 Network diagram of a 5-bus system

Each generator in this system is assumed to have a quadratic generation cost curve and the objective function is to minimize the total generation cost, i.e.

$$\min \sum_{i=4,5} (c_{2,i} P_{g,i}^2 + c_{1,i} P_{g,i} + c_{0,i}) \tag{5.29}$$

where the cost coefficients $c_{2,i}$, $c_{1,i}$ and $c_{0,i}$ of each generator are listed in Table 5-1:

Table 5-1 Generator Cost Coefficients

Bus i	$c_{2,i}$ ($/MW^2)	$c_{1,i}$ ($/MW)	$c_{0,i}$ ($)
4	50.4395	200.4335	1200.6485
5	200.55	500.746	1857.201

Both generators have a capacity of 800MW and a minimal real output of 100MW. On the other hand, the upper and lower bounds of voltage magnitudes are 0.90p.u. and 1.10p.u. at load buses, and 0.95p.u. and 1.10p.u. at generator buses, respectively. The upper limits of branch currents are chosen as 125% of the power flow in the base case. Loads are modelled as correlated Gaussian distributions with a variation coefficient of 3% and a correlation coefficient ρ = 0.3 or 0.5. The constraint probability for chance constraints in Equation (5.23) is set to be 0.95. The convergence tolerance of power flow is 1e-6p.u. and the tolerance for constraint violation is 0.5e-5p.u..

The S-OPF solution converged after 2 iterations and the results are listed in Table 5-2:

Table 5-2 Results Comparison between S-OPF and D-OPF

OPF	S-OPF			D-OPF
ρ	0	0.3	0.5	
Total cost ($)	7907.98	7939.80	7960.92	7703.20
V_1 (p.u.)	0.9132	0.9144	0.9151	0.90
V_2 (p.u.)	1.0987	1.0980	1.0983	1.10
V_3 (p.u.)	1.0888	1.0895	1.0900	1.0818
V_4 (p.u.)	1.0654	1.0649	1.0646	1.0697
V_5 (p.u.)	1.10	1.10	1.10	1.10
$P_{g,4}$ (MW)	502.38	496.74	493.15	550.56
$P_{g,5}$ (MW)	254.29	258.97	261.96	215.68
$Q_{g,4}$ (Mvar)	152.32	149.78	148.21	177.80
$Q_{g,5}$ (Mvar)	239.69	237.49	236.12	261.94

It can be seen in Table 5-2 that the total generation cost of S-OPF is about 2.6%-3.3% higher than that of D-OPF, resulting from the influence of uncertainties. In contrast, the margins of control variables V_4 and $P_{g,4}$ as well as dependent variables V_1, $Q_{g,4}$ and $Q_{g,5}$ are larger in S-OPF, which leaves more possibility of further adjustment to the system operation. On the other

hand, the total generation cost increases as the correlation coefficient ρ increases, which indicates the necessity of taking correlation into consideration.

Figure 5-3 illustrates the difference between the probability density curves of V_1 when $\rho = 0$ and 0.5 respectively.

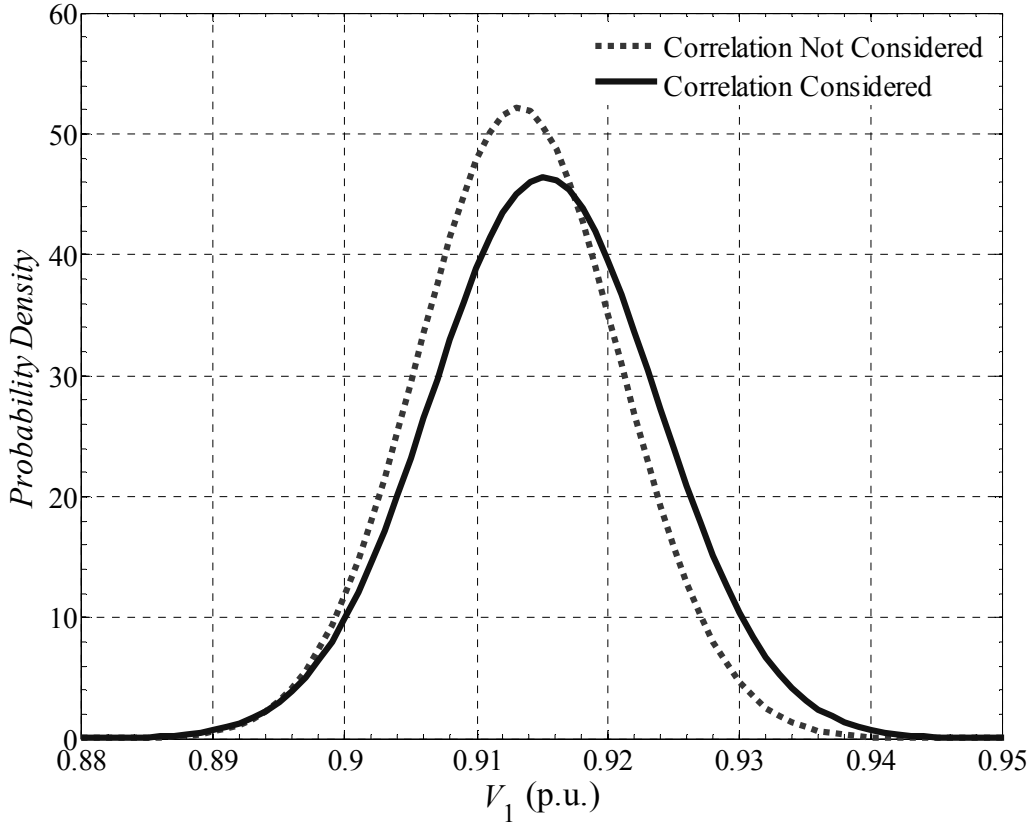

Figure 5-3 Probability density curve of the voltage magnitude at bus 1

According to Figure 5-3, V_1 varies in a larger range when loads are positively correlated. Similar phenomena are also observed in the branch flows, e.g. as Figure 5-4 shows.

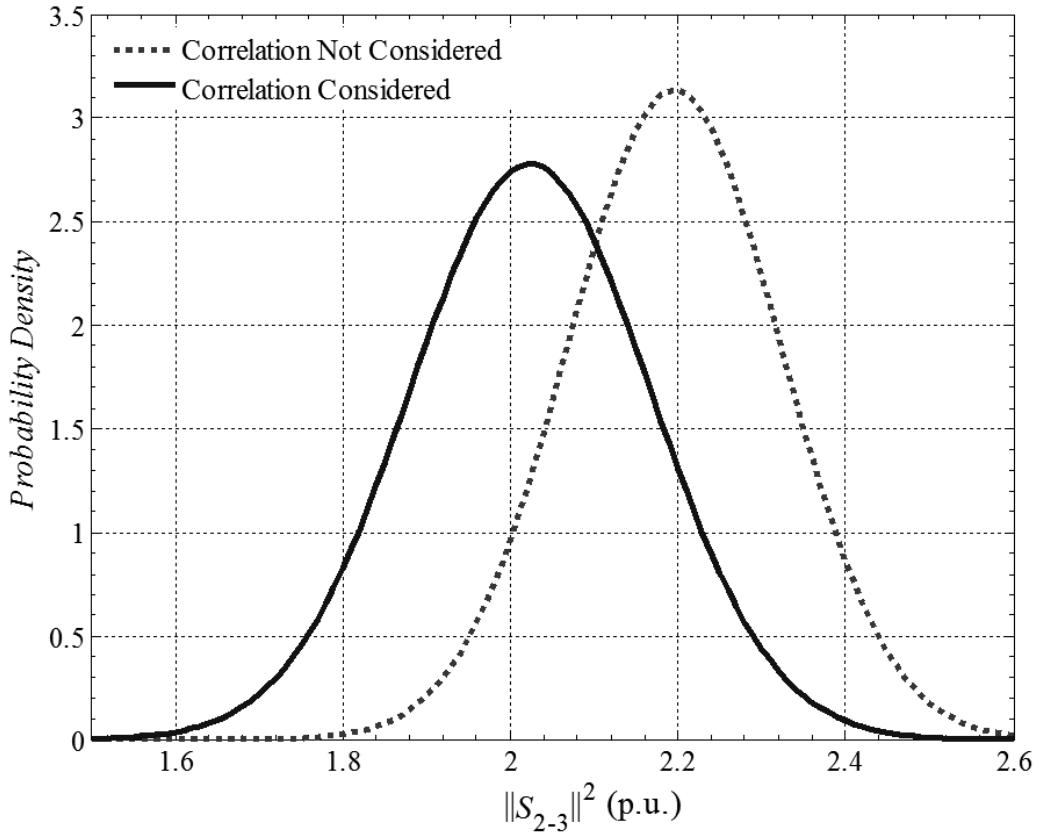

Figure 5-4 Probability density curve of the apparent power flow in branch 2-3

The second test system is a modified IEEE 118-bus system [98], in which wind generation is included with a significant penetration level of about 18.89%. The diagram of this test system is shown in Figure 5-5, where three groups of wind farms depicted in solid rectangles are integrated into this system.

In order to maintain the system load level, the wind power has substituted the conventional generation, which has been reduced proportionally. The detailed data of the wind generation are given in Table 5-3.

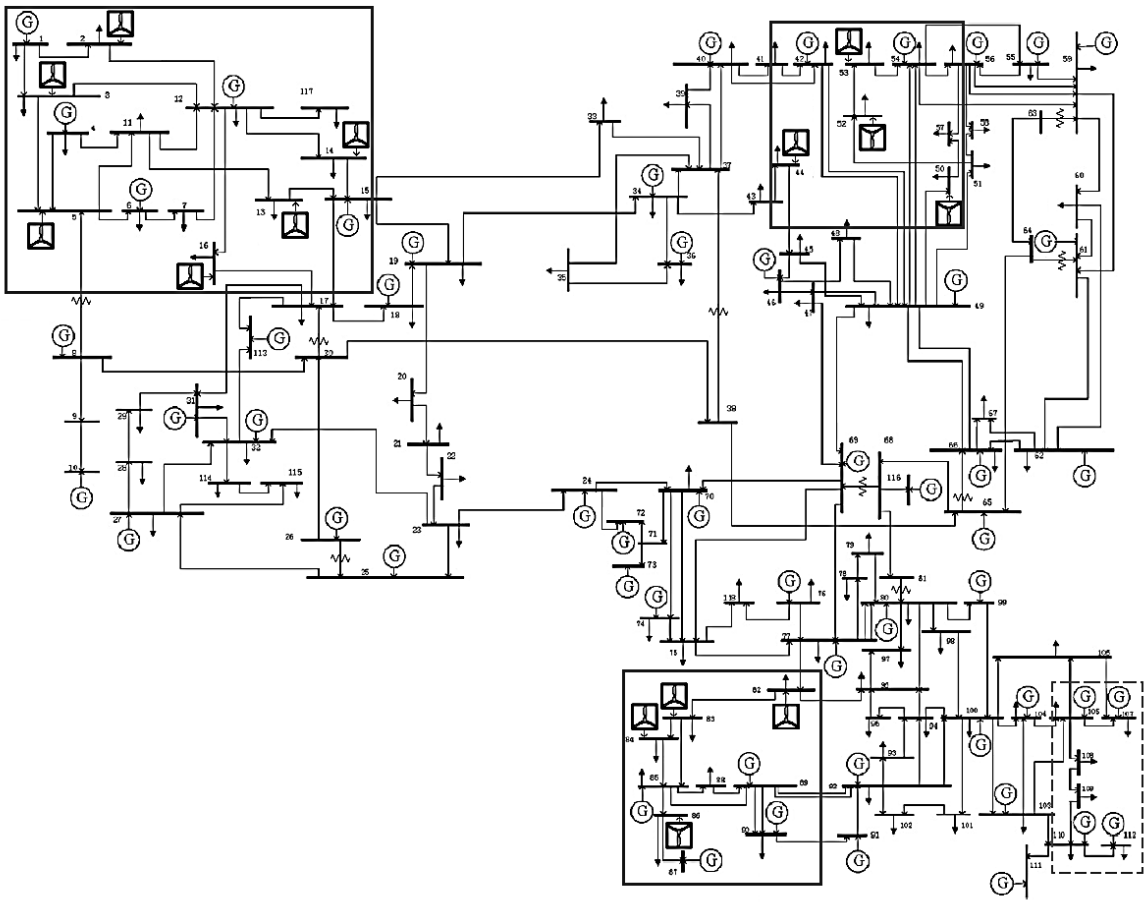

Figure 5-5 Network diagram of modified IEEE 118-bus system

Table 5-3 Wind Farm Data included in Modified IEEE 118-Bus System

Wind Farm	Bus	Group	Wind Power (MW)	Standard Deviation (MW)	Rated Power (MW)
1	52	1	59.3	25.6	98
2	44	1	31	13.2	51
3	53	1	14.8	6.48	25
4	50	1	8.5	3.66	14
5	84	2	20.1	9.4	36
6	86	2	17	7.2	28
7	83	2	33	15.11	58
8	82	2	50.3	20.84	82
9	2	3	33	14.1	55
10	5	3	20	9.4	36
11	16	3	27	11.2	44
12	13	3	37.5	16.1	62
13	3	3	27	10.5	42
14	14	3	37.5	16.1	62

The wind generation shown above is the forecasted production. The total installed wind power is 693MW. The forecasted wind generation in this situation, 416MW, is 60% of the rated wind power. Thus, it can be seen from the values of their standard deviations that the actual wind generation outputs may differ widely from the forecasted values.

In Table 5-3, the groups of wind farms with correlated generation outputs are shown, but wind farms belonging to different groups are considered uncorrelated. The uncertainties of wind farm generation outputs are modelled as correlated Beta distributions. Correlation coefficients between the wind farms of the same groups are also given:

$$\underset{\text{Group1}}{\begin{bmatrix} 1 & 0.38 & 0.47 & 0.41 \\ 0.38 & 1 & 0.45 & 0.47 \\ 0.47 & 0.45 & 1 & 0.55 \\ 0.41 & 0.47 & 0.55 & 1 \end{bmatrix}} \quad \underset{\text{Group2}}{\begin{bmatrix} 1 & 0.72 & 0.65 & 0.6 \\ 0.72 & 1 & 0.65 & 0.68 \\ 0.65 & 0.65 & 1 & 0.59 \\ 0.6 & 0.68 & 0.59 & 1 \end{bmatrix}} \quad \underset{\text{Group3}}{\begin{bmatrix} 1 & 0.35 & 0.46 & 0.23 & 0.32 & 0.21 \\ 0.35 & 1 & 0.28 & 0.33 & 0.19 & 0.22 \\ 0.46 & 0.28 & 1 & 0.25 & 0.15 & 0.17 \\ 0.23 & 0.33 & 0.25 & 1 & 0.19 & 0.21 \\ 0.32 & 0.19 & 0.15 & 0.19 & 1 & 0.22 \\ 0.21 & 0.22 & 0.17 & 0.21 & 0.22 & 1 \end{bmatrix}}$$

The coefficients have been chosen to be purposely low, in order to show that even in this case it is still necessary to consider correlation.

On the other hand, the uncertainties of forecasted loads are modelled as Gaussian distributions, whose mean values are equal to the base case data while their variation coefficients are set arbitrarily as follows [101]: 7% from bus 1 to bus 33, 4% from bus 34 to bus 59, 9% from bus 60 to bus 79, and 5% from bus 80 to bus 118. It has been considered that the loads at four buses (107, 108, 109, and 110) in the dash rectangle are correlated with a correlation matrix:

$$\begin{bmatrix} 1 & 0.3 & 0.4 & 0.25 \\ 0.3 & 1 & 0.64 & 0.3 \\ 0.4 & 0.64 & 1 & 0.29 \\ 0.25 & 0.3 & 0.29 & 1 \end{bmatrix}$$

As for the parameters of OPF, the control variables are simply the real generation outputs and voltage magnitudes of generator buses; the objective function is the total generation cost ($/hour); each generator is supposed to have a quadratic cost curve; the voltage magnitudes at load buses are all bounded between 0.96p.u. and 1.06p.u.. Detailed information can be found in MATPOWER sample cases [175].

On the other hand, the constraint probability of the chance constraints in Equation (5.23) is set to be 0.95. Moreover, the convergence tolerance for power flow is 1e-6p.u. and the tolerance for constraint violation is 0.5e-5p.u..

The S-OPF solution converged at 113420.28$/h after 7 iterations and iteration information about total cost and constraint violation is listed in the following table:

Table 5-4 Iteration Information during S-OPF Solution

Iteration	Total Cost ($/h)	Number of Constraint Violations		
		V_d	Q_g	$\|\|I_{br}\|\|$
1	113329.95	4	13	1
2	113375.16	1	4	1
3	113415.39	2	3	1
4	113419.37	1	1	1
5	113420.15	1	0	1
6	113420.27	0	0	1
7	113420.28	0	0	0

As shown in Table 5-4, due to the influence of uncertainty, the total generation cost is slightly larger than that of the D-OPF problem with all random system inputs set at their mean values.

On the other hand, the S-OPF problem without the correlation among wind farms and loads was also solved, and the total generation cost is 113381.58$/h after 6 iterations.

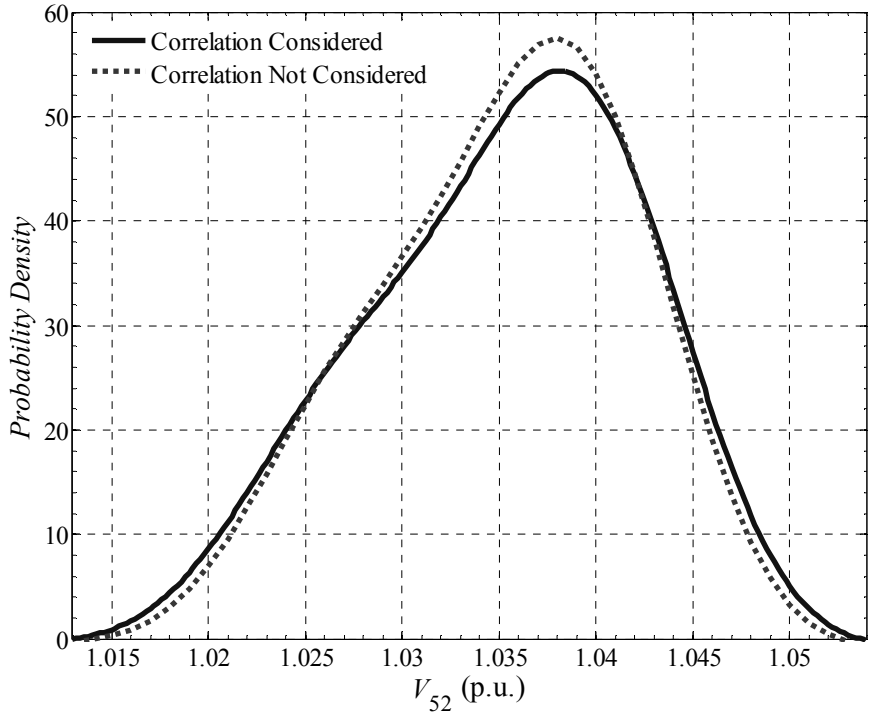

Figure 5-6 Probability density curve of the voltage magnitude at bus 52

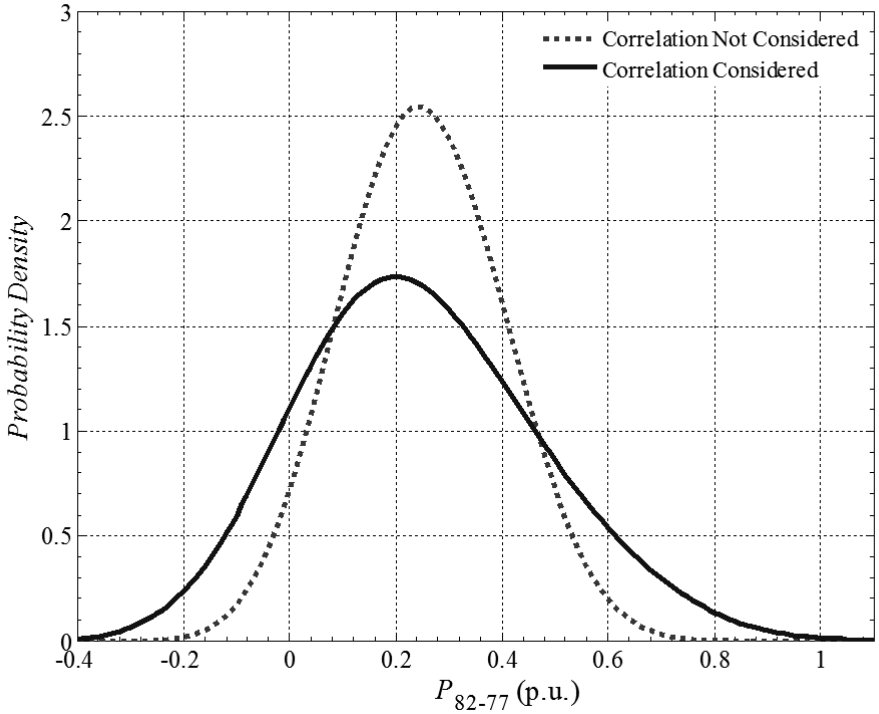

Figure 5-7 Probability density curve of the real power flow in branch 82-77

In Figure 5-6 and Figure 5-7, the probability density curves of a bus voltage magnitude and a branch power flow near the wind farms under different situations are compared: It can be seen that the influence of correlation is apparent, and such influence becomes more significant in the neighbourhood of the wind farms. This indicates again the necessity of considering the correlation between random system inputs in the S-OPF problem. Moreover, the bus voltages and branch power flows tend to be asymmetric due to the influence of the asymmetric distributed wind farm generation outputs.

Moreover, the S-OPF problems with different constraint probabilities of chance constraints were also tested, and the results are listed in Table 5-5:

Table 5-5 Results Comparison under Different Constraint Probabilities

Constraint Probability	Total Iteration	Total Cost ($/h)
0.90	6	113393.68
0.91	9	113399.54
0.92	14	113402.56
0.93	10	113407.74
0.94	8	113413.57
0.95	7	113420.28
0.96	8	113428.25
0.97	9	113438.14
0.98	9	113451.43
0.99	10	113472.58

As shown in Table 5-5, the iteration count tends to be irregular with the constraint probability. In contrast, the total real generation cost increases as the constraint probability increases.

The impact of the system input variation on the S-OPF problem was also investigated, where the variation coefficients of all the Gaussian loads were increased gradually to 1.5 times as large as their original values, and the results are listed in Table 5-6. It can be seen that both the iteration count and the total real generation cost increase as the variation of stochastic

loads become larger. The reason that the total real generation cost only increase slightly is because the real capacity of the modified IEEE 118-bus system is adequate (5400MW in total) to handle the variation of the loads (4242MW in total).

Table 5-6 Results Comparison under Different Load Variation Coefficients

Variation Coefficient (%)	Total Iteration	Total Cost ($/h)
100	7	113420.28
110	8	113421.02
120	8	113421.82
130	9	113422.69
140	9	113423.63
150	10	113424.63

5.5 Chapter Summary

In this chapter, a heuristic solution approach has been proposed for the chance-constrained S-OPF problem, which is able to not only incorporate non-Gaussian distributed system inputs, e.g. the generation outputs of wind farms, but also handle the possible correlation between any random system inputs.

Case studies have indicated the effectiveness and good convergence of the proposed S-OPF approach. However, because this approach still searches the optimal results in the neighbourhood of that of a corresponding D-OPF problem, it could not assure the global optimality of the obtained results. Therefore, this issue needs further investigation and improvement in future.

CHAPTER 6 RESEARCH SUMMARY

6.1 Conclusion and Contribution

Nowadays, stochastic analysis and optimization of the power system is more and more important as renewable energy and electric vehicles are developing fast and integrated into the power grids, because these new sources and loads tend to be highly uncertain. This research covers three levels of stochastic analysis and optimization of power system steady-state, i.e. modelling, algorithm, and optimization:

1. Because it has to factorize the Jacobian matrix at each iteration, the time efficiency of the conventional Newton-Raphson (NR) power flow is relatively low. Although the Fast Decouple (FD) power flow is a good substitute for the NR power flow in a lot of case, its applicability is still limited by some assumptions, e.g. the low R/X ratio of branches. Therefore, the Accelerated Newton-Raphson (ANR) power flow has been proposed in this study as an alternative. It combines the constant Jacobian matrix and a correction multiplier of the power mismatch vector, so that the time efficiency is improved without sacrificing convergence robustness. Numerical results have shown that the ANR power flow has super-linear convergence characteristics and achieves a speed-up of up to about 50% in comparison to the NR power flow. Moreover, the convergence of the ANR power flow is not influenced by the R/X ratio of branches. However, when the loading level of the power system is high, it is suggested to fix the Jacobian matrix after 1 or 2 full Newton iterations, in order to ensure the convergence.

2. As the fast popularisation of electric vehicles, their charging demand is becoming an important part of the system load. Due to the uncertainty existing in the factors that influence

their charging behaviour, the overall charging demand of electric vehicles tends to be uncertain. Therefore, a methodology has been established in this study to model the overall charging demand of electric vehicles in a certain area. Such a modelling methodology takes key factors that determine the charging behaviour of electric vehicles into consideration, and run a stochastic simulation of electric vehicle charging process. The probability model of their charging demand is then obtained through statistical analysis of the simulation results. Using this modelling methodology, the charging demand of electric vehicles in two typical scenarios, i.e. at an electric vehicle charging station and in a local residential community, have been identified as the Weibull distribution and the Gaussian distribution, respectively. These probability distributions can be further employed in probabilistic power flow or stochastic optimal power flow to evaluate the impact of electric vehicle charging on the power system.

3. According to the comparison study of three mainstream methods of probabilistic power flow (PPF) calculations, the Cumulant Method (CM) is the fastest one because the deterministic power flow is calculated only once. In contrast, the Monte Carlo Simulation (MCS) requires a large number of deterministic power flow calculations to obtain meaningful statistical results. The Point Estimate Method (PEM) reduces the number of deterministic power flow calculations to be proportional to the number of random system inputs, but as the scale of the power system increases, it gradually loses time efficiency. However, the CM relies on the assumption that random system inputs are independent with each other, which could be unrealistic especially for renewable generation. Therefore, the CM has been improved in this study to take the possible correlation between random system inputs into consideration, where the part of system state variables and outputs corresponding to correlated system inputs are iteratively accumulated from them. Numerical results have indicated the accuracy and efficiency of the improved CM in comparison with MCS and PEM. It is also

identified that the necessity of considering correlation, otherwise it could lead to negative effects on the result of PPF calculations. However, because the CM is based on linearized power flow equations, the variation of random system inputs should be not too large, i.e. their variation coefficient should empirically be less than 20%.

4. In comparison to deterministic optimal power flow (D-OPF), stochastic optimal power flow (S-OPF) is more suitable when the uncertainty of system inputs should be considered. In the chance constrained S-OPF, the randomness of system input is directly represented in the optimisation model and influences the optimal solution. However, existing solution approaches to chance constrained S-OPF only considers Gaussian distributed system inputs, and the correlation between random system inputs are neglected. Therefore, a heuristic solution approach has been developed in this study, which is able to not only incorporate non-Gaussian distributed system inputs, but also handle the possible correlation between random system inputs. The proposed S-OPF approach searches the optimal solution in the neighbourhood of the solution of a corresponding D-OPF problem, and adjusts its violated equivalent chance constraints until no violation happens. Numerical results of two cases indicate its effectiveness and good convergence. However, the proposed approach also requires that the variation of the random system inputs is not too large, so that its optimal solution is in the neighbourhood of the corresponding D-OPF problem. On the other hand, the global optimality of the proposed approach is still to be identified.

6.2 Future Research

Conventional power system reliability evaluation criteria and indices are based on deterministic analysis, which are not adequate for stochastic analysis. As for the topics in this research, it is necessary to do further study on the following aspects:

1. The modelling methodology of electric vehicle charging demand has not considered the control policies on electric vehicle charging, e.g. the charging current could be adjusted according to the real-time electricity price. Moreover, electric vehicles are potential distributed energy storage units, so in a suitable constitution they could provide a certain kind of auxiliary service to the power grid, e.g. load peak clipping or voltage secondary regulation. On the other hand, it is still an open topic to be addressed in future how to model the spatial uncertainty of the number of electric vehicles in a certain area.

2. Except for Monte Carlo simulation, currently other methods of PPF calculations are not able to consider power flow adjustments (for instance, changing transformer tap ratio) or limits (for instance, enforcing generator reactive power limits). Therefore, in order to extend the application of cumulant method of PPF calculations in online analysis and dispatching, there is still a lot of work to do.

3. The proposed heuristic approach to the chance-constrained S-OPF problem utilises the new quantitative results achieved in the thesis on the power flow calculations. This opens a door to improving the optimality of control variables. Hence, the proposed suboptimal solution of the chance-constrained S-OPF problem can be seen as leading to the control inputs of much improved optimality when compared to the existing approaches. However, its convergence and sub-optimality property need further research work to be done.

APPENDIX MATHEMATICAL FUNDAMENTALS

1 Numerical Characteristics of Random Variable [176]

1.1 Moment and Cumulant

Raw Moment: The raw moment of a real-valued continuous random variable X is defined as

$$\mu_n' = E(X^n) = \int_{-\infty}^{+\infty} x^n dF(x) = \int_{-\infty}^{+\infty} x^n f(x) dx \tag{1}$$

where n is the raw moment order;

E is the expectation operator;

$F(x)$ is the cumulative distribution function of X;

$f(x)$ is the probability density function of X, i.e. the derivative of $F(x)$ if exists.

The raw moment of a real-valued discrete random variable X is defined as

$$\mu_n' = E(X^n) = \sum_{i}^{N} x_i^n p(x_i) \tag{2}$$

where n is the raw moment order;

E is the expectation operator;

N is the number of possible values of X;

$p(x_i)$ is the probability mass function of X, i.e. the probability density function.

The 1st order raw moment μ_1' is the *Mean* (also called *Expected Value*) of X, usually denoted as μ.

If there exists $\varepsilon > 0$ such that

$$\psi(t) \equiv E(e^{tx}) \quad t \in R \tag{3}$$

for $|t| < \varepsilon$, then $\psi(t)$ is called the *moment generating function* of X.

For a continuous random variable X,

$$\begin{aligned}\psi(t) &\equiv \int_{-\infty}^{+\infty} e^{tx} dF(x) = \int_{-\infty}^{+\infty} \left(1 + \sum_{n=1}^{\infty} t^n \frac{x^n}{n!}\right) dF(x) \\ &= \int_{-\infty}^{+\infty} dF(x) + \sum_{n=1}^{\infty} \frac{t^n}{n!} \int_{-\infty}^{+\infty} x^n dF(x) \\ &= 1 + \sum_{n=1}^{\infty} \frac{\mu_n'}{n!} t^n\end{aligned} \tag{4}$$

Apparently, raw moments appear as the coefficients in the Maclaurin series of moment generating function $\psi(t)$.

Central Moment: The central moment of a real-valued continuous random variable X is defined as

$$\mu_n = E[(X - \mu)^n] = \int_{-\infty}^{+\infty} (x - \mu)^n dF(x) = \int_{-\infty}^{+\infty} (x - \mu)^n f(x) dx \tag{5}$$

where n is the central moment order;

E is the expectation operator;

$F(x)$ is the cumulative distribution function of X;

$f(x)$ is the probability density function of X, i.e. the derivative of $F(x)$ if exists.

The raw moment of a real-valued discrete random variable X is defined as

$$\mu_n = E[(X-\mu)^n] = \sum_{i}^{N} (x_i - \mu)^n \, p(x_i) \tag{6}$$

where n is the central moment order;

E is the expectation operator;

N is the number of possible values of X;

$p(x_i)$ is the probability mass function of X, i.e. the probability density function.

The 2nd order central moment μ_2 is the *Variance* of X, usually denoted as σ^2.

The positive square root of variance σ^2 is the *Standard Deviation* of X, usually denoted as σ.

The ratio of standard deviation to mean, i.e. σ/μ, is called the *Variation Coefficient* of X.

The ratio of μ_n to σ^n, i.e. μ_n/σ^n, is called the *Normalized* (or *Standardized*) *Central Moment* of X. Note that, normalized central moments are dimensionless quantities, so they represent the distribution independently of any linear change of scale.

The 3rd order normalized central moment μ_3/σ^3 is called the *Skewness* of X, often denoted as γ.

The 4th order central moment μ_4/σ^4 minus 3 is called the *Kurtosis* (also known as *excess kurtosis* in older works) of X, often denoted as κ. The "minus 3" in this definition is often explained as a correction to make the kurtosis of the Gaussian distribution equal to zero.

The moments of a random variable can be viewed as the quantitative measure of its distribution shape. For example, variance measures the "width" of its possible values in one dimension or measures the cloud area of its possible values in higher dimensions as it could be fitted by an ellipsoid; skewness measures the lopsidedness of the distribution, where a left

skewed distribution has a negative skewness, while a right skewed distribution has a positive skewness; kurtosis measures whether the distribution is tall and skinny or short and squat in comparison with the standard Gaussian distribution. If a distribution has a peak at its mean and long tails, its kurtosis positive (leptokurtic); conversely, a bounded distributions tends to have low kurtosis (platykurtic). Any probability distribution can be characterized by a number of features (such as its mean, variance, skewness, etc.), and the moments of a function, such as probability density function or cumulative distribution function, describe the nature of its distribution.

However, a key problem with moments and their generating function is that they may not exist, as sometimes the integrals in Equations (1)-(6) would not converge absolutely. Thus cumulants provide an alternative to moments.

Cumulant: For a real valued random X, define its *characteristic function* as

$$\varphi(t) = E(e^{itx}) \quad t \in R \tag{7}$$

Then its cumulant κ_n is defined by

$$\ln \varphi(t) = \sum_{n=1}^{\infty} \kappa_n \frac{(it)^n}{n!} \tag{8}$$

where n is the cumulant order;

E is the expectation operator;

i is the imaginary unit, i.e. $i^2 = -1$;

$\ln \varphi(t)$ is called the *cumulant generating function* of X.

Cumulants appear as the coefficients in the Maclaurin series of cumulant generating function $\ln\varphi(t)$. Note that, the characteristic function $\varphi(t)$ always exists, because it is the integral of a bounded function on a space of finite measure. Even when $\ln\varphi(t)$ does not have a Maclaurin series beyond linear order in the argument t, it can still be used directly in analyzing and, particularly, adding random variables.

In some cases, theoretical treatments of problems in terms of cumulants are simpler than those using moments due to the special properties of cumulants.

Property 1: For a random variable X, its n-th order cumulant is $\kappa_n(X)$, then the n-th order cumulant of $aX + b$ is

$$\kappa_n(aX+b) = \begin{cases} a\kappa_1(X) + b & n = 1 \\ a^n\kappa_n(X) & n \geq 2 \end{cases} \tag{9}$$

where a and b are real constants.

Property 2: For uncorrelated random variable X and Y, their n-th order cumulants are $\kappa_n(X)$ and $\kappa_n(Y)$ respectively, then the n-th order cumulant of $X + Y$ is

$$\kappa_n(X+Y) = \kappa_n(X) + \kappa_n(Y) \tag{10}$$

Moments determine cumulants in the sense that any two probability distributions whose moments are identical will have identical cumulants as well, and similarly cumulants determine moments. More specifically,

$$\psi(it) = 1 + \sum_{n=1}^{\infty} \frac{\mu'_n}{n!}(it)^n = \exp\left(\sum_{n=1}^{\infty} \kappa_n \frac{(it)^n}{n!}\right) \tag{11}$$

Therefore, the cumulant generating function is actually the logarithm of the moment generating function.

The relationship between cumulants and moments were summarized in [177] as follows

$$\kappa_n = \mu'_n - \sum_{i=1}^{n-1} \binom{n-1}{i} \kappa_{n-i} \mu'_i \tag{12}$$

$$\mu'_n = \kappa_n + \sum_{i=1}^{n-1} \binom{n-1}{i} \kappa_{n-i} \mu'_i \tag{13}$$

$$\kappa_n = \mu_n - \sum_{i=2}^{n-2} \binom{n-1}{i} \kappa_{n-i} \mu'_i \quad n \geq 2 \tag{14}$$

$$\mu_n = \kappa_n + \sum_{i=2}^{n-2} \binom{n-1}{i} \kappa_{n-i} \mu_i \quad n \geq 2 \tag{15}$$

$$\mu_n = \sum_{i=0}^{n} \binom{n}{i} \mu'_i (-\mu)^{n-i} \tag{16}$$

$$\mu'_n = \sum_{i=0}^{n} \binom{n}{i} \mu_i \mu^{n-i} \tag{17}$$

1.2 Covariance and Correlation

Covariance: The covariance of two real-valued random variables X and Y is defined as

$$\operatorname{cov}(X, Y) = E[(X - \mu_X)(Y - \mu_Y)] = E(XY) - \mu_X \mu_Y \tag{18}$$

where $\mu_X = E(X)$ and $\mu_Y = E(Y)$.

According to its definition, covariance has following properties:

$$\begin{cases} \operatorname{cov}(X, a) = 0 \\ \operatorname{cov}(aX, Y) = a \operatorname{cov}(Y, X) \\ \operatorname{cov}(X + a, Y) = \operatorname{cov}(X, Y) \\ \operatorname{cov}(X + Y, Z) = \operatorname{cov}(X, Z) + \operatorname{cov}(Y, Z) \\ \operatorname{cov}(X, Y) = \operatorname{cov}(Y, X) \end{cases} \tag{19}$$

where a is a real constant.

Moreover, variance σ^2 is a special case of covariance when two variables are identical.

For a set of random variables, the covariance of all pairs constitutes a *Covariance Matrix*, i.e.

$$\begin{aligned} \boldsymbol{\Sigma} &= E\{[\boldsymbol{X} - E(\boldsymbol{X})][\boldsymbol{X} - E(\boldsymbol{X})]^T\} \\ &= \begin{bmatrix} \operatorname{cov}(X_1, X_1) & \operatorname{cov}(X_1, X_2) & \cdots & \operatorname{cov}(X_1, X_n) \\ \operatorname{cov}(X_2, X_1) & \operatorname{cov}(X_2, X_2) & \cdots & \operatorname{cov}(X_2, X_n) \\ \vdots & \vdots & \ddots & \vdots \\ \operatorname{cov}(X_n, X_1) & \operatorname{cov}(X_n, X_2) & \cdots & \operatorname{cov}(X_n, X_n) \end{bmatrix} \end{aligned} \tag{20}$$

where $\boldsymbol{X} = [X_1, X_2, \ldots, X_n]^T$.

Covariance matrix is symmetric and positive definite, thus its Cholesky decomposition always exists and can be applied to decouple correlated random variables.

Covariance provides a measure of how much two random variables change together, i.e. the strength of their correlation: if X and Y are uncorrelated, by using the linearity property of expectation operator, $\operatorname{cov}(X,Y) = E(X)E(Y) - \mu_X\mu_Y = 0$; otherwise, their covariance will be nonzero. In fact, if $\operatorname{cov}(X,Y) > 0$, then Y tends to increase as X increases, and if $\operatorname{cov}(X,Y) < 0$, then Y tends to decrease as X increases. However, the magnitude of covariance is not that easy

to interpret, but its normalized version, correlation coefficient, shows by its magnitude the strength of the linear correlation.

Correlation Coefficient: The correlation coefficient of two real-valued random variables X and Y is defined as

$$\rho_{X,Y} = \frac{\operatorname{cov}(X,Y)}{\sigma_X \sigma_Y} \tag{21}$$

where $\sigma_X^2 = E[(X - \mu_X)^2]$ and $\sigma_Y^2 = E[(X - \mu_Y)^2]$.

Equation (21) is the most common Pearson's correlation, which is a measure of the linear relationship between two random variables. Similar to covariance, $\rho_{X,Y} = \rho_{Y,X}$, and $\rho_{X,X} = \rho_{Y,Y} = 1$. Moreover, according to the Cauchy-Schwarz inequality, there is $|\rho_{X,Y}| \leq 1$, and the stronger the linear relationship is, the closer to 1 $|\rho_{X,Y}|$ is. However, when $\rho_{X,Y}$ is 0, X and Y are uncorrelated, which only means that there is no linear relationship between them.

For a set of random variables $\boldsymbol{X} = [X_1, X_2, \ldots, X_n]^T$, the correlation coefficient of all pairs constitutes the *Correlation Matrix*, i.e.

$$\boldsymbol{\rho_\Sigma} = \begin{bmatrix} 1 & \rho_{X_1,X_2} & \cdots & \rho_{X_1,X_n} \\ \rho_{X_2,X_1} & 1 & \cdots & \rho_{X_2,X_1} \\ \vdots & \vdots & \ddots & \vdots \\ \rho_{X_n,X_1} & \rho_{X_n,X_2} & \cdots & 1 \end{bmatrix} \tag{22}$$

which is a symmetric positive-semidefinite matrix.

2 Probability Distribution Function Approximation

2.1 Orthogonal Polynomial Approximation [178]

Numerical characteristics such as moments and cumulants provide an alternative description of a probability distribution. However, not like the cumulative distribution function or the probability density function, numerical characteristics cannot uniquely determine a probability distribution. Fortunately, if parts of a random variable's numerical characteristics are known, it is possible to approximate its probability functions by orthogonal polynomials.

Assume that a non-negative function $w(x)$ is integrable over a real interval $[a, b]$ ($a = -\infty$ and $b = +\infty$ are allowed). If polynomials span $\{\varphi_0(x), \varphi_1(x), \ldots, \varphi_n(x)\}$ have the inner product as follows

$$\langle \varphi_i(x), \varphi_j(x) \rangle = \int_a^b \varphi_i(x)\varphi_j(x)w(x)dx \tag{23}$$

and $\langle \varphi_i(x), \varphi_j(x) \rangle = 0$ ($i \neq j$), then span $\{\varphi_0(x), \varphi_1(x), \ldots, \varphi_n(x)\}$ are called *Orthogonal Polynomials* over $[a, b]$, and $w(x)$ is called their *Weighting Function*.

Several common orthogonal polynomials are listed in the following table:

Common Orthogonal Polynomials

Name	Recursion ($n \geq 1$)	$w(x)$	$[a, b]$
Hermite	$H_0(x) = 1$ $H_1(x) = x$ $H_{n+1}(x) = xH_n(x) - H_n'(x)$	$\frac{e^{-\frac{1}{2}x^2}}{\sqrt{2\pi}}$	$(-\infty,+\infty)$
Laguerre	$La_0(x) = 1$ $La_1(x) = -x + 1$ $La_{n+1}(x) = \frac{1}{n+1}[(2n+1-x)La_n(x) - nLa_{n-1}(x)]$	e^{-x}	$[0,+\infty)$

Legendre	$Le_0(x)=1$ $Le_1(x)=x$ $Le_{n+1}(x)=\frac{1}{n+1}[(2n+1)xLe_n(x)-nLe_{n-1}(x)]$	1	$[-1,+1]$
Chebyshev	$T_0(x)=1$ $T_1(x)=x$ $T_{n+1}(x)=2xT_n(x)-T_{n-1}(x)]$	$\frac{1}{\sqrt{1-x^2}}$	$[-1,+1]$

For a random variable X, if its first n orders of raw moments exist, then its probability density function $f(x)$ can be approximated over $[a, b]$ by

$$f(x) \approx w(x)\sum_{i=0}^{n} c_i \varphi_i(x) \quad x \in [a,b]$$
$$c_i = \frac{1}{i!}\sum_{k=0}^{i} C_{i,k}\mu'_k \tag{24}$$

where $C_{i,k}$ is the coefficient of x^k in the orthogonal polynomial $\varphi_i(x)$;

μ'_k is the k-th order raw moment of X.

2.2 Series Expansion Approximation

Most of series expansions are stilled based on orthogonal functions and their properties. Their effectiveness of approximation depends on the similarity between the actual probability distribution and the orthogonal functions.

Gram-Charlier Series [179]: For a random variable X, if its first n order cumulants exist, then its probability distribution approximation by the Gram-Charlier series expansion is

$$F(x) \approx \Phi(\frac{x-\mu}{\sigma}) + \varphi(\frac{x-\mu}{\sigma})\sum_{i=1}^{n} c_i H_{i-1}(\frac{x-\mu}{\sigma})$$
$$f(x) \approx \varphi(\frac{x-\mu}{\sigma})\left[1+\sum_{i=1}^{n} c_i H_i(\frac{x-\mu}{\sigma})\right]\Big/\sigma \quad (25)$$

where μ is the mean of X;

σ is the standard deviation of X;

$H_i(x)$ is the i-th order Hermite polynomial;

$\Phi(x)$ is the cumulative distribution function of the standard Gaussian distribution;

$\varphi(x)$ is the probability density function of the standard Gaussian distribution.

The coefficients c_i in Equation (25) is calculated from the cumulants of X as follows

$$c_1 = c_2 = 0$$
$$c_3 = \kappa_3 \big/ 6\sigma^3 , c_4 = \kappa_4 \big/ 24\sigma^4 , c_5 = \kappa_5 \big/ 120\sigma^5 \quad (26)$$
$$c_i = \frac{\kappa_i}{i!\sigma^i} + \frac{1}{2}\sum_{j=3}^{i-3} c_j c_{i-j} \quad (i \geq 6)$$

where κ_i is the i-th order cumulant of X.

The convergence property of the Gram-Charlier series generally depends on how the form of X is similar to the Gaussian distribution. It is proved that the Gram-Charlier series converges for every x if the integral

$$\int_{-\infty}^{+\infty} e^{\frac{x^2}{4}} dF(x) \tag{27}$$

is convergent, and $f(x)$ is of bounded variation in $(-\infty,+\infty)$ when $n \to \infty$. An inference is that $f(x)$ should fall to zero faster than $e^{x^2/4}$ does to assure the convergence of this series expansion, which leads to restrictions for its application.

Edgeworth Series [180]: The Edgeworth series and the Gram-Charlier series are actually the same, but the arrangement of their terms (and thus the accuracy of series truncation) differs. The Edgeworth series expansion using the first five order cumulants of X is given by

$$\begin{aligned}
F(x) \approx \Phi(\frac{x-\mu}{\sigma}) &+ \frac{\kappa_3}{3!\sigma^3}\varphi^{(2)}(\frac{x-\mu}{\sigma}) - \frac{\kappa_4}{4!\sigma^4}\varphi^{(3)}(\frac{x-\mu}{\sigma}) - \frac{10\kappa_3^2}{6!\sigma^6}\varphi^{(5)}(\frac{x-\mu}{\sigma}) \\
&+ \frac{\kappa_5}{5!\sigma^5}\varphi^{(4)}(\frac{x-\mu}{\sigma}) + \frac{35\kappa_3\kappa_4}{7!\sigma^5}\varphi^{(6)}(\frac{x-\mu}{\sigma}) + \frac{280\kappa_3^3}{9!\sigma^9}\varphi^{(8)}(\frac{x-\mu}{\sigma}) \\
&- \frac{\kappa_6}{6!\sigma^6}\varphi^{(5)}(\frac{x-\mu}{\sigma}) - \frac{35\kappa_4^2}{8!\sigma^8}\varphi^{(7)}(\frac{x-\mu}{\sigma}) - \frac{56\kappa_3\kappa_5}{8!\sigma^8}\varphi^{(7)}(\frac{x-\mu}{\sigma}) \\
&- \frac{2100\kappa_3^2\kappa_4}{10!\sigma^{10}}\varphi^{(9)}(\frac{x-\mu}{\sigma}) - \frac{15400\kappa_3^4}{12!\sigma^{12}}\varphi^{(11)}(\frac{x-\mu}{\sigma}) \\
f(x) \approx \Big[\varphi(\frac{x-\mu}{\sigma}) &- \frac{\kappa_3}{3!\sigma^3}\varphi^{(3)}(\frac{x-\mu}{\sigma}) + \frac{\kappa_4}{4!\sigma^4}\varphi^{(4)}(\frac{x-\mu}{\sigma}) + \frac{10\kappa_3^2}{6!\sigma^6}\varphi^{(6)}(\frac{x-\mu}{\sigma}) \\
&- \frac{\kappa_5}{5!\sigma^5}\varphi^{(5)}(\frac{x-\mu}{\sigma}) - \frac{35\kappa_3\kappa_4}{7!\sigma^5}\varphi^{(7)}(\frac{x-\mu}{\sigma}) - \frac{280\kappa_3^3}{9!\sigma^9}\varphi^{(9)}(\frac{x-\mu}{\sigma}) \\
&+ \frac{\kappa_6}{6!\sigma^6}\varphi^{(6)}(\frac{x-\mu}{\sigma}) + \frac{35\kappa_4^2}{8!\sigma^8}\varphi^{(8)}(\frac{x-\mu}{\sigma}) + \frac{56\kappa_3\kappa_5}{8!\sigma^8}\varphi^{(8)}(\frac{x-\mu}{\sigma}) \\
&+ \frac{2100\kappa_3^2\kappa_4}{10!\sigma^{10}}\varphi^{(10)}(\frac{x-\mu}{\sigma}) + \frac{15400\kappa_3^4}{12!\sigma^{12}}\varphi^{(12)}(\frac{x-\mu}{\sigma}) \Big] / \sigma
\end{aligned} \tag{28}$$

where μ is the mean of X;

σ is the standard deviation of X;

κ_i (i = 1, 2, …, 5) is the i-th order cumulant of X;

$\Phi(x)$ is the cumulative distribution function of the standard Gaussian distribution;

$\varphi(x)$ is the probability density function of the standard Gaussian distribution.

It has been investigated that under fairly general conditions the Edgeworth series has asymptotic property, which means that the approximation effectiveness of the Edgeworth series expansion could be not better as the number of truncated terms increases.

Cornish-Fisher Series [181]: The Cornish-Fisher series is used to approximate the quantile function of a probability distribution, i.e. the inversion of the cumulative distribution function. The Cornish-Fisher series expansion using the first five order cumulants of a random variable X with its mean of 0 and standard deviation of 1 is given by

$$\begin{aligned} Q(p) \approx \psi(p) &+ \frac{\psi^2(p)-1}{6}\kappa_3 + \frac{\psi^3(p)-3\psi(p)}{24}\kappa_4 \\ &- \frac{2\psi^3(p)-5\psi(p)}{36}\kappa_3^2 + \frac{\psi^4(p)-6\psi^2(p)+3}{120}\kappa_5 \\ &- \frac{\psi^4(p)-5\psi^2(p)}{24}\kappa_2\kappa_3 + \frac{12\psi^4(p)-53\psi^2(p)}{324}\kappa_3^3 \end{aligned} \tag{29}$$

where $x = Q(p)$ is the quantile function of X;

κ_i (i = 1, 2, …, 5) is the i-th order cumulant of X;

$\psi(p)$ is the quantile function of the standard Gaussian distribution.

If X has some other mean μ and standard deviation σ, Equation (29) can be applied to its normalization $(X–\mu)/\sigma$, so it is not a problem to obtain the quantile of X itself through Cornish-Fisher series expansion.

Moreover, a recursion implementation was proposed in [182], which allows the higher order Cornish-Fisher series. However, because $\psi(p)$ has no closed-form representation using basic algebraic functions, the probability density function $f(x)$ can be approximated by spline differentiation of $F(x) = Q^{-1}(x)$.

It should be noted that since these three series are all based on the Gaussian distribution, the approximation is expected to be more accurate to fit a nearly Gaussian distribution. But the Cornish-Fisher series usually performs better than the other two in the approximation of asymmetric probability distributions. For example, the probability functions of an asymmetric lognormal distribution are plotted in Figure 1 and Figure 2 along with their series expansion approximation. Obviously, the Cornish-Fisher series gives a much better approximation.

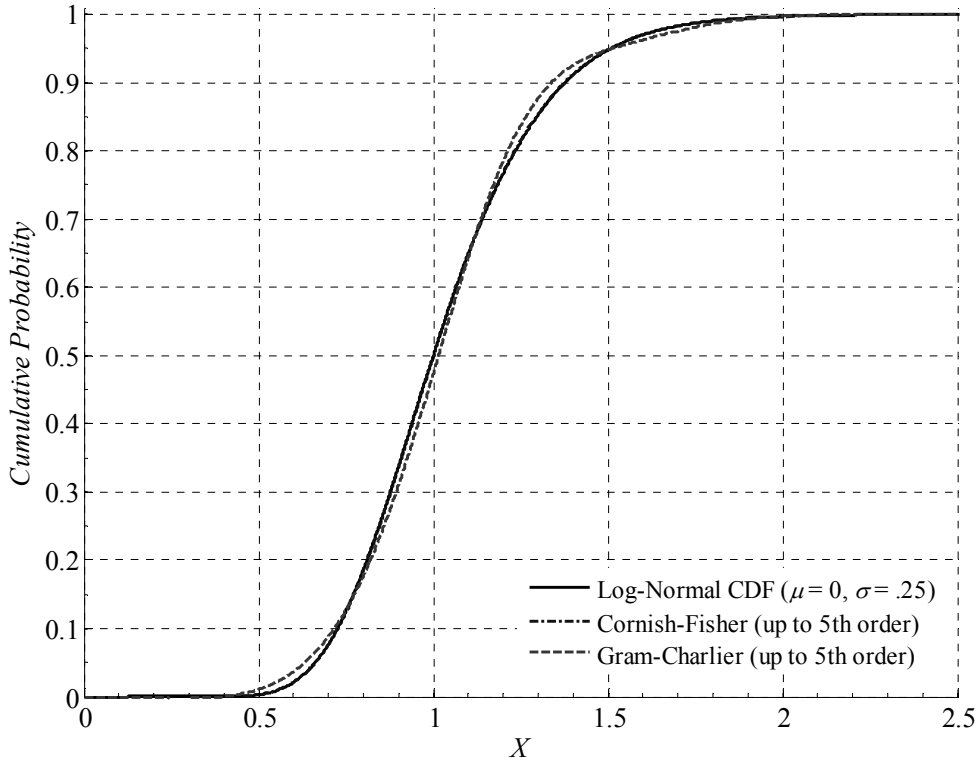

Figure 1 Cumulative distribution approximation by series expansions (up to 5th order)

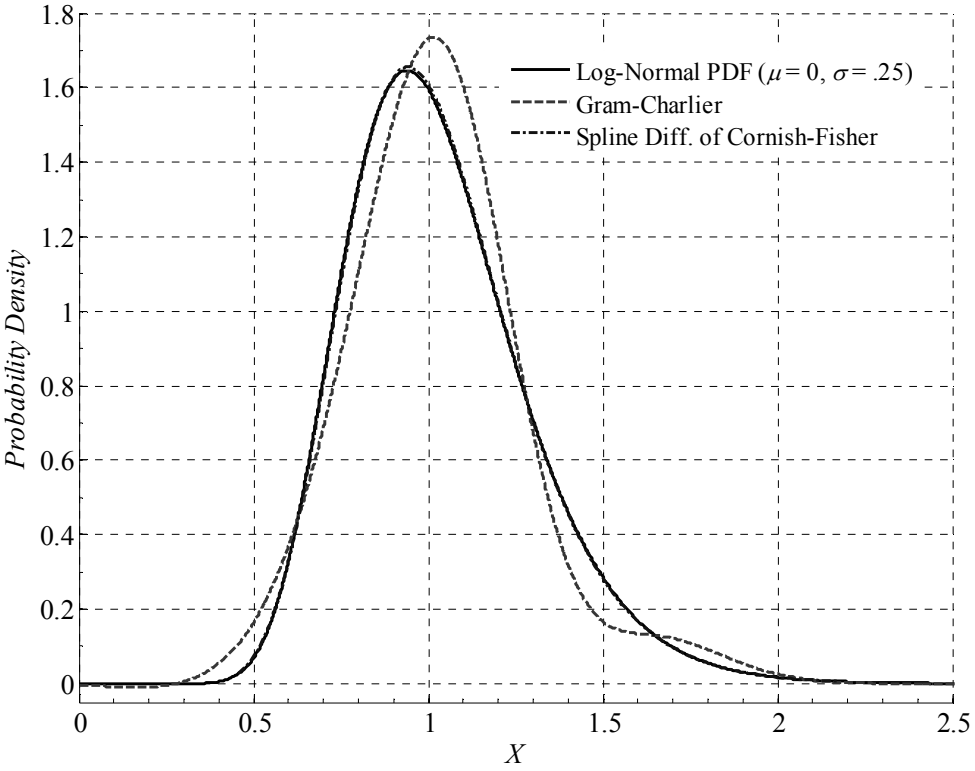

Figure 2 Probability density approximation by series expansions (up to 5th order)

On the other hand, the convergence and accuracy of these series do not necessarily improve with increasing orders of truncation of the series. For example, the Gram-Charlier series of 7 orders turns to be worse than that of 5 orders in the approximation of a Beta distribution:

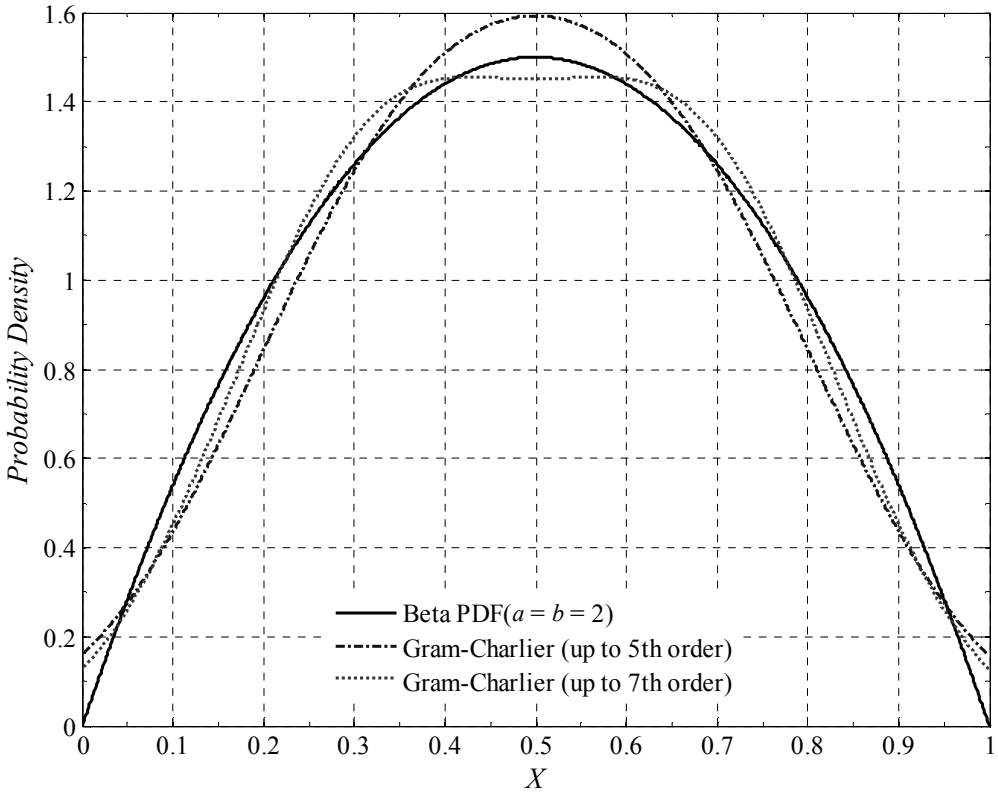

Figure 3 Asymptotic property of series expansions

Moreover, these three series do not guarantee monotonicity of the cumulative distribution function. In some circumstances, the Gram-Charlier or Edgeworth series expansions of the cumulative distribution function could exceed [0, 1]. For example, the left tail of the Gram-Charlier series falls below 0 in Figure 2, which means non-monotonicity.

2.3 Staircase Function Approximation

The cumulative distribution function of a discrete random is a staircase function. Von Mises proposed a method in [183] to approximate a probability distribution using a discrete distribution, given enough raw moments of the former.

For a real valued random variable Y, if its first $2n-1$ orders of raw moments $\mu_1', \mu_2', \ldots, \mu_{2n-1}'$ exist, its cumulative distribution function $F_Y(x)$ can be approximated by a discrete distribution X of $n-1$ points. The discrete points of X are the roots of the following polynomial:

$$x^n + c_{n-1}x^{n-1} + \cdots + c_1 x + c_0 \tag{30}$$

where coefficients c_i ($i = 0,1, \ldots, n-1$) are the solution of another equation set

$$\begin{bmatrix} 1 & \mu_1' & \cdots & \mu_{n-1}' \\ \mu_1' & \mu_2' & \cdots & \mu_n' \\ \vdots & \vdots & \ddots & \vdots \\ \mu_{n-1}' & \mu_n' & \cdots & \mu_{2n-2}' \end{bmatrix} \begin{bmatrix} c_0 \\ c_1 \\ \vdots \\ c_{n-1} \end{bmatrix} = \begin{bmatrix} -\mu_n' \\ -\mu_{n+1}' \\ \vdots \\ -\mu_{2n-1}' \end{bmatrix} \tag{31}$$

It is proved that the roots of the polynomial in Equation (30) are all real and unique [183]. The probability p_i corresponding to each root x_i ($i = 1, 2, \ldots, n-1$) can be obtained from

$$\begin{bmatrix} 1 & 1 & \cdots & 1 \\ x_1 & x_2 & \cdots & x_n \\ \vdots & \vdots & \ddots & \vdots \\ x_1^{n-1} & x_2^{n-1} & \cdots & x_n^{n-1} \end{bmatrix} \begin{bmatrix} p_1 \\ p_2 \\ \vdots \\ p_n \end{bmatrix} = \begin{bmatrix} \mu_1' \\ \mu_2' \\ \vdots \\ \mu_{n-1}' \end{bmatrix} \tag{32}$$

Note that, the coefficient matrix in Equation (32) is a Vandermonde matrix, so solving Equation (32) is equivalent to finding the coefficients of the polynomial as follows [183]

$$\prod_{\substack{k=0 \\ k \neq i}}^{n-1} \frac{x - x_k}{x_i - x_k} = \sum_{k=0}^{n-1} C_k x^k \tag{33}$$

This equivalence reduces complexity of solving Equation (32) from $O(n^3)$ to $O(n^2)$.

Figure 4 shows an example of the staircase function approximation, in which the staircase cumulative distribution function of X, denoted as $F_X(x)$, will cross $F_Y(x)$ at $2n-1$ points.

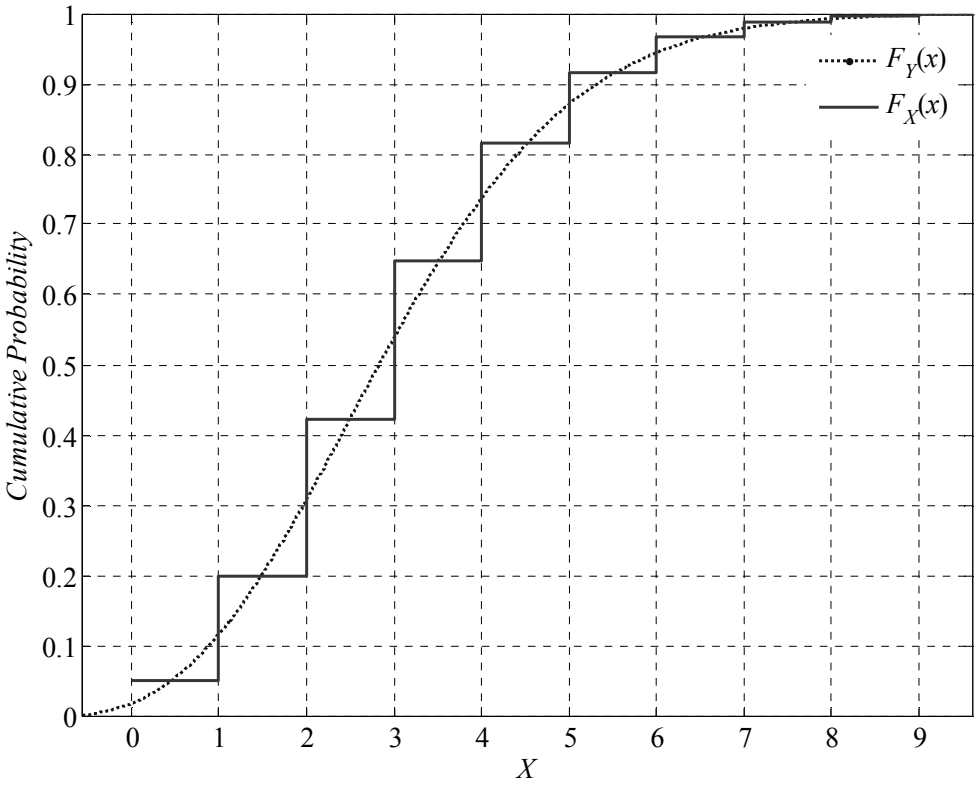

Figure 4 Staircase function approximation example

Moreover, there is

$$\begin{cases} F_X(x_{i-1}) < F_Y(x_i) < F_X(x_i) \\ F_Y(x) \le F_X(x_i) \end{cases} \tag{34}$$

where (i = 1,2, …, n) and $F_X(x_0) = 0$.

As the number of discrete points n grows, the approximation becomes better, but the computational burden to solve Equations (30)-(32) will increase accordingly. Therefore, it is suggested to apply the staircase function approximation when other methods fail.

3 Convolution of Probability Distributions

The convolution of two real functions *f* and *g* is defined as follows

$$(f * g)(x) = \int_{-\infty}^{+\infty} f(y)g(x-y)dy = \int_{-\infty}^{+\infty} f(x-y)g(y)dy \tag{35}$$

If *f* and *g* are defined on a certain integer set, their convolution can be given by

$$(f * g)(n) = \sum_{m=-\infty}^{+\infty} f(m)g(n-m) = \sum_{m=-\infty}^{+\infty} f(n-m)g(m) \tag{36}$$

There are several ways of deriving formulae for the convolution of probability distributions. Often the manipulation of integrals can be avoided by use of some type of generating function. One of the straightforward techniques is to use the characteristic function, which always exists and is unique to a given probability distribution.

The probability distribution of the sum of two or more independent random variables is the convolution of their individual distributions. The term is motivated by the fact that the probability mass function or probability density function of a sum of random variables is the convolution of their corresponding probability mass functions or probability density functions respectively. For example,

$$\sum_{i=1}^{n} \mathrm{N}(\mu_i, \sigma_i^2) \sim \mathrm{N}(\sum_{i=1}^{n} \mu_i, \sum_{i=1}^{n} \sigma_i^2)$$

$$\sum_{i=1}^{n} \mathrm{Ber}(p) \sim \mathrm{Bin}(n, p) \tag{37}$$

$$\sum_{i=1}^{n} \mathrm{Bin}(N_i, p) \sim \mathrm{Bin}(\sum_{i=1}^{n} N_i, p)$$

4 Common Probability Distributions

4.1 Continuous Probability Distribution

Continuous Uniform Distribution (*Rectangular Distribution*):

Notation	$\mathrm{U}(a,b)$
Parameter	$-\infty < a < b < +\infty$
Support	$x \in [a,b]$
$F(x)$	$\begin{cases} 0 & x < a \\ \dfrac{x-a}{b-a} & x \in [a,b) \\ 1 & x \geq b \end{cases}$
$f(x)$	$\begin{cases} 1/(b-a) & x \in [a,b] \\ 0 & x < a \text{ or } x > b \end{cases}$
μ	$(a+b)/2$
σ^2	$(b-a)^2/12$
γ	0
κ	$-6/5$
μ_n'	$\dfrac{1}{n+1}\sum_{i=0}^{n} a^i b^{n-i}$

Note that, U(0,1) is called a *Standard Uniform Distribution*, which is fundamental to generating samples of other distributions.

Beta Distribution

Notation	$\mathrm{Beta}(\alpha,\beta)$
Parameter	$\alpha > 0, \beta > 0$
Support	$x \in (0,1)$

$F(x)$	$\mathrm{I}(x;\alpha,\beta)=\frac{\mathrm{B}(x;\alpha,\beta)}{\mathrm{B}(\alpha,\beta)}$
$f(x)$	$\frac{x^{\alpha-1}(1-x)^{\beta-1}}{\mathrm{B}(\alpha,\beta)}$
μ	$\frac{\alpha}{\alpha+\beta}$
σ^2	$\frac{\alpha\beta}{(\alpha+\beta)^2(\alpha+\beta+1)}$
γ	$\frac{2(\beta-\alpha)\sqrt{\alpha+\beta+1}}{(\alpha+\beta+2)\sqrt{\alpha\beta}}$
κ	$6\frac{(\alpha-\beta)^2(\alpha+\beta+1)-\alpha\beta(\alpha+\beta+2)}{\alpha\beta(\alpha+\beta+2)(\alpha+\beta+3)}$
μ_n'	$\frac{\mathrm{B}(\alpha+n,\beta)}{\mathrm{B}(\alpha,\beta)}$
Sampling	See [184]-[185]

Exponential Distribution:

Notation	$\mathrm{Exp}(\lambda)$
Parameter	$\lambda>0$
Support	$x\in[0,+\infty)$
$F(x)$	$\begin{cases}0 & x<0\\ 1-e^{-\lambda x} & x\geq 0\end{cases}$
$f(x)$	$\begin{cases}0 & x<0\\ \lambda e^{-\lambda x} & x\geq 0\end{cases}$
μ	$1/\lambda$
σ^2	$1/\lambda^2$
γ	2
κ	6
μ_n'	$\frac{n!}{\lambda^n}$
μ_n	$\frac{!n}{\lambda^n}$
Sampling	$-\ln U(0,1)/\lambda$

Gaussian Distribution (*Normal Distribution*):

Notation	$\mathrm{N}(\mu,\sigma^2)$
Parameter	$\mu\in R,\sigma>0$
Support	$x\in R$

$F(x)$	$\frac{1}{2}\left[1+\operatorname{erf}\left(\frac{x-\mu}{\sqrt{2\sigma^2}}\right)\right]$
$f(x)$	$\frac{1}{\sqrt{2\pi}\sigma}e^{\frac{(x-\mu)^2}{2\sigma^2}}$
μ	μ
σ^2	σ^2
γ	0
κ	0
μ_n'	$\begin{cases}\mu_1'=\mu, \\ \mu_2'=\mu^2+\sigma^2 \\ \mu_n'=\mu\mu_{n-1}'+(n-1)\sigma^2\mu_{n-2}' & n\geq 3\end{cases}$
μ_n	$\begin{cases}\mu_1=0, \\ \mu_2=\sigma^2 \\ \mu_n=(n-1)\sigma^2\mu_{n-2} & n\geq 3\end{cases}$
κ_n	$\begin{cases}\kappa_1=\mu, \\ \kappa_2=\sigma^2 \\ \kappa_n=0 & n\geq 3\end{cases}$
Sampling	$\begin{cases}\mu+\sigma\sqrt{-2\ln U_1}\cos(2\pi U_2) \\ \mu+\sigma\sqrt{-2\ln U_1}\sin(2\pi U_2)\end{cases}$ U_1, U_2 i.i.d. U(0,1)

Note that, N(0,1) is called a *Standard Gaussian Distribution*.

Bivariate Gaussian Distribution (*Bivariate Normal Distribution*):

Notation	$\mathrm{N}(\mu_1,\mu_2,\sigma_1^2,\sigma_2^2)$
Parameter	$\mu_1\in R,\mu_2\in R,\sigma_1>0,\sigma_2>0$
Support	$\boldsymbol{x}\in\boldsymbol{\mu}+span\{\boldsymbol{\Sigma}\}\subseteq\boldsymbol{R}^2$ $\boldsymbol{\mu}=[\mu_1,\mu_2]^{\mathrm{T}},\boldsymbol{\Sigma}=\begin{bmatrix}\sigma_1^2 & \rho\sigma_1\sigma_2\\ \rho\sigma_1\sigma_2 & \sigma_2^2\end{bmatrix}$ $\rho=\frac{\operatorname{cov}(X_1,X_2)}{\sigma_1\sigma_2}$
$F(x)$	No analytic expression
$f(x)$	$\frac{1}{2\pi\sigma_1\sigma_2\sqrt{1-\rho^2}}e^{-\frac{z}{2(1-\rho^2)}},z\equiv\frac{(x-\mu_1)^2}{\sigma_1^2}-2\rho\frac{(x-\mu_1)(x-\mu_2)}{\sigma_1\sigma_2}+\frac{(x-\mu_2)^2}{\sigma_2^2}$
μ	$\boldsymbol{\mu}$
σ^2	$\boldsymbol{\Sigma}$
Sampling	$\boldsymbol{\mu}+\boldsymbol{AN}$

	$\boldsymbol{N} = \begin{bmatrix} \sqrt{-2\ln U_1}\cos(2\pi U_2) \\ \sqrt{-2\ln U_1}\sin(2\pi U_2) \end{bmatrix}$, U_1 and U_2 i.i.d. U(0,1); If $\boldsymbol{\Sigma}$ is positive-definite, $\boldsymbol{A}$ is the Cholesky decomposition of $\boldsymbol{\Sigma}$, i.e. $\boldsymbol{A}\boldsymbol{A}^{\mathrm{T}} = \boldsymbol{\Sigma}$. If $\boldsymbol{\Sigma}$ is nonnegative-definite, $\boldsymbol{A} = \boldsymbol{Q}\boldsymbol{\Lambda}^{\frac{1}{2}}$, where $\boldsymbol{Q}\boldsymbol{\Lambda}\boldsymbol{Q}^{\mathrm{T}} = \boldsymbol{\Sigma}$.

Lognormal Distribution

Notation	$\ln\mathrm{N}(\mu,\sigma^2)$
Parameter	$\mu \in R, \sigma > 0$
Support	$x \in (0,+\infty)$
$F(x)$	$\frac{1}{2}\left[1+\operatorname{erf}\left(\frac{\ln x-\mu}{\sqrt{2\sigma^2}}\right)\right]$
$f(x)$	$\frac{1}{x\sqrt{2\pi}\sigma}e^{-\frac{(\ln x-\mu)^2}{2\sigma^2}}$
μ	$e^{\mu+\frac{1}{2}\sigma^2}$
σ^2	$(e^{\sigma^2}-1)e^{2\mu+\sigma^2}$
γ	$(e^{\sigma^2}+2)\sqrt{e^{\sigma^2}-1}$
κ	$e^{4\sigma^2}+2e^{3\sigma^2}+3e^{2\sigma^2}-6$
μ_n'	$e^{n\mu+\frac{1}{2}n^2\sigma^2}$
Sampling	$e^{\mu+\sigma\,\mathrm{N}(0,1)}$

Weibull Distribution

Notation	$\mathrm{Wbl}(\mu,\sigma^2)$
Parameter	$\lambda > 0, k > 0$
Support	$x \in [0,+\infty)$
$F(x)$	$\begin{cases} \frac{k}{\lambda}(x/\lambda)^{k-1}e^{-(x/\lambda)^k} & x \geq 0 \\ 0 & x < 0 \end{cases}$
$f(x)$	$1-e^{-(x/\lambda)^k}$
μ	$\lambda\Gamma(1+1/k)$
σ^2	$\lambda^2\Gamma(1+2/k)-\mu^2$
γ	$[\lambda^3\Gamma(1+3/k)-3\mu\sigma^2-\mu^3]/\sigma^3$
κ	$[\lambda^4\Gamma(1+4/k)-4\gamma\mu\sigma^3-6\mu^2\sigma^2-\mu^4]/\sigma^4-3$
μ_n'	$\lambda^n\Gamma(1+n/k)$

Sampling	$\sqrt[k]{-\frac{1}{\lambda}\ln \mathrm{U}(0,1)}$

4.2 Discrete Probability Distribution

Bernoulli Distribution

Notation	$\mathrm{Ber}(p)$
Parameter	$0 < p < 1$
Support	$x = \{0,1\}$
$F(x)$	$\begin{cases} 0 & x < 0 \\ 1-p & 0 \le x < 1 \\ 1 & x \ge 1 \end{cases}$
$f(x)$	$\begin{cases} 1-p & x = 0 \\ p & x = 1 \end{cases}$
μ	p
σ^2	$p(1-p)$
γ	$\frac{1-2p}{\sqrt{p(1-p)}}$
κ	$\frac{1}{p(1-p)} - 6$
μ_n'	p
Sampling	$\begin{cases} 0 & \mathrm{U}(0,1) \le 1-p \\ 1 & \mathrm{U}(0,1) > 1-p \end{cases}$

Binomial Distribution

Notation	$\mathrm{Bin}(N, p)$
Parameter	$N \in N_0, 0 < p < 1$
Support	$x = \{0,1,\cdots,N\}$
$F(x)$	$\mathrm{I}(1-p; N-x, x+1) = \sum_{i=0}^{\lfloor x \rfloor} \binom{N}{i} p^i (1-p)^{N-i}$
$f(x)$	$\binom{N}{x} p^x (1-p)^{N-x}$
μ	Np
σ^2	$Np(1-p)$
γ	$\frac{1-2p}{\sqrt{Np(1-p)}}$

κ	$\frac{1}{Np(1-p)}-\frac{6}{N}$
κ_n	$\begin{cases}\kappa_1 = Np \\ \kappa_n = p(1-p)\frac{d\kappa_{n-1}}{dp} \quad n \geq 2\end{cases}$
Sampling	$\begin{cases}0 & \mathrm{U}(0,1) \leq F(0) \\ i & F(i-1) < \mathrm{U}(0,1) \leq F(i), i = \{1,2,\cdots,N-1\} \\ N & \mathrm{U}(0,1) > F(N-1)\end{cases}$

LIST OF PUBLICATIONS

[1] G. Li and X.-P. Zhang, "Modelling of Plug-in Hybrid Electric Vehicle Charging Demand in Probabilistic Power Flow Calculations," *IEEE Transactions on Smart Grid*, vol. 3, no. 1, pp. 492-499, Mar. 2012.

[2] G. Li and X.-P. Zhang, "Stochastic Optimal Power Flow Approach Considering Correlated Probabilistic Load and Wind Farm Generation," in *Proceedings of 2011 IET Conference on Reliability of Transmission and Distribution Networks*, London, UK, vol. CP580, pp. 3A1-3A7, Nov. 22-24 2011.

[3] G. Li, X.-P. Zhang, and X. Wang, "Accelerated Newton-Raphson Power Flow," *European Transactions on Electrical Power*, vol. 22, no. 4, pages 504–517, May 2012

[4] G. Li, X.-P. Zhang, "Comparison between Two Probabilistic Load Flow Methods for Reliability Assessment," in *Proceedings of 2009 IEEE Power and Energy Society General Meeting*, Calgary, Alberta, AB, Canada, pp. 1-7, Jul. 26-30 2009.

[5] Z. Bie, H. Liu, G. Li, et al., "Voltage Fluctuation Analysis of a Power System with Wind Farms Integrated by Probabilistic Load Flow," *Journal of Xi'an Jiaotong University*, vol. 42, no. 12, pp. 1500-1505, Dec. 2008.

[6] Z. Bie, G. Li, H. Liu, et al., "Studies on Voltage Fluctuation in the Integration of Wind Power Plants Using Probabilistic Load Flow," in *Proceedings of 2008 IEEE Power and Energy Society General Meeting*, Pittsburgh, PA, USA, pp. 1-7, Jul. 20-24 2008.

LIST OF REFERENCES

[1] S. Newman, *The Final Energy Crisis, 2nd Edition*. London: Pluto Press, 2008.

[2] H. Michael and K. Snorre, "Depletion of Fossil Fuels and the Impacts of Global Warming," *Resource and Energy Economics*, vol. 18, no. 2, pp. 115-136, Jun. 1996.

[3] European Wind Energy Association, *Wind Energy - The Facts*. London: Earthscan, 2009.

[4] E. Ungar and K. Fell, "Plug in, Turn on, and Load up," *IEEE Power and Energy Magazine*, vol. 8, no. 3, pp. 30-35, May 2010.

[5] D. Seligsohn, R. Heilmayr, X. Tan, and L. Weischer, China, the United States, and the Climate Change Challenge, *World Resources Institute*, Tech. Report, Oct. 2009, [Online]. Available: http://www.wri.org/publication/china-united-states-climate-change-challenge/.

[6] S. M. Amin and B. F. Wollenberg, "Toward a Smart Grid: Power Delivery of the 21st Century," *IEEE Power and Energy Magazine*, vol. 3, no. 5, pp. 34-41, Sept. 2005.

[7] X. Zhou, "Present Situation and Trend of Energy Consumption in Traffic and Transportation Industry," *Sino-Global Energy*, vol. 15, no. 7, pp. 9-18, Jul. 2010.

[8] R. D. Richardson and G. M. Mcnerney, "Wind Energy Systems,", *Proceedings of the IEEE*, vol. 81, no. 3, pp. 378-389, Mar. 1993.

[9] P. Musgrove, "Wind Energy," Cambridge: Cambridge University Press, 2009.

[10] World Wind Energy Association Head Office, World Wind Energy Half-Year Report 2011, *World Wind Energy Association*, Tech. Report, Aug. 2011.

[11] RenewableUK, "UK Wind Energy Database Statistics," March 2012, [Online]. Available: http://www.bwea.com/statistics/.

[12] A. Smith, "Two Terawatts Average Power Output: The UK Offshore Wind Resource," Sept. 2010, [Online]. Available: http://www.claverton-energy.com/two-terawatts-average-power-output-the-uk-offshore-wind-resource.html/.

[13] J. Oswald, M. Raine, and H. Ashraf-Ball, "Will British Weather Provide Reliable Electricity?," *Energy Policy*, vol. 36, no. 8, pp. 2312-2325, Jun. 2008.

[14] M. Etezadi-Amoli, K. Choma, and J. Stefani, "Rapid-Charge Electric-Vehicle Stations," *IEEE Transactions on Power Delivery*, vol. 25, no. 3, pp. 1883-1887, Jul. 2010.

[15] European Commission, “Reducing Emissions from Transport,” Jan. 2011, [Online]. Available: http://ec.europa.eu/clima/policies/transport/index_en.htm/.

[16] A. K. Srivastava, B. Annabathina, and S. Kamalasadan, “The Challenges and Policy Options for Integrating Plug-in Hybrid Electric Vehicle into the Electric Grid,” *The Electricity Journal*, vol. 23, no. 3, pp. 83-91, Mar. 2010.

[17] D. Sperling, and G. Deborah, *Two Billion Cars: Driving toward Sustainability*. New York: Oxford University Press, 2009.

[18] D. B. Sandalow, *Plug-In Electric Vehicles: What Role for Washington?*. Washington: The Brookings Institution, 2009.

[19] C. Woodyard, “Obama Pushes Electric Cars, Battery Power This Week,” *USA Today*, Jul. 2010.

[20] K. Bradsher, “In China, Power in Nascent Electric Car Industry,” *New York Times*, Dec. 2011.

[21] C. Schweinsberg, “U.S. Hybrid Sales Hit 2 Million Mark,” *WardsAuto*, Jun. 2011.

[22] A. Shimbun, “Hybrids Now 16% of Market in Japan as Prius Wins Annual Sales Crown Again,” *Integrity Exports*, Apr. 2012.

[23] A. Vaughan, “UK Government Launches £5,000 Electric Car Grant Scheme,” Jan. 2011, [Online]. Available: http://www.guardian.co.uk/environment/2011/jan/01/electric-car-grant-uk/.

[24] D. Vince, “Our Electric Highway Will Kick Start Britain's Green Car Revolution,” Jul. 2011, [Online]. Available: http://www.guardian.co.uk/environment/2011/jul/27/ electric-motorway-green-cars/.

[25] Society of Motor Manufacturers and Traders, “December 2011 – EV and AFV Registrations,” Jan. 2012, [Online]. Available: http://www.smmt.co.uk/2012/01/ december-2011-%E2%80%93-ev-and-afv-registrations/.

[26] J. Siegel, “Electric Vehicle Market Will Grow 20 Percent Annually,” Dec. 2011, [Online]. Available: http://www.greenchipstocks.com/articles/electric-vehicle-market-growth/1467/.

[27] Y. Wu, “Research on Reliability Evaluation and Expansion Planning of Power System including Wind Farms,” Ph.D. dissertation, School of Electric Engineering, Hefei University of Technology, Hefei, Anhui, China, 2006.

[28] Z. Hu, Y. Song, Z. Xu, et al., “Impacts and Utilization of Electric Vehicles into Power Systems,” *Proceedings of the CSEE*, vol. 32, no. 4, pp. 1-11, Feb. 2012.

[29] C. Gao and L. Zhang, “A Survey of Influence of Electrics Vehicle Charging on Power Grid,” *Power System Technology*, vol. 35, no. 2, pp. 127-131, Feb. 2011.

[30] W. F. Tinney and C. E. Hart, “Power Flow Solution by Newton's Method,” *IEEE Transactions on Power Apparatus and Systems*, vol. 86, no. 11, pp. 1449-1460, Nov. 1967.

[31] E. Moore K. Ganesan, W. J. Vetter, “On Convergence of Newton's Method for Load Flow Problems,” *International Journal for Numerical Methods in Engineering*, vol. 7, no.3, pp. 325-336, Jul. 1973.

[32] B. Stott, “Review of Load-Flow Calculation Methods,” *Proceedings of IEEE*, vol.62, no. 7, pp. 916-929, Jul. 1974.

[33] B. Scott and O. Alsac, “Fast Decoupled Load Flow,” *IEEE Transactions on Power Apparatus and Systems*, vol. 93, no. 3, pp. 859-869, May 1974.

[34] V. Ajjarapu and C. Christy, “The Continuation Power Flow: A Tool for Steady-State Voltage Stability Analysis,” *IEEE Transactions on Power Systems*, vol. 7, no. 1, pp. 416-423, Feb. 1992.

[35] S. Iwamoto and Y. Tamura, “A Load Flow Method for Ill-Conditioned Power Systems,” *IEEE Trans. on Power Apparatus and Systems*, vol. 100, no.4, pp. 1736-1743, Apr. 1981.

[36] V. M. da Costa, N. Martins, and J. L. R. Pereira, “Developments in the Newton Raphson Power Flow Formulation Based on Current Injections,” *IEEE Transactions on Power Systems*, vol. 14, no. 4, pp. 1320-1326, Nov. 1999.

[37] V. M. da Costa, J. L. R. Pereira, and N. Martins, “An Augmented Newton-Raphson Power Flow Formulation Based on Current Injections,” *International Journal of Electrical Power & Energy Systems*, vol. 23, no. 4, pp. 305-312, May 2001.

[38] C. A. Ferreira and V. M. da Costa, “A Second Order Power Flow Based on Current Injection Equations,” *International Journal of Electrical Power & Energy Systems*, vol. 27, no. 4, pp. 254-263, May 2005.

[39] T. Kulworawanichpong, “Simplified Newton-Raphson Power-Flow Solution Method,” *International Journal of Electrical Power & Energy Systems*, vol. 32, no. 6, pp. 551-558, Jul. 2010.

[40] V. M. da Costa and A. Rosa, “A Comparative Analysis of Different Power Flow Methodologies," in *Proceedings of 2008 IEEE/PES Transmission and Distribution Conference and Exposition: Latin America*, Bogota, Colombia, pp.1-7, Aug. 13-15 2008.

[41] F. Milano, “Continuous Newton’s Method for Power Flow Analysis,” *IEEE Transactions on Power Systems*, vol. 24, no. 1, pp. 50-57, Feb. 2009.

[42] S. Iwamoto and Y. Tamura, “A Load Flow Calculation Method for Ill-Conditioned Power Systems,” *IEEE Transactions on Power Apparatus and Systems*, vol. 100, no. 4, pp.1736-1743, Apr. 1981.

[43] L. M. C. Braz, C. A. Castro, and C. A. F. Murati, “A Critical Evaluation of Step Size Optimization Based Load Flow Methods,” *IEEE Transactions on Power Systems*, vol. 15, no. 1, pp.202-207, Feb. 2000.

[44] J. E. Tate and T. J. Overbye, “A Comparison of the Optimal Multiplier in Polar and Rectangular Coordinates,” *IEEE Transactions on Power Systems*, vol. 20, no. 4, pp. 1667- 1674, Nov. 2005.

[45] R. S. Salgado and A. F. Zeitune, “Power Flow Solutions through Tensor Methods,” *IET Generation, Transmission & Distribution*, vol. 3, no. 5, pp. 413-424, May 2009.

[46] A. C. Z. de Souza, C. B. Rosa, I. L. Lopes, and et al., “Non-Iterative Load-Flow Method as A Tool for Voltage Stability Studies,” *IET Generation Transmission & Distribution*, vol. 1, no. 3, pp. 499-505, May 2007.

[47] A. Karami, and M. S. Mohammadi, “Radial Basis Function Neural Network For Power System Load-Flow,” *International Journal of Electrical Power & Energy Systems*, vol. 30, no. 1, pp. 60-66, Jan. 2008.

[48] P. ACHARJEE and S. K. GOSWAMI, “Chaotic Particle Swarm Optimization Based Robust Load Flow,” *International Journal of Electrical Power & Energy Systems*, vol. 32, no. 2, pp. 141-146, Feb. 2008.

[49] A. Semlyen and F. de Leon, “Quasi-Newton Power Flow Using Partial Jacobian Updates,” *, IEEE Transactions on Power Systems*, vol. 16, no. 3, pp.332-339, Aug. 2001.

[50] G. Radman and J. Shultz, “An Effective Calculation Procedure for the Newton-Raphson Power Flow Analysis,” in *Proceedings of 7th ISATED International Multi-*

Conference on Power and Energy Systems, Calgary, Canada, pp. 149-153, Feb. 24-26 2003.

[51] P. J. Lagace, M. H. Vuong and I. Kamwa, "Improving Power Flow Convergence by Newton Raphson with a Levenberg-Marquardt Method," in *Proceedings of 2008 IEEE Power and Energy Society General Meeting*, Pittsburgh, PA, USA, pp.1-6, 20-24 Jul. 2008.

[52] K. L. Lo and Z. J. Meng, "Newton-Like Method for Line Outage Simulation," *IEE Proceedings of Generation, Transmission and Distribution*, vol. 151, no. 2, pp. 225-231, Mar. 2004.

[53] N. S. Krejić and Z. Luźanin, "Newton-Like Method with Modification of the Right-Hand-Side Vector," *Mathematics of Computation*, vol. 71, no. 237, pp. 237-250, Jan. 2002.

[54] R. S. Dembo, S. C. Eisenstat, and T. Steihaug, "Inexact Newton Methods," *SIAM Journal on Numerical Analysis*, vol. 19, no. 2, pp. 400-408, Apr. 1982.

[55] S. C. Eisenstat and H. F. Walker, "Choosing the Forcing Terms in an Inexact Newton Method," *SIAM Journal on Scientific Computing*, vol. 17, no. 1, pp. 16-32, Jan. 1996.

[56] D. Herceg, N. S. Krejić, and Z. Luźanin, "Quasi-Newton's Method with Correction," *Novi Sad Journal of Mathematics*, vol. 26, no. 1, pp. 115-127, Jan. 1996

[57] G. Zhou and L. Qi, "On the Convergence of an Inexact Newton-Type Method," *Operations Research Letters*, vol. 34, no. 6, pp. 647-652, Nov. 2006.

[58] C. Xu, N. Wang, and M. Wang, "Study of Accelerated Newton-Like Method with Modification of the Right-Hand-Side Vector," *Journal of Huazhong University of Science and Technology (Nature Science Edition)*, vol. 34, no. 4, pp. 119-121, Apr. 2006.

[59] I. K. Argyros, S. Hilout, "Inexact Newton-type Methods," *Journal of Complexity*, vol. 26, no. 6, pp. 577-590, Dec. 2010.

[60] A. K. Srivastava, B. Annabathina, and S. Kamalasadan, "The Challenges and Policy Options for Integrating Plug-in Hybrid Electric Vehicle into the Electric Grid," *The Electricity Journal*, vol. 23, no. 3, pp. 83-91, Apr. 2010.

[61] T. H. Bradleya and A. A. Frankb, "Design, Demonstrations and Sustainability Impact Assessments for Plug-In Hybrid Electric Vehicle," *Renewable and Sustainable Energy Reviews*, vol. 13, no. 1, pp. 115-128, Jan. 2009.

[62] S. S. Williamson, “Electric Drive Train Efficiency Analysis Based on Varied Energy Storage System Usage for Plug-In Hybrid Electric Vehicle,” in *Proceedings of 2007 IEEE Power Electronics Specialists Conference*, Orlando, FL, USA, pp.1515-1520, Jul. 17-21 2007.

[63] G. T. Heydt, “The Impact of Electric Vehicle Deployment on Load Management Strategies,” *IEEE Transactions on Power Apparatus & System*, vol. 1, no. 144, pp. 1253-1259, May 1983.

[64] A. Heider and H. J. Haubrich, “Impact of Wide-Scale EV Charging on the Power Supply Network,” in *Proceedings of IEE Colloquium on Electric Vehicles: A Technology Roadmap for the Future*, London, UK, vol. 6, no. 262, pp. 1-4, May 5 1998.

[65] K. Schneider, C. Gerkensmeyer, M. Kintner-Meyer, and M. Fletcher, “Impact Assessment of Plug-In Hybrid Electric Vehicles on Pacific Northwest Distribution Systems,” in *Proceedings of 2008 IEEE Power and Energy Society General Meeting*, Pittsburgh, PA, USA, pp. 1-6, Jul. 20-24 2008.

[66] K. Mets, T. Verschueren, W. Haerick, et al., “Optimizing Smart Energy Control Strategies for Plug-In Hybrid Electric Vehicle Charging,” in *Proceedings of 12th IEEE/IFIP Network Operations and Management Symposium Workshops*, Osaka, Japan, pp. 293-299, Apr. 19-23 2010.

[67] N. Rotering and M. Ilic, “Optimal Charge Control of Plug-In Hybrid Electric Vehicles in Deregulated Electricity Markets,” *IEEE Transactions on Power Systems*, vol. 26, no. 3, pp. 1021-1029, Aug. 2011.

[68] W. Kempton and J. Tomic, “Vehicle-to-Grid Power Fundamentals: Calculating Capacity and Net Revenue,” *Journal of Power Sources*, vol. 144, no. 1, pp. 268-279, Jun. 2005.

[69] W. Kempton and J. Tomic, “Vehicle-to-Grid Power Implementation: From Stabilizing the Grid to Supporting Large-Scale Renewable Energy,” *Journal of Power Sources*, vol. 144, no. 1, pp. 280-294, Jun. 2005.

[70] H. Turton and F. Moura, “Vehicle-to-Grid Systems for Sustainable Development: An Integrated Energy Analysis,” *Technological Forecasting and Social Change*, vol. 75, no. 8, pp. 1091-1108, Oct. 2008.

[71] C. Guille and G. Gross, "A Conceptual Framework for the Vehicle-to-Grid (V2G) Implementation," *Energy Policy*, vol. 37, no. 11, pp. 4379-4390, Nov. 2009.

[72] W. Kempton and J. Tomic, "Vehicle-to-Grid Power Fundamentals: Calculating Capacity and Net Revenue," *Journal of Power Sources*, vol. 144, no. 1, pp. 268-279, Jun. 2005.

[73] W. Kempton and J. Tomic, "Vehicle-to-Grid Power Implementation: From Stabilizing the Grid to Supporting Large-Scale Renewable Energy," *Journal of Power Sources*, vol. 144, no. 1, pp. 280-294, Jun. 2005.

[74] M. Etezadi-Amoli, K. Choma, and J. Stefani, "Rapid-Charge Electric-Vehicle Stations," *IEEE Transactions on Power Delivery*, vol. 25, no. 3, pp. 1883-1887, Jul. 2010.

[75] K. Clement-Nyns, E. Haesen, and J. Driesen, "The Impact of Charging Plug-In Hybrid Electric Vehicles on a Residential Distribution Grid", *IEEE Transactions on Power Systems*, vol. 25, no. 1, pp. 371-380, Feb. 2010.

[76] U. N. Bhat, *An Introduction to Queueing Theory: Modeling and Analysis in Applications*. New York: Birkhäuser Boston & Springer Science, 2008.

[77] R. Garcia-Valle, and J. G. Vlachogiannis, "Electric Vehicle Demand Model for Load Flow Studies", *Electric Power Components & Systems*, vol. 37, no. 5, pp. 577-582, May 2009.

[78] J. G. Vlachogiannis, "Probabilistic Constrained Load Flow Considering Integration of Wind Power Generation and Electric Vehicles", *IEEE Transactions on Power Systems*, vol. 24, no. 4, pp. 1808-1817, Nov. 2009.

[79] S. Meliopoulos, Power System Level Impacts of Plug-In Hybrid Vehicles, *Power Systems Engineering Research Center (PSERC)*, Tech. Report, Oct. 2009, [Online]. Available: www.pserc.wisc.edu/research/public_reports/td.aspx/.

[80] B. Borkowska, "Probabilistic Load Flow," *IEEE Transactions on Power Apparatus and Systems*, vol. 93, pp. 752-759, May 1974.

[81] A. M. L. d. Silva and V. L. Arienti, "Probabilistic Load Flow by a Multi-linear Simulation Algorithm," *IEE Proceedings of Generation Transmission and Distribution*, vol. 137, pp. 276-282, Jul. 1990.

[82] R. Billinton and W. Li, *Reliability Assessment of Electric Power Systems Using Monte Carlo Methods*. New York: Plenum, 1994.

[83] P. Jirutitijaroen and C. Singh, "Comparison of Simulation Methods for Power System Reliability Indexes and Their Distributions," *IEEE Transactions on Power Systems*, vol. 23, pp. 486-493, Apr. 2008.

[84] R. N. Allan, B. Borkowska, and C. H. Grigg, "Probabilistic Analysis of Power Flows," *Proceedings of the Institute of Electrical Engineers*, vol. 121, no 12, pp. 1551-1556, Dec. 1974.

[85] R. N. Allan and M. R. G. Al-Shakarchi, "Probabilistic Techniques in A.C. Load-Flow Analysis," *Proceedings of the Institute of Electrical Engineers*, vol. 124, pp. 154-160, Feb. 1977.

[86] R. N. Allan and M. R. G. Al-Shakarchi, "Linear Dependence between Nodal Powers in Probabilistic A.C. Load Flow", *Proceedings of IEE*, vol. 124, no. 6, pp. 529-534, Jun. 1977.

[87] R. N. Allan, A. M. L. da Silva, and R. C. Burchett, "Evaluation Methods and Accuracy in Probabilistic Load Flow Solutions," *IEEE Transactions on Power Apparatus and Systems*, vol. 100, pp. 2539-2546, May 1981.

[88] R. N. Allan and A. M. L. Dasilva, "Probabilistic Load Flow Using Multi-linearizations," *IEE Proceedings of Generation Transmission and Distribution*, vol. 128, no. 5, pp. 280-287, May 1981.

[89] A. M. L. d. Silva, V. L. Arienti, and R. N. Allan, "Probabilistic Load Flow Considering Dependence between Input Nodal Powers," *IEEE Transactions on Power Apparatus and Systems*, vol. 103, pp. 1524-1530, Jun. 1984.

[90] M. Brucoli and F. Torelli, "Quadratic Probabilistic Load Flow with Linearly Modeled Dispatch," *International Journal of Electrical Power & Energy Systems*, vol. 7, pp. 138-146, Jul. 1985.

[91] A. M. L. Dasilva, R. N. Allan, S. M. Soares, and V. L. Arienti, "Probabilistic Load Flow Considering Network Outages," *IEE Proceedings of Generation Transmission and Distribution*, vol. 132, pp. 139-145, May 1985.

[92] L. A. Sanabria and T. S. Dillon, "Stochastic Power Flow Using Cumulants and Von Mises Functions," *International Journal of Electrical Power & Energy Systems*, vol. 8, pp. 47-60, Jan. 1986.

[93] S. Patra and R. B. Misra, "Probabilistic Load Flow Solution Using Method of Moments," in *Proceedings of 2nd International Conference on Advances in Power*

System Control, *Operation & Management*, Hong Kong, vol. 1 and 2, pp. 922-934 & 991, Dec. 7-10 1993.

[94] P. Zhang and S. T. Lee, "Probabilistic Load Flow Computation Using the Method of Combined Cumulants and Gram-Charlier Expansion," *IEEE Transactions on Power Systems*, vol. 19, pp. 676-682, Feb. 2004.

[95] Z. Hu and X. Wang, "A Probabilistic Load Flow Method Considering Branch Outages," *IEEE Transactions on Power Systems*, vol. 21, pp. 507-514, May 2006.

[96] M. Lu, Z. Y. Dong, and T. K. Saha, "A Probabilistic Load Flow Method Considering Transmission Network Contingency," in *Proceedings of 2007 IEEE Power Engineering Society General Meeting*, Tampa, FL, USA, pp. 1-6, Jun. 24-28 2007.

[97] J. Usaola, "Probabilistic Load Flow with Wind Production Uncertainty Using Cumulants and Cornish-Fisher Expansion," *International Journal of Electrical Power & Energy Systems*, vol. 31, no. 9, pp. 474-481, Sept. 2009.

[98] J. Usaola, "Probabilistic Load Flow with Correlated Wind Power Injections," *Electric Power Systems Research*, vol. 80, no. 5, pp. 528-536, May 2010.

[99] F. J. Ruiz-Rodriguez, J. C. Hernández, and F. Jurado, "Probabilistic Load Flow for Photovoltaic Distributed Generation Using the Cornish-Fisher Expansion," *Electric Power Systems Research*, vol. 89, no. 8, pp. 129-138, Aug. 2012.

[100] C.-L. Su, "Probabilistic Load-Flow Computation Using Point Estimate Method," *IEEE Transactions on Power Systems*, vol. 20, pp. 1843-1851, Nov. 2005.

[101] J. M. Morales and J. Perez-Ruiz, "Point Estimate Schemes to Solve the Probabilistic Power Flow," *IEEE Transactions on Power Systems*, vol. 22, pp. 1594-1601, Nov. 2007.

[102] J. M. Morales, L. Baringo, A. J. Conejo, et al., "Probabilistic Power Flow with Correlated Wind Sources," *IET Generation, Transmission & Distribution*, vol. 4, no. 5, pp. 641-651, May 2010.

[103] M. T. Schilling, A. M. Leite da Silva, R. Billinton, et al., "Bibliography on Power System Probabilistic Analysis (1962-88)," *IEEE Transactions on Power Systems*, vol. 5, pp. 1-11, 1990.

[104] P. Chen, Z. Chen, and B. Bak-Jensen, "Probabilistic Load Flow: A Review," in *Proceedings of 3rd International Conference on Electric Utility Deregulation and*

Restructuring and Power Technologies, Nanjing, Jiangsu, China, pp.1586-1591, Apr. 6-9 2008.

[105] J. Carpentier, "Optimal Power Flows," *International Journal of Electrical Power & Energy Systems*, vol.1, no. 1, pp. 3-15, Apr. 1979.

[106] Y. Taiyou and R. H. Lasseter, "Stochastic Optimal Power Flow: Formulation and Solution," in *Proceedings of 2000 IEEE Power Engineering Society Summer Meeting*, Seattle, WA, USA, vol. 1, pp. 237-242, 2000.

[107] A. Schellenberg, "Probabilstic and Stochastic Optimal Power Flow," Ph.D. dissertation, Department of Electric and Computer Engineering, University of Calgary, Alberta, Canada, 2006.

[108] G. L. Viviani and G. T. Heydt, "Stochastic Optimal Energy Dispatch," *IEEE Transactions on Power Apparatus and Systems*, vol. 100, no. 07, pp. 3221-3227, Jul. 1981.

[109] M. Madrigal, K. Ponnambalam, and V. H. Quintana, "Probabilistic Optimal Power Flow," in *Proceedings of 1998 IEEE Canadian Conference on Electrical and Computer Engineering*, Toronto, Canada, pp. 385-388, May 24-28 1998.

[110] A. Schellenberg, W. Rosehart, and J. Aguado, "Cumulant Based Probabilistic Optimal Power Flow (P-OPF)," in *Proceedings of 2004 International Conference on Probabilistic Methods Applied to Power Systems*, Ames, LA, USA, pp. 506-511, Sept. 12-16 2004.

[111] A. Schellenberg, W. Rosehart, and J. Aguado, "Cumulant-Based Probabilistic Optimal Power Flow (P-OPF) with Gaussian and Gamma Distributions," *IEEE Transactions on Power Systems*, vol. 20, no. 2, pp. 773-781, May 2005.

[112] G. Verbic, and C. A. Canizares, "Probabilistic Optimal Power Flow in Electricity Markets Based on a Two-Point Estimate Method," *IEEE Transactions on Power Systems*, vol. 21, no. 4, pp. 1883-1893, Nov. 2006.

[113] G. Verbic, A. Schellenberg, W. Rosehart, et al., "Probabilistic Optimal Power Flow Applications to Electricity Markets," in *Proceedings of 2006 International Conference on Probabilistic Methods Applied to Power Systems*, Stockholm, Sweden, pp. 348-353 & 1244, Jun. 11-15 2006.

[114] X. Li, Y. Z. Li, and S. H. Zhang, "Analysis of Probabilistic Optimal Power Flow Taking Account of the Variation of Load Power," *IEEE Transactions on Power Systems*, vol. 23, no. 3, pp. 992-999, Aug. 2008.

[115] M. E. El-Hawary, and G. A. N. Mbamalu, "Stochastic Optimal Load Flow Using a Combined Quasi-Newton and Conjugate Gradient Technique," *International Journal of Electrical Power & Energy Systems*, vol.11, no. 2, pp. 85-93, Apr. 1989.

[116] Z. Hu and X. Wang, "Stochastic Optimal Power Flow Approach Considering Load Probabilistic Distributions," *Automation of Electric Power Systems*, vol. 31, no. 16, pp. 14-17 & 44, Nov. 2007.

[117] Z. Hu, X. Wang, and G. Taylor, "Stochastic Optimal Reactive Power Dispatch: Formulation and Solution Method," *International Journal of Electrical Power & Energy Systems*, vol. 32, no. 6, pp. 615-621, Jul. 2010.

[118] H. Zhang and P. Li, "Probabilistic Analysis for Optimal Power Flow under Uncertainty," *IET Generation, Transmission & Distribution*, vol. 4, no. 5, pp. 553-561, May 2010.

[119] Y. Yuan, Q. Li, and W. Wang, "Optimal Operation Strategy of Energy Storage Unit in Wind Power Integration Based on Stochastic Programming," *IET Renewable Power Generation*, vol. 5, no.2, pp. 194-201, May 2011.

[120] B. Liu, Theory *and Practice of Uncertain Programming, 2nd Edition*. Berlin: Springer Press, 2009.

[121] P. F. Correia, J. M. Ferreira de Jesus, "Simulation of Correlated Wind Speed and Power Variates in Wind Parks," *Electric Power Systems Research*, vol. 80, no. 5, pp. 592-598, May 2010.

[122] W. H. Press, S. A. Teukolsky, W. T. Vetterling, et al., *Numerical Recipes: The Art of Scientific Computing, Third Edition*. Cambridge: Cambridge University Press.

[123] T. A. Davis, *Direct Methods for Sparse Linear Systems - Fundamentals of Algorithms*. Philadelphia: Society for Industrial and Applied Mathematics, 2006.

[124] J. E. Dennis Jr. and R. B. Schnabel, *Numerical Methods for Unconstrained Optimization and Nonlinear Equations*. Philadelphia: Society for Industrial Mathematics, 1983.

[125] G. A. Korn and T. M. Korn, *Mathematical Handbook for Scientists and Engineers*. New York: Dover Publications, 2000.

[126] S. M. Chan, and V. Brandwajn, "Partial Matrix Refactorization," *IEEE Transactions on Power Systems*, vol. 1, no. 1, pp. 193-200, Jan. 1986.

[127] Y. Zhang, and W. F. Tinney, "Partial Refactorization with Unrestricted Topology Changes," *IEEE Transactions on Power Systems*, vol. 10, no. 3, pp. 1361-1368, Jul. 1995.

[128] J. Walter, M. Koch, G. Winkler, and D Bellot, "Basic Linear Algebra Library," Nov. 2010, [Online]. Available: http://www.boost.org/libs/numeric/.

[129] T. A. Davis, and E. P. Natarajan, "KLU: Sparse LU Factorization," May 2007, [Online]. Available: http://www.cise.ufl.edu/research/sparse/klu/.

[130] B. Dawes, "Boost Timer Library," Oct. 2011, [Online]. Available: www.boost.org/doc/libs/release/libs/timer/.

[131] H. Fischer, *A History of the Central Limit Theorem: from Classical to Modern Probability Theory*. New York: Springer, 2010.

[132] R. V. Hogg, J. W. McKean, and A. T. Craig, *Introduction to Mathematical Statistics, 6th Edition*. Upper Saddle River, New Jersey: Prentice Hall, 2004.

[133] N. L. Johnson, A. W. Kemp, and S. Kotz, *Univariate Discrete Distributions, 3rd Edition*. Hoboken, NJ: Wiley-Interscience, 2005.

[134] W. T. Pennell and A. H. Miller, "Procedures for Modeling Wind Turbine Performance from Site Wind Data," in *Proceedings of 5th Annual Energy-Sources Technology Conference and Exhibition*, New Orleans, LA, USA, 82-PET-7, Mar. 7-10 1982.

[135] G. J. Bowden, P. R. Barker, V. O. Shestopal, and J. W. Twidell, "The Weibull Distribution Function and Wind Power Statistics," *Wind Energy*, vol. 7, no. 2, pp. 85-98, Apr. 1983.

[136] R. B. Corotis, A. B. Sigl, and J. Klein, "Probability Models of Wind Velocity Magnitude and Persistence," *Solar Energy*, vol. 20, no. 6, pp. 483-493, Jun. 1978.

[137] S. H. Jangamshetti and V. G. Rau, "Site Matching of Wind Turbine Generators: A Case Study," *IEEE Transactions on Energy Conversion*, vol. 14, no. 4, pp. 1537-1543, Dec. 1999.

[138] A. E. Feijoo, J. Cidras, and J. L. G. Dornelas, "Wind Speed Simulation in Wind Farms for Steady-State Security Assessment of Electrical Power Systems", *IEEE Transactions on Energy Conversion*, vol.14, no. 4, pp. 1582-1588, Dec. 1999.

[139] A. Garcia, J. L. Torres, E. Prieto, and A. de Francisco, "Fitting Wind Speed Distributions: A Case Study," *Solar Energy*, vol. 62, no. 2, pp. 139-144, Feb. 1998.

[140] A. Balouktsis, D. Chassapis, and T. D. Karapantsios, "A Nomogram Method for Estimating the Energy Produced by Wind Turbine Generators," *Solar Energy*, vol. 72, no. 3, pp. 251-259, Mar. 2002.

[141] Y. Muluge and F. Drake, "Assessment of Solar and Wind Energy Resources in Ethiopia II: Wind Energy," Solar Energy, vol. 57, no. 4, pp. 323-334, Oct. 1996.

[142] S. H. Jangamshetti and V. Rau, "Optimum Siting of Wind Turbine Generators," *IEEE Transactions on Energy Conversion*, vol. 16, no. 1, pp. 8-13, Mar. 2001.

[143] A. Van den Bos, *Parameter Estimation for Scientists and Engineers*. Hoboken, NJ: Wiley-Interscience, 2007.

[144] L. Ranch, New Mexico Wind Resource Assessment, *Sandia National Laboratories*, Tech. Report, Feb. 2003, Online. Available: http://www.sandia.gov/wind/other/ LeeRanchData-2002.pdf/.

[145] G. N. Kariniotakis and P. Pinson, "Uncertainty of Short-term Wind Power Forecasts: A Methodology for On-line Assessment," in *Proceedings of 2004 International Conference on Probabilistic Methods Applied to Power Systems*, Ames, IA, USA, pp.729-736, Sept. 16 2004.

[146] S. F. Castro and R. N. Allan, "Generation Availability Assessment of Wind Farms," *Proceedings of IEE Generation, Transmission and Distribution*, vol.143, no.5, pp.507-518, Sept. 1996.

[147] X. Zhang; W. Wang, "Wind Farm and Wake Effect Modeling for Simulation of a Studied Power System," in *Proceedings of 2009 Power Systems Conference and Exposition*, Seattle, WA, USA, pp.1-6, Mar. 15-18 2009.

[148] A. Marinopoulos, J. Pan, M. Zarghami, et al., "Investigating the Impact of Wake Effect on Wind Farm Aggregation," in *Proceedings of 2011 IEEE Trondheim PowerTech*, Trondheim, Norway, pp.1-5, Jun. 19-23 2011.

[149] J. K. Sethi, D. Deb, M. Malakar, "Modeling of a Wind Turbine Farm in Presence of Wake Interactions," in *Proceedings of 2011 International Conference on Energy, Automation, and Signal*, Bhubaneswar, India, pp.1-6, Dec. 28-30 2011.

[150] A. Fabbri, T. GomezSanRoman, J. RivierAbbad, et al., "Assessment of the Cost Associated with Wind Generation Prediction Errors in a Liberalized Electricity

Market," *IEEE Transactions on Power Systems*, vol.20, no.3, pp. 1440-1446, Aug. 2005.

[151] M. Lange, "On the Uncertainty of Wind Power Predictions - Analysis of the Forecast Accuracy and Statistical Distribution of Errors," *Journal of Solar Energy Engineering*, vol. 127, no. 2, pp. 177-185, May 2005.

[152] J. Usaola and J. Angarita, "Bidding Wind Energy under Uncertainty," in *Proceedings of 2007 International Conference on Clean Electrical Power*, Capri, Italy, pp.754-759, May 21-23 2007.

[153] H. Bludszuweit, J. A. Dominguez-Navarro, and A. Llombart, "Statistical Analysis of Wind Power Forecast Error", *IEEE Transactions on Power Systems*, vol. 23, no. 3, pp. 983-991, Aug. 2008.

[154] K. T. Chau and Y. S. Wong, "Overview of Power Management in Hybrid Electric Vehicles", *Energy Conversion and Management*, vol. 43, no. 15, pp. 1953-1968, Oct. 2002.

[155] L. Sanna, "Driving the Solution the Plug-In Hybrid Electric Vehicle", *EPRI Journal*, pp. 8-17, Sept. 2005.

[156] S. M. Ross, *Stochastic Processes, 2nd Edition*. New York: Wiley, 1996.

[157] K. Morrow, D. Karner, and J. Francfort, Plug-in Hybrid Electric Vehicle Charging Infrastructure Review, *Idaho National Laboratory*, Tech. Report, 2008, [Online]. Available: avt.inl.gov/pdf/phev/phevInfrastructureReport08.pdf/.

[158] P. Sharer, R. Leydier, and A. Rousseau, Impact of Drive Cycle Aggressiveness and Speed on HEVs Fuel Consumption Sensitivity, *Argonne National Lab*, Tech. Report, Apr. 2007, [Online]. Available: www.transportation.anl.gov/pdfs/HV/416.pdf

[159] G. W. Corder and D. I. Foreman, *Nonparametric Statistics for Non-Statisticians*. New York: Wiley, 2009.

[160] G. Papaefthymiou, "Integration of Stochastic Generation in Power Systems," Ph.D. dissertation, Faculty of Electrical Engineering, Mathematics and Computer Science, Delft University of Technology, Delft, Netherlands, 2007.

[161] J. M. Morales, R. Mínguez, and A. J. Conejo, "A Methodology to Generate Statistically Dependent Wind Speed Scenarios," *Applied Energy*, vol. 87, no. 3, pp. 843-855, Mar. 2010.

[162] A. C. Aitken, *Statistical Mathematics, 8th Revised Edition*. Edinburgh and London: Oliver & Boyd, 1957.

[163] I. M. Sobol', *A Primer for the Monte Carlo Method*. Chicago: CRC Press, 1994.

[164] M. H. Kalos and P. A. Whitlock, *Monte Carlo Methods, 2nd Edition*. Weinheim: Wiley-VCH, 2008.

[165] Gan Li and Xiao-Ping Zhang, "Comparison between Two Probabilistic Load Flow Methods for Reliability Assessment," in *Proceedings of 2009 IEEE Power & Energy Society General Meeting*, Calgary, Canada, pp.1-7, 26-30 July 2009.

[166] Y. G. Zhao and T. Ono, "New Point Estimates for Probability Moments," *Journal of Engineering Mechanics*, vol. 126, no. 4, pp. 433-436, Apr. 2000.

[167] T. C. John and B. B. Gregory, "The Point-Estimate Method with Large Numbers of Variables," *International Journal for Numerical and Analytical Methods in Geomechanics*, vol. 26, no. 15, pp. 1515-1529, Aug. 2002.

[168] H. S. Li, Z. Z. Lu, and X. K. Yuan, "Nataf Transformation Based Point Estimate Method", *Chinese Science Bulletin*, vol. 53, no. 17, pp. 2586-2592, Sept. 2008.

[169] WANG, Y. and TUNG, Y.-K.: 'Improved Probabilistic Point Estimation Schemes for Uncertainty Analysis', *Applied Mathematical Modeling*, vol. 33, no. 2, pp. 1042-1057, Feb. 2009.

[170] A. Hoese, and F. Garcés, "Stochastic Correlated Simulation: An Extension of the Cumulant Method to Include Time-Dependent Energy Sources," *International Journal of Electrical Power & Energy Systems*, vol. 21, no. 1, pp. 13-22, Jan. 1999.

[171] Z. Hu, "Static Security Analysis of Power System Considering Stochastic Factors," Ph.D. dissertation, School of Electric Engineering, Xi'an Jiaotong University, Xi'an, Shaanxi, China, 2005.

[172] C. Foote, P. Djapic, G. Ault, et al., United Kingdom Generic Distribution System Phase One Standard Data Format, *University of Manchester*, Tech. Report, Aug. 2005, [Online]. Available: http://monaco.eee.strath.ac.uk/ukgds/.

[173] S. Song, Z. Lu, and Z. Song, "Reliability Sensitivity Analysis Involving Correlated Random Variables by Directional Sampling," in *Proceedings of 2011 International Conference on Quality, Reliability, Risk, Maintenance, and Safety Engineering*, Chengdu, China, pp. 845-850, Jun. 17-19 2011.

[174] H. Wang, C. E. Murillo-Sánchez, R. D. Zimmerman, and R. J. Thomas, "On Computational Issues of Market-based Optimal Power Flow," *IEEE Transactions on Power Systems*, vol. 22, no. 3, pp. 1185-1193, Mar. 2007.

[175] R. D. Zimmerman, C. E. Murillo-Sánchez, and R. J. Thomas, "MATPOWER Steady-State Operations, Planning and Analysis Tools for Power Systems Research and Education," *IEEE Transactions on Power Systems*, vol. 26, no. 1, pp. 12-19, Jan. 2011.

[176] M. Abramowitz and I. A. Stegun, *Handbook of Mathematical Functions with Formulas, Graphs, and Mathematical Tables, 9th Edition*. New York: Dover, 1972.

[177] P. J. Smith, "A Recursive Formulation of the Old Problem of Obtaining Moments from Cumulants and Vice Versa," *The American Statistician*, vol. 49, no. 2, Feb. 1995.

[178] H. Cramer, *Mathematical Methods of Statistics*, Princeton: Princeton University Press, 1946.

[179] P. Sauer, G. Heydt, "A Convenient Multivariate Gram-Charlier Type A Series," *IEEE Transactions on Communications*, vol. 27, no. 1, pp. 247-248, Jan. 1979.

[180] S. Blinnikov, R. Moessner, "Expansions for Nearly Gaussian Distributions," *Astronomy and Astrophysics Supplement Series*, vol. 130, no. 1, pp. 193-205, May 1998.

[181] G. W. Hill, and A. W. Davis, "Generalized Asymptotic Expansions of Cornish-Fisher Type," *Annals of Mathematical Statistics*, vol. 39, no. 4, pp. 1264-1273, Apr. 1968.

[182] Y.-S. Lee and T.-K. Lin, "Algorithm AS 269: High Order Cornish-Fisher Expansion," *Journal of the Royal Statistical Society. Series C (Applied Statistics)*, vol. 41, no. 1, pp. 233-240, Jan. 1992.

[183] R. Von Mises, *Mathematical Theory of Probability and Statistics*. New York and London: Academic Press, 1964.

[184] J. Ahrens and U. Dieter, "Computer Methods for Sampling from Gamma, Beta, Poisson and Binomial Distributions," *Computing*, vol. 12, no. 3, pp. 223-246, Sept. 1974.

[185] J. Ahrens and U. Dieter, "Generating Gamma Variates by A Modified Rejection Technique," *Communications of the ACM*, vol. 25, no.1, pp. 47-54, Jan. 1982.